Lignin Biomaterial – from Enzyme-Responsive Vehicles to Carbon Precursor

Doungporn Yiamsawas

Dissertation

Lignin Biomaterial - from Enzyme-Responsive Vehicles to Carbon Precursor

Dissertation

zur Erlangung des Grades

"Doktor der Naturwissenschaften"

dem Fachbereich Chemie, Pharmazie und Geowissenschaften

der Johannes Gutenberg-Universität Mainz

vorgelegt von

Doungporn Yiamsawas

Geboren in Samut Sakhon, Thailand

Mainz 2016

Dekan:

1. Berichterstatter:

2. Berichterstatter:

Tag der mündlichen Prüfung :

Abstract

This thesis presents the first report on enzymatic triggered release of active agents from lignin nanoparticles prepared by a variety of chemistry via the miniemulsion process. The nanoparticles are found very promising as novel drug delivery vehicles in agriculture.

The first approach is to prepare lignin hollow nanocapsules by interfacial polyaddition in inverse miniemulsion. The obtained cross-linked lignin nanocontainers can be loaded with hydrophilic substances which can be released by an enzymatic trigger, namely laccases, present in natural plants. The second strategy for the nanocarrier formation is the modification of lignin by esterification of hydroxyl groups present in lignin with methacrylic anhydride. Then lignin nanocarriers with different morphologies such as solid, core-shell, and porous structure were produced by a combination of miniemulsion polymerization and a solvent evaporation process. A hydrophobic dye is used to investigate the release behavior of the lignin nanocarriers depending on their morphology. To verify the enzymatic response of lignin nanocarriers, the enzyme laccase was used to trigger the release of the dye from the lignin nanocarriers.

Lignin can act as drug delivery vehicles for fungal diseases in plants. For this, biodegradable lignin nanoparticles were loaded with pyroclostrobin, an antifungal drug against a disease of grapevine called Esca; studies in plants were performed by injecting aqueous dispersion of nanoparticles into Esca-infected *vitis vinifera* (grapevines). This work was carried out in collaboration with Prof. Dr. Eckhard Thines of the Institute of Biotechnology and Drug Research in Kaiserslautern. The enzymes secreted by Esca degraded the lignin nanoparticles and released the drug to cure infected wine plants. All treated plants with the fungicide-filled lignin nanoparticles recovered from the Esca infection.

The effect of biodegradable lignin nanoparticles and non-degradable polystyrene nanoparticles with encapsulated iron oxide on the development of mung beans and their bio-distribution was studied. Magnetic polystyrene nanoparticles influenced the growth of the root and the stem development during seeding, while the lignin particles did not have any visible effect. Both types of nanoparticles could penetrate the epidermis of the root tissue, were accumulated in root cells, and could be transported through the vascular cylinder to

leaves. The lignin nanoparticles were further loaded with a model antifungal drug that was distributed within the plant after incubation or injection of the bean with the nanoparticle dispersion.

This thesis shows tremendous potential of lignin nanoparticles in drug delivery for agricultural purposes and also in water purification by carbonization of lignin particles synthesized by the miniemulsion process. The resulting carbon particles exhibited a high surface area and showed efficient adsorption of the methylene blue dye.

These results prove that the abundant biopolymer lignin can be used as an efficient material for the preparation of nanoparticles with variable morphologies that can be applied in agriculture as biodegradable drug carrier or as adsorbent after carbonization.

Acknowledgements

Table of Contents

1. Introduction

"You can make anything out of lignin... except money"

Old industry saying

Introduction & Motivation

Surviving on a planet with limited resources to support our increasing global population is probably the greatest challenge humanity has faced so far. The largest problem is that many technologies driven our economy are not sustainable. There is the necessity of developing sustainable technology, together with increasing concerns over environment protection. The questions about future availability of petrochemical feedstock have pushed research and development toward degradable materials and renewable resources, which are environmentally friendly and should be more sustainable than currently used petroleum-based materials.[1] Within this context, lignin, a major polymeric component in plants, arises as a promising candidate for some applications due to its chemical versatility. Lignin is one of the most abundant natural polymers, together with cellulose and hemicellulose, and it forms part of the secondary cell walls of plants and helps to maintain the integrity of the cellulose/hemicellulose/pectin matrix. Apart from this, lignin is obtained from paper industry, when extracting cellulose in the pulping process. The composition and ratio of lignin in plants depends on the botanical species. In softwood lignin represents about 30% of the total mass, while in hardwood this amount decreases to 20–25%. The variable molecular mass of this biopolymer is a consequence of the randomly cross-linked polymerization of phenolic moieties, originating from radical-coupling reactions between phenolic radicals.

Among the recent technologies, nanotechnology takes a predominated position in many applications especially in the field of electronics[2], energy[3], and medicine[4], but its application to crop protection is still in its early stages. Nanoparticles have a great potential for the use as "magic bullets" that are loaded with herbicides, chemicals, or nucleic acids and then targeted at specific plant tissues or areas where they release their loads. In recent years the development of nanocarriers for the targeted delivery and controlled release of agrochemicals has been reported.[5, 6] The encapsulation of some pesticides into nanocarriers can lead to improvements during their application, and allows the slow and constant release of the active ingredient, reducing the use of organic solvent. The miniemulsion process is an efficient method for the preparation of polymer particles in the size range between about 30 and 500 nm. Using this technique, a wide variety of different materials ranging from liquid to

solid, from organic to inorganic, and from molecularly dissolved to aggregated species can be encapsulated into polymeric solid nanoparticles or nanocapsules with a liquid core. The use of renewable sources like lignin in the miniemulsion process breakthrough might help to overcome the petrochemical source limitation in diverse applications.

In this thesis, the syntheses of lignin nanoparticles by the miniemulsion process and their potential in agriculture applications are described. The methods for the preparation of nanoparticles from lignin are based on an inverse miniemulsion polymerization process for the encapsulation of hydrophilic compounds and on a miniemulsion process including a solvent evaporation for the encapsulation of hydrophobic compounds. For possible applications in agriculture, the entrapment of agrochemicals and their triggered release by laccase, an enzyme degrading lignin, from lignin nanoparticles has been studied. In addition, the lignin particles loaded with fungicide were tested in a vinery field test for Esca disease treatment. Furthermore, the uptake and toxicity to the plant of the lignin nanoparticles have been compared to magnetic polystyrene nanoparticles which are currently attractive nanoparticles in medical application. Moreover lignin is a carbon-rich renewable resource which composes of 50% carbon, 40% oxygen, 6% hydrogen and a small amount of nitrogen and mineral.[7, 8] Thus the carbonization of lignin particles was also investigated with different conditions and surface structure of carbon material from the lignin particles is finally explored.

2. Theoretical Background

2.1 Lignin as renewable raw material

2.1.1 Historical background of lignin in polymer science

Polymeric components in plants, such as cellulose, hemicellulose, and lignin interpenetrate with each other to form complex higher ordered structures in the secondary cell walls in living plants. The location of lignin in wood is presented in Figure 2.1. The history of lignin science holds over a period of one hundred years and many scientists had made effectively efforts to extract lignin from wood in order to purify cellulose in the pulping process. Since lignin has been considered as an unwelcome by-product, several attempts have been made to cultivate wood species having a small amount of lignin content using new biotechnologies. Thus, synthetic pathways of lignin in living plant organs and also enzymatic or chemical degradation processes have been investigated.[9]
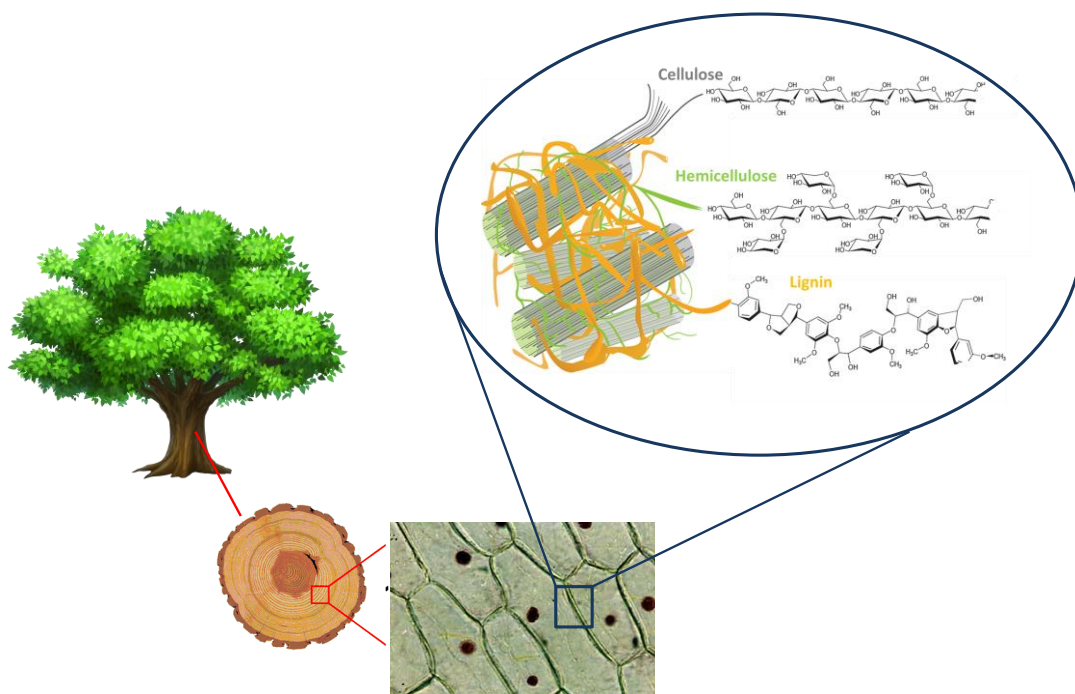
Figure 2.1 Occurrence of lignin in the plant cell walls of a tree. (Reprinted from Trends in Biotechnology, Nov, 28(11), Vanholme R, Van Acker R, Boerjan W., Potential of Arabidopsis systems biology to advance the biofuel field, 543-7., Copyright (2010) with permission from Elsevier)[10, 11]

The term "lignin" – coming from the Latin word lignum meaning "wood" - is used for the first time by the Swiss botanist A. P. de Candolle (1778–1841).[12] Lignin shows a complex structure, depending on its origin. The chemical structures of lignin have been investigated in detail by chemical and spectroscopic methods. In 1908, Klason first suggested that lignin had a macromolecular structure and later by 1917, it was found that it consisted of coniferyl alcohol units bonding together by ether linkages.[13] Due to the advanced development in instrumentation specifically spectroscopic techniques such as ultraviolet-visible (UV-Vis spectroscopy, infrared (IR), and nuclear magnetic resonance (NMR) spectroscopy, and mass spectrometry (MS) as well as new molecular weight determination instruments in the middle of 20th century, this greatly assisted the chemist to investigate the physical and polymer chemistry of lignin. In 1949, Aulin-Erdtman proved that lignins were undoubtedly aromatic by using UV-Vis spectroscopy and proposed that they were a condensation polymer of coniferyl aldehyde. [13]

The most complete structural model of lignin widely accepted until today was proposed by Adler in 1977.[14] The proposed structure with its main highlighted functional groups is demonstrated in Figure 2.2. Unlike other natural biopolymers lignin is a rather randomly crosslinked macromolecule and had no optical activity and no stereoregularity. It is generally accepted that there are three basic phenol derivatives, the so-called monolignols, that make up almost all types of lignin found in nature: *p*-coumaryl alcohol, coniferyl alcohol, and sinapyl alcohol (Figure 2.3). Each monolignol produces p-hydroxyphenyl, guaiacyl, and syringyl residues in the polymer.

The physic-chemical nature of lignin as a biopolymer has been investigated for a long time. In early 1960, Goring performed a lot of studies in order to analyze the polymeric properties of lignin including the molecular weight, shape, electrolyte swelling, solubility behavior, glass transition temperature and adhesive property of different lignins.[15-18] The main problem to measure the physical properties of isolated lignin is its limited solubility in organic solvent. The uncertainty of the molecular mass determination of isolated lignin is unavoidable since the soluble fraction of lignin is likely lower than that of an isolated sample. This issue turns out to be even more complicated because the solution properties of lignin do not only depend on the plant species but also on the isolation process. Thus, the polymeric character of lignin can be deduced only by estimation

The molecular mass of lignin has been determined by typical techniques included viscosimetry,[19] light scattering,[20] and gel permeation chromatography (GPC).[21] They are in the range of 10^3–10^5 g·mol^{-1} depending on the plant species, isolation method, and as well as the measuring method.
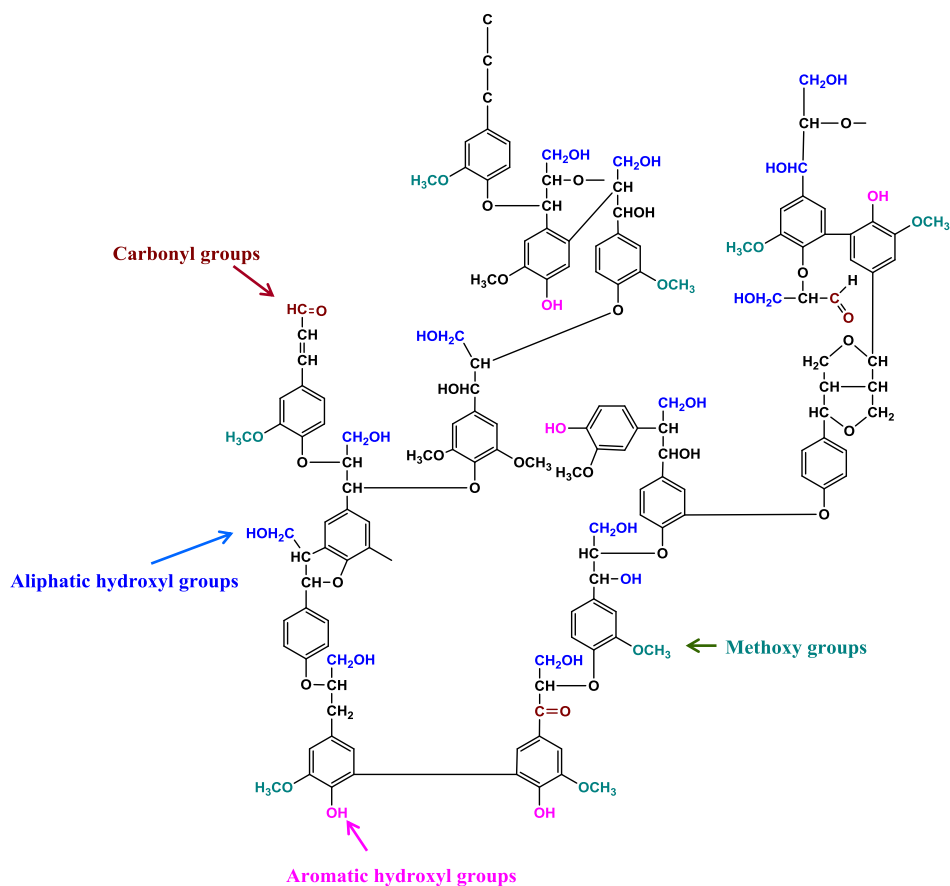
Figure 2.2 Structure of lignin proposed by Alder with main functional groups highlighted.
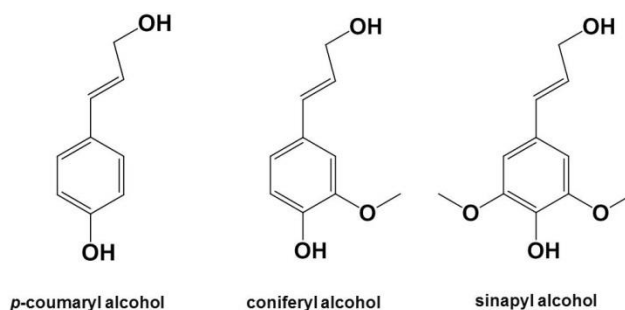
Figure 2.3 Monolignol units as precursors for lignin biosynthesis.

2.1.2 Variety of lignins

Lignocellulosic material such as wood is composed of carbohydrate polymers (cellulose, hemicellulose), and an aromatic polymer (lignin). Typically, lignin is isolated from cellulose in paper industry. Therefore lignins are usually classified according to the isolation method. Two approaches are typically used for the separation of lignins from lignocellulosic materials. First, acidolytic methods are based on the hydrolysis of polysaccharide parts of lignocellulose. Extraction of lignin after ball milling or enzymatic treatments of lignocellulosics gives milled wood lignin (MWL). Nevertheless, for practical approaches of effective utilization of lignins, it is important to pay attention for using commercial lignins such as by-products of pulping processes or biomass production processes since they are considered as waste of the paper industry. The commercial lignins from pulping and biomass process are explained below.

Lignins from solvent pulping.[12, 22, 23] Many lignin preparations have been developed from different organic solvent-based procedures, and these are known as organosolv lignins. Lignin is extracted from biomass with an organic solvent/water mixture at a high temperature/pressure. The most widely used solvents are alcohols, together with other mixtures of solvents and reagents. The lignin is isolated by acidic precipitation after the process. Organosolv lignins are sulfur-free and have a less modified structure than other types of lignins.

Lignins from Kraft pulping.[12, 22, 23] Kraft pulping is the dominant chemical pulping process in the world. It uses strong alkali (e.g. NaOH) and sodium sulfide (Na_2S) in a temperature range of 155–175 °C for several hours to separate lignin (black liquid fractions) from the cellulose fibers (solid fraction). Kraft lignin is obtained then by precipitation of the black liquid, neutralized with an acid (pH value of pH 1–2), and dried to a solid form. Kraft lignin is a hydrophobic material with a lower molecular mass than the original lignin.

Lignins from sulfite pulping.[12, 22, 23] As a source of papermaking grade bleached pulp, the sulfite process, using several salts of sulfurous acid (sulfites or bisulfites) to extract the lignin from wood, has been displaced by the Kraft (alkaline) pulping. However, lignosulfonates obtained from waste sulfite pulping liquors from softwood are the most

important commercial source of lignin today with global production being about 1 million metric tons per year. Lignosulfonates contains sulfonate ($-SO_3^-$) groups bonded to the polymer and are therefore soluble in water at a wide range of pH values. The molecular mass of the lignosulfonate is higher than the Kraft lignin, rendering a structure that is more similar to the original lignin. The common applications of lignosulfonates are binders, dispersants, and emulsifying agents.

Lignins from biomass conversion technologies.[22] Tremendous effort is currently being expanded to find feasible pathways to produce fuel ethanol from the cellulose contained in agricultural residues and waste wood. If a cellulosic ethanol industry is established, large amounts of lignin will be produced as a by-product. The biomass conversion technologies used typically involves in hydrolytic pretreatment which is either catalyzed by mineral acid or autocatalyzed by biomass-derived organic acids. Most schemes propose to use the separated lignin as a fuel to run the ethanol plant. However, a process that converts all of the input biomass to fuel is unlikely to be economically feasible. To improve the economic feasibility, a portion of the lignin needs to be converted to higher-values chemicals or materials.[22]

2.1.3 Biodegradation of lignin by enzymes

In nature, lignin can be degraded by white-rot fungi such as *Phanerochaete chrysosporium*, which produce an extracellular lignin peroxidase enzyme to start the degradation process. Other fungal strains produce manganese peroxidase and laccase enzymes that are also active in breaking down the lignin structure. Table 2.1 summarizes the main cofactors or substrates and the principal effects or the reactions of each enzyme.[24] The broad substrate specificity of laccases and their ability to utilize atmospheric oxygen as electron donor instead of hydrogen peroxide used by peroxidases makes these enzymes a promising candidate for diverse industrial applications. These include the use as a bleaching agent in pulp delignification and as a stabilizer in wine production, the use in detoxification of phenolic compounds in waste water and organic pollutants,[25] in textile decolorization of synthetic dyes (anthraquinone, azo, indigo and triarylmethane), in laccase-based cathode for

biofuel cells[26, 27] and biosensors,[28, 29] in the manufacture of antibiotics and anti-cancer drugs, and for the modification of polymer and fiber surface.[30]

In this thesis, the ability of laccase to degrade lignin was used as an enzymatic trigger to release agrochemicals from lignin nanoparticles. The responsive material is described in chapter 2.2.

Table 2.1 Enzyme involved in the degradation of lignin and their main reaction.

Enzyme Activity	Cofactor or Substrate (Mediator)	Main Effect or Reaction
Lignin peroxidase	H_2O_2, veratryl alcohol	Aromatic ring oxidized to cation radical
Maganese peroxidase	H_2O_2, Mn organic acid, thiol, unsaturated lipids	Mn(II) oxidized to Mn(III); chelated Mn(II) oxidizes phenolic compound to phenolic radicals
Laccase	O_2; mediator,e.g. hydroxylbenzotriazole	Phenol are oxidized to phenol radical; other reactions in the presence of mediators
Gyoxal oxidase	Glyoxal, methyl glycoal	Glyoxal oxidized to glyoxylic acid; H_2O_2 production
Aryl alcohol oxidase	Aromatic alcohol	Aromatic alcohol oxidized to aldehyde; H_2O_2 production
Other H_2O_2 producing enzymes	Many organic compounds	O_2 reduced to H_2O_2

2.1.4 Utilization of lignin

Lignin has been previously considered as a waste material or a low value by-product of pulping with its utilization mainly limited to use as a fuel to fire the pulping boilers. The time changes this view by several factors including the increasingly stringent environmental waste regulations and a limitation of petrochemical based materials. Today, a large number of studies on lignin focus on finding a higher value application.

Theoretical Background

Many approaches have been studied for lignin utilization. For example, lignosulfonates, which contain sulfonate (-SO$_3^-$) groups and are water soluble, currently represent the only lignin type that has been established as a large scale industrial commodity with around 1,000,000 tons/year.[31] It can be used without any further processing; although some specialty applications may need further purification to decrease its molecular weight distribution or the sulfur content. The largest use for lignosulfonates is to mix it with concrete followed by using it as binders in applications such as animal feed pellets or dust control. Kraft lignin has far fewer established uses as a raw material than lignosulfonates. However, since the water-insoluble Kraft lignin is the most common form of industrial lignin, it has been in the focus of many researchers to incorporate it into existing polymeric systems or to create novel materials. Kraft lignin has been explored as an additive or extender in thermoset systems, such as in polyurethane, phenol formaldehyde (PF), and epoxy thermosetting resins.[9] It has inherent properties that can also be useful in thermoplastic materials. Especially, its aromatic structure suggests that it could be used as a free radical scavenger in existing commodity thermoplastics. Recently, the German researchers Pfiter and Nägele from the Fraunhofer Institute of Chemical Technology have developed a new thermoplastic as a bioplastic material which is made by mixing specific types of low-content sulfur lignins with natural fibers from several plants and natural additives, named ARBOFORM®[12] as shown in Figure 2.4. Additional lignin applications are in the field of carbon fibers, activated carbon, and also antioxidants.

Another avenue is to depolymerize lignin to aromatic chemicals. Lignins have been degraded into different low molar mass compounds, such as vanillin, dimethyl sulfoxide, acetic acid, quinines, aldehydes and many other aromatic chemical compounds.[12] Plastics and synthetic fibers could be further synthesized using some of these chemicals. Thermochemical and biochemical processes or the fragmentation of lignin - includes pyrolysis, oxidation, hydrogenation, hydrolysis, gasification and microbial conversion.

Figure 2.4 Promotional tokens made of Arboform® and its product applications.[32]

A third method is used to take advantage of the numerous possible reaction sites on the lignin backbone (e.g. hydroxyl, methoxyl, carbonyl and carboxyl groups) and to engineer the properties of the lignin by chemical modification or to alter its viscosity or solubility properties. Esterification is one of the simple methods to modify hydroxyl groups of lignin. Different esterifying agents including acidic compounds, acid anhydrides, and acid chlorides have been applied for the lignin esterification to improve the solubility of Kraft lignin in nonpolar solvents such as styrene-containing thermoset resins. The final resulting lignin ester can be used in unsaturated polyester thermosets.[33]

A last approach that should be mentioned here is grafting-onto-polymerization on lignin. Recently, numerous researchers have used lignin as a - macromonomer for (co)polymer synthesis.[34-37] Kraft lignin grafted to hydrophilic polymers such as polyacrylamide or poly(acrylic acid), has been prepared using reversible addition−fragmentation chain transfer (RAFT) polymerization and was investigated as surfactant.[38] UV absorbent lignin-based graft copolymers, lignin-*graft*-poly(methyl methacrylate-*co*-butyl acrylate) (lignin-*g*-P(MMA-*co*-BA)), was successfully prepared via atom transfer radical polymerization (ATRP) and were evaluated as sustainable thermoplastic elastomers (TPEs) for applications in UV-blocking coatings.[39]

2.2 Stimuli-responsive materials

Stimuli-responsive materials are smart materials which show noticeable changes in their properties with environmental stimulus variations. They can be classified according to the stimuli they response to such as; physical, chemical, and biological stimuli as demonstrated in Figure 2.5.[40]
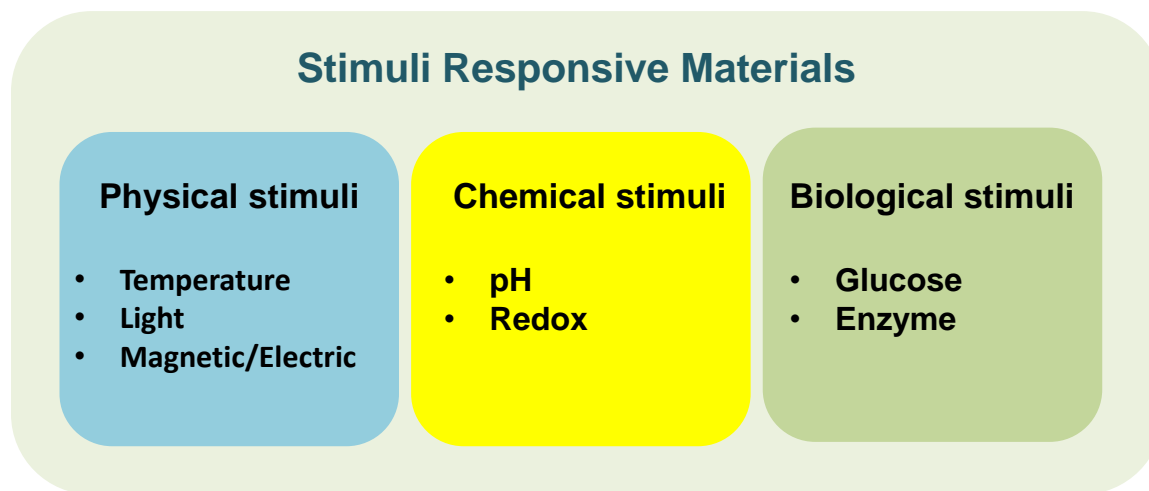
Figure 2.5 Classification of responsive materials.

2.2.1. Physical stimuli

Temperature as a stimulus. Among all available physical stimuli, a change in temperature has played great attention, because this stimulus can easily be applied and monitored from outside. Thermal-responsive materials are typically linked with properties, such as solubility displaying a non-linear relationship with temperature. They present a critical solution temperature at which the solution system undergoes a phase change within a small temperature range. A typical thermo-responsive material exhibits a lower critical temperature (LCST) below which a one phasic solution exists and above which phase separation occurs. The upper critical temperature (UCST) of material in solutions are monophasic above a specific temperature and turn into bi-phasic below that temperature. Poly(*N*-isopropylacrylamide) (PNIPAM) is one of the most investigated LCST polymers in

aqueous solution for biomedical application, due to the fact that its LCST is 32 °C. PNIPAM usually forms a hydrogel, which is polymer network extensively swollen with water. When heated above 32 °C, it undergoes a LCST phase transition from a swollen hydrated state to a shrunken dehydrated state. Therefore PNIPAM is suitable for a drug delivery system under sol-gel transition, induced by temperature change after introduction to body (called *in situ* gelling).[41] In addition besides polyacrylamide hydrogels, other synthetic polymers as polyvinylethers,[42] polyoxazolines,[43, 44] as well as poly(oligoethylene oxide)methacrylate[45, 46] have also been investigated for their responsive activities.

Light as a stimulus. Light as a stimulus can not only be easily realized by exposure of a sample to light at a specific wavelength. Virtually the whole light spectrum, beginning in the UV up to the deep infrared, allows diversity in applications which cannot be offered by other stimuli. Furthermore, light allows a localized stimulation within a defined area or volume. Within light responsive materials, the impact on the corresponding light responsive moiety can be associated with photoinduced isomerization and/or photochromism,[47, 48] which renders light as a versatile stimulus. The most attractive materials for photo-responsive properties are azobenzene (trans–cis isomerization)[49] and spiropyran (spiro- to merocyanine form).[50] In addition the formation of photo-controllable block copolymer micelles has also found broad interest.[51]

Magnetic/Electric signal as a stimulus. Electric and magnetic fields are the most practical stimuli with respect to signal control via magnitude, duration of the pulse and interval between the pulses. Electrical responsive materials are typically conducting polymers which can change their shape via swelling, shrinking, or bending when exposed to an electric field. Commonly materials responding to an electric field are polythiophene[52] and sulfonated-polystyrene.[53] In general, the polymers or materials that respond to changes of the magnetic fields are typically polymer composites of elastomers or gels filled with small magnetic particles such as iron (III) oxide particles, ferromagnetic particles and nickel powder. Polymer matrixes for magnetic responsive materials are mostly based on poly(ε-caprolactone) and poly(ethylene glycol) mono-ethylether methacrylate.[54-56]

2.2.2 Chemical stimuli

pH as a stimulus. A material is considered as pH responsive when it consists of moieties that are capable of donating or accepting protons upon an environmental change in pH.[57-60] A change of the pH value induces a change of conformation of polymer chains in aqueous solution induced by the electrostatic repulsion between generated charges. Polyacids and polybases are typically pH responsive materials. Highly explored pH responsive polymer include chitosan,[61-63] albumin,[64, 65] gelatin,[66, 67] poly(acrylic acid),[68, 69] poly (ethylene imine),[70] and poly(lysine).[71]

Redox as a stimulus. A redox stimulus occurs due to a change of oxidation state of the redox-sensitive groups. Organic compounds such as dithienylethenes,[72] ferrocene[73, 74] or disulfides[75] display aredox sensitivity. In addition, the redox-responsive moiety of paramagnetic organic molecules, such as tetramethylpiperidine-1-oxyl (TEMPO) derivatives can be oxidized or reduced in a reversible fashion by their an unpaired electron.[76, 77]

2.2.3 Biological stimuli

Glucose response. Materials that respond to glucose have received considerable attention because of their potential application in both glucose sensing and insulin delivery. Glucose responsive materials are typically synthesized by conjugating glucose oxidase (GOx) with a pH responsive polymer. When such polymer comes in contact with glucose, GOx oxidizes glucose to gluconic acid which causes a pH value change of the environment. The pH-response generally causes swelling or collapsing of the polymer matrix that contains insulin. For example, a membrane system consisting of a poly(acrylic acid) (PAA)-*graft*-cellulose film was conjugated to GOx for insulin delivery in response to glucose concentration.[78] At neutral pH value in the absence of glucose the carboxylic groups of PAA are negatively charged. Repulsion between negative charges should make the polymer chain extended and closed the pores of the membrane. In the presence of glucose gluconic acid is produced by GOx protonated PAA, making the polymer chains coil-like and opening the pores membrane to enhance insulin permeation. Another similar approach is the formation of glucose-responsive gating membranes based on PAA-grafted poly(vinylidene fluoride).[79]

GOx-based responsive materials were also grafted - to poly(ethylene glycol) (PEG) [80,81] and other nontoxic, nonimmunogenic, biocompatible polymers, such as chitosan.[82] The glucose responsive materials based on boronic acid–diol complexation were also widely investigated for insulin delivery system.[83]

Enzyme response. -Enzyme-responsive materials provide additional advantages over responsive materials using pH or temperature as stimuli. Enzyme-responsive materials are typically composed of an enzyme-sensitive substrate and another component that directs or controls interactions that lead to macroscopic transitions. Catalytic action of the enzyme on the substrate can lead to changes in supramolecular architectures, swelling/collapse, or the surface transformation of the substrate. Sensitivity of the enzyme stimulus- is unique because enzymes are highly selective in their reactivity, are operable under mild conditions present *in vivo*, and are vital components in many biological pathways. Because a variety of enzymes is already present in the body, the stimulus does not need to be added externally but can be supplied by the biological environment itself, provided that the naturally present enzyme matches the triggering enzyme of the responsive material. Therefore enzyme responsive materials are important for drug development. For instance, peptide-based nanocapsules and nanoparticles have been developed for the delivery of bioactive molecules due to its cleavability by protease.[84, 85] The utilization of enzyme responsive materials is not only interesting in drug delivery systems but also in smart antibacterial devices.[86] A principal idea of smart antibacterial devices is based on the release of an antibacterial agent by the presence of the bacteria themselves. This thesis presents lignin as an enzyme responsive material for applications in agrochemical delivery and is considered as smart trigger release system in chapter 3.1.3.

2.3 Miniemulsion and miniemulsion polymerization

2.3.1 Definition of different kinds of emulsions

Oil-in water dispersions (two-phase systems) can be classified into macroemulsions, miniemulsions, or microemulsions. A major distinction between these three categories is the stability of the emulsion. In this context, the "stability" usually refers to the time elapsed prior to degradation of the emulsion as indicated by the formation of droplets much larger than in the original emulsion, typically noted by the macroscopic separation of the oil phase in creaming experiments.[87, 88]

Figure 2.6 illustrates in a generalized fashion with the droplet size, appearance, and the emulsion stability for the three types of emulsions. Macroemulsions are the coarser of the three in that the droplet size is relatively large (1-100 µm) and the stability is limited since they are meta-stable (kinetically stable) and thermodynamically unstable. Surfactants are required to reduce the interfacial tension between two phases and increase the stability for a certain time. The droplet size is dependent on the system components (oil, stabilizer, phase ratio) mixing characteristics (impeller type and speed). Microemulsions, on the other hand, are thermodynamically stable (i.e. indefinitely stable) with droplet sizes varying from 10 to 100 nm. Relatively large quantities of mixed emulsifiers, typically consisting of an ionic surfactant (e.g. sodium dodecyl sulfate, SDS) and a short chain alcohol (e.g. pentanol), are usually used to prepare these emulsions.

Miniemulsions are considered as an intermediate between macroemulsions and microemulsions in term of droplet size and emulsion stability. Droplets generally range in size from 50 to 500 nm with narrow size distribution and the miniemulsion can be stable for some days or even months. The droplets are usually created by high shear forces (ultrasound, high pressure homogenization, etc.) on a conventional emulsion formulated from two immiscible liquids.
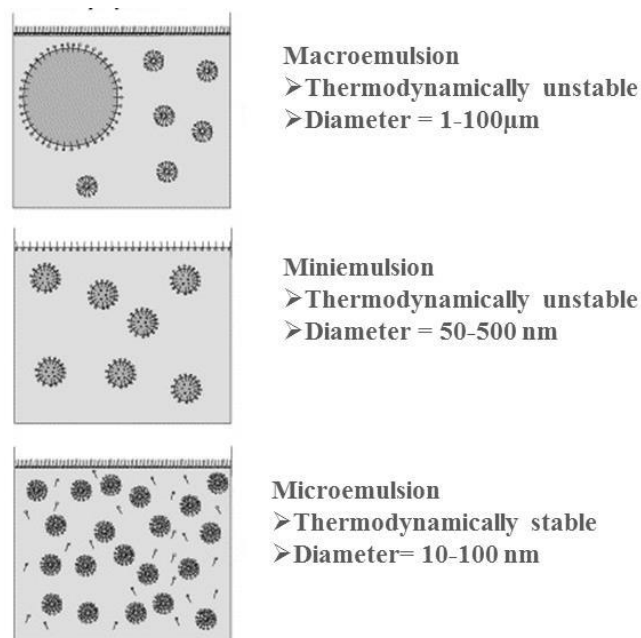
Figure 2.6 Classification of emulsion. (This figure was modified and reprinted from Prog. Polym. Sci., 27(4), Antonietti M., Landfester K., Polyreactions in miniemulsions, 689-757, Copyright (2002) with permission from Elsevier)

2.3.2 Stability of miniemulsion

The two possible mechanisms for the growth of droplets in emulsions are illustrated in Figures 2.7. If the small droplets are not stabilized against Ostwald ripening they will disappear by diffusion of molecules from the small droplets to larger droplets.[89] The Ostwald ripening is driven by the difference of Laplace pressures ($P_{Laplace}$) or the droplet's pressure between the smaller and bigger droplets. To create a stable miniemulsion of small droplets, the droplets must be stabilized against Ostwald ripening by diffusion processes and against coalescence by collisions. Stabilization against coalescence is obtained by adding an appropriate surfactant. Cationic, anionic, and nonionic surfactants can be used for the formulation of a miniemulsion. In case of Ostwald ripening, diffusional stabilization is achieved by adding a small quantity of a costabilizer or an osmotic pressure agent. In general, the costabilizer, often called "(ultra)hydrophobe" (direct or oil-in-water miniemulsion) or "lipophobe" (inverse or water-in-oil miniemulsion), has to be a compound with an extremely low solubility in the continuous phase. For direct miniemulsions, a monomer-soluble or water insoluble agent such as hexadecane can be used (solubility in

distilled water: 9×10^{-6} mg·l^{-1} at 25 °C).[90] The costabilizer creates an osmotic pressure inside the droplets, counteracting the Laplace pressure that is responsible for diffusional degradation (Ostwald ripening).[91]
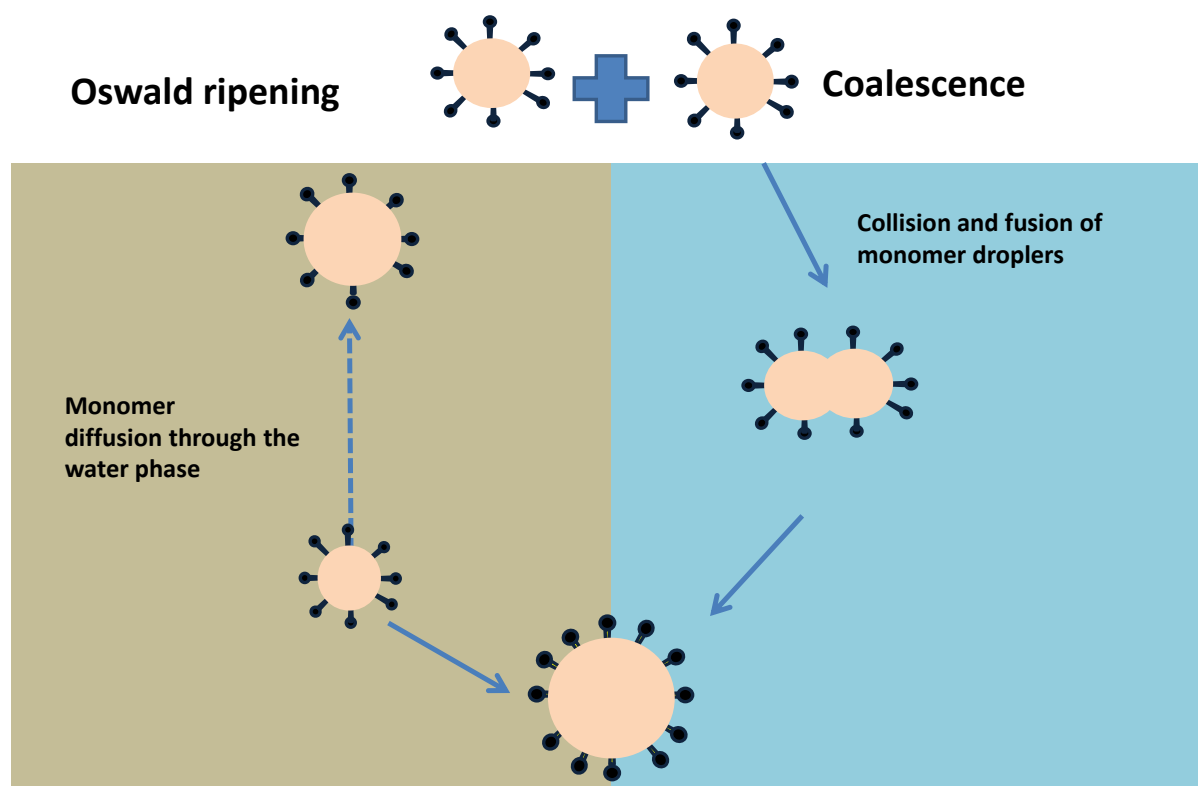
Figure 2.7 Two possible mechanisms for the growth of emulsion droplets.[92] (This figure was modified from lecture material of the "Principles of miniemulsion" course from Prof. Dr. Katharina Landfester).

2.3.3 Principle of the miniemulsion polymerization

Miniemulsion and classical emulsion polymerizations proceed with different mechanisms. This is primarily attributed to the different initial conditions before the start of the polymerization that have a profound influence on the subsequent particle nucleation and growth mechanisms. In the conventional emulsion polymerization, the most widely accepted particle nucleation mechanisms include micellar nucleation and homogeneous nucleation. Emulsified monomer droplets (> 10 μm in diameter) generally do not contribute to particle nucleation to any appreciable extent due to their small droplet surface area compared to the much smaller micelles.

The idea of miniemulsion polymerization is to initiate the polymerization in each of the small, stabilized droplets, meaning that polymerization takes place in small nanodroplets. Each droplet can be called "nanoreactor" since it acts as an independent nanoreactor without being seriously disturbed by all the other events. This concept is not limited to polymerizations (both chain growth and step growth) but can be used for many reactions such as sol-gel processes,[93] and olefin cross metathesis.[94] Figure 2.8 shows a scheme of the miniemulsion process: in the first step of the miniemulsion process, small stable droplets ranging in size of 50-500 nm are formed by shearing a system containing the dispersed phase, the continuous phase, a surfactant, and an osmotic pressure agent. The system is called "direct" miniemulsion, if the dispersed phase is hydrophobic and an "inverse" miniemulsion, if the dispersed phase is hydrophilic. In a second step, these droplets can undergo a reaction without changing their identity.

In miniemulsions, for the achievement of the formation and stabilization of the nanodroplets, several parameters such as high-shear input, choices of surfactants and stabilizers have to be considered. To generate small nanodroplets high-energy input to overcome the interfacial energy of the two phases is required. The required free energy with respect of the thermodynamic follows the equation:

$$\Delta G = \gamma \Delta A \qquad \text{Equation 2.1}$$

Where ΔG = free Gibbs energy difference,

γ = surface/interfacial tension between two phase; $J \cdot m^{-2}$ or $N \cdot m^{-1}$,

ΔA = the newly formed interface area
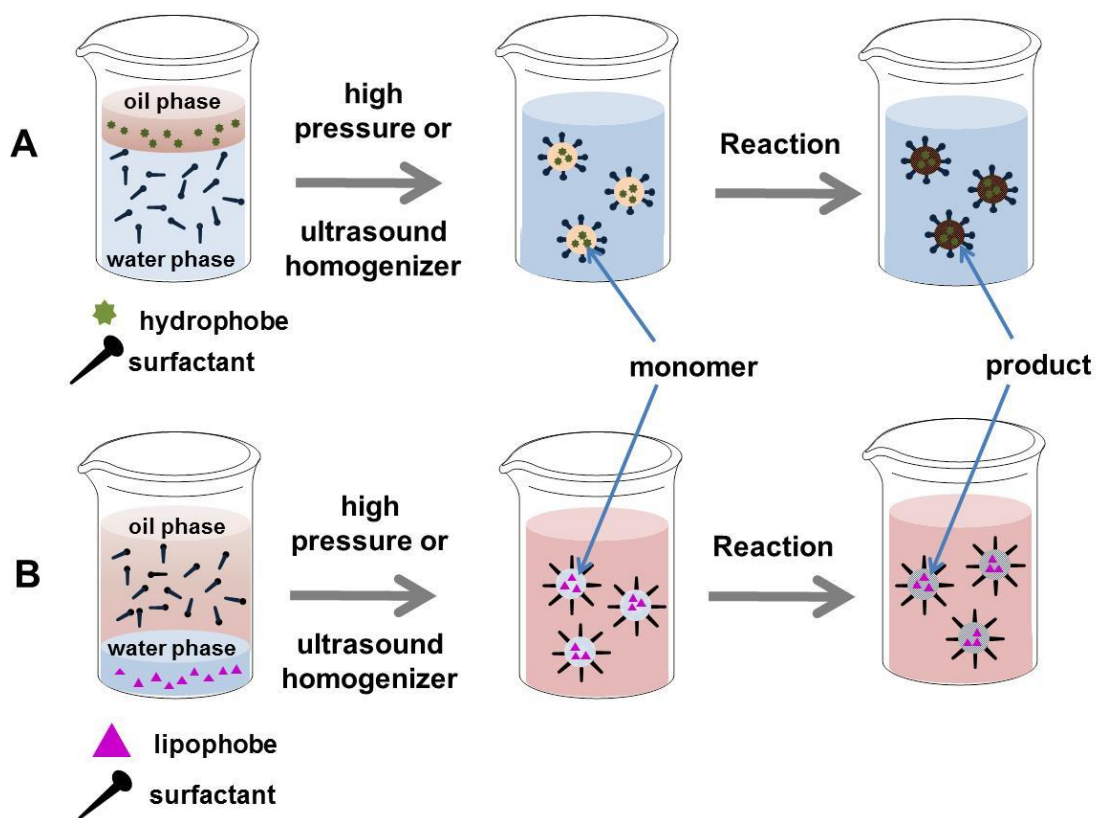
Figure 2.8 Principle of the miniemulsion polymerization, (A) direct miniemulsion, (B) inverse miniemulsion. After being subjected to high shear, the two immiscible phases result in narrowly distributed nanodroplets (containing the osmotic pressure agent; hydrophobe for direct miniemulsion and lipophobe for inverse miniemulsion). Ideally, no change of the droplets is observed during the consecutive reaction process.

As high shear device ultrasonication is used especially for the homogenization of small quantities, whereas microfluidizers or high-pressure homogenizers are favorable for the emulsification of larger quantities. The presence of surfactants in miniemulsions decreases the interfacial tension between the continuous and disperse phase and therefore helps the emulsification process. The concentration of the surfactant in the continuous phase in the final miniemulsion is chosen below the critical micelle concentration (CMC) and the surfactant can be added after homogenization for poststabilization to prevent fusion by collision, via steric or electrostatic repulsive forces.

The destabilization of nanodroplets by Ostwald ripening after the homogenization process can efficiently be minimized by a small quantity of an osmotic pressure agent to the

dispersed phase. The osmotic pressure agent can counteract the Laplace pressure by suppressing the diffusion of monomer molecules from smaller droplets to larger ones. The Laplace pressure inside the original miniemulsion droplet is given by the interfacial tension of the interface between two liquid phases:

$$P_{(Laplace)} = \frac{2\gamma_{LL}}{R}$$
Equation 2.2

Where γ_{LL} = the surface tension between the two liquid phases ($J \cdot m^{-2}$ or $N \cdot m^{-1}$)

R   = the radius of the droplets (m)

This Laplace pressure is counterbalanced by an osmotic pressure from an osmotic agent inside the droplets which is given by;

$$\Pi_{osm} = \frac{RTC}{M}$$
Equation 2.3

Where R = the ideal gas constant ($8.314\ J \cdot K^{-1} \cdot mol^{-1}$)

T = the temperature (K)

C = concentration of osmotic agent ($mol \cdot l^{-1}$)

M = molecular weight of osmotic agent ($g \cdot mol^{-1}$)

In direct miniemulsions, the osmotic pressure does not necessarily fully compensate the Laplace pressure; however, the droplets are stable, due to different stabilization mechanisms: miniemulsions are not thermodynamically stable, but are in a critically stabilized steady-state. Importantly, since the growth of the nanodroplets takes place on a much greater time scale compared to the polymerization time, thus miniemulsion can provide a situation very close to a one-to-one copy of the monomer droplets to the polymer particles as mentioned above, i.e. each nanodroplet acts as nanoreactor. This advantage allows that not only free radical polymerization can be carried out in miniemulsion but also other reactions like polycondensation for polyester nanoparticles,[95] polyaddition for polyepoxide[96] or polyurethane particles,[97, 98] or anionic polymerization in non-aqueous miniemulsions for

polyamide nanoparticles[99] and in aqueous phase for polybutylcyanoacrylate (PBCA) nanoparticles.[100] Recently, hollow nanocapsules with an aqueous core via olefin cross metathesis of acrylated dextran[94] have been prepared. Moreover, the miniemulsion is excellently suited for the encapsulation of a variety of different materials, ranging from hydrophobic to hydrophilic, from solid to liquid, and from inorganic to organic substances. These encapsulated substances can be released or not as desired.[101]

2.3.4 Encapsulation in particulate structures

Encapsulation is defined as a process to entrap substances within a carrier material and to protect it by a physical barrier from the environment. The main purpose of the encapsulation in a colloid is to stabilize active ingredients and/ or controlling their release . Different encapsulation technologies hold significant potential for a variety of applications and are well developed within the biomedical,[102] cosmetic,[103] food,[104] and printing industries.[105] Considering the nano-encapsulation, miniemulsion is one of the most promising methods. There are two main types of encapsulations: 1) matrix type and 2) core-shell type (Figure 2.9).
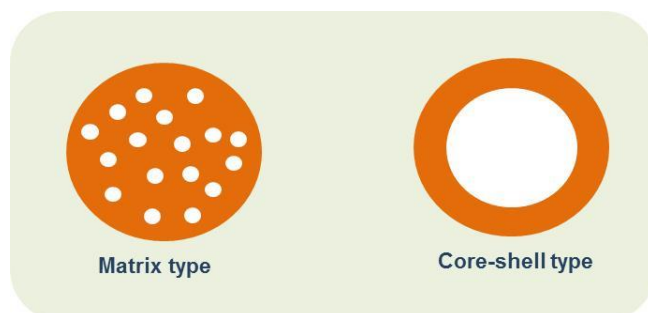
Figure 2.9 Two main types of encapsulation strategies: matrix and core-shell type.

2.3.4.1 Encapsulation of active ingredients soluble in the dispersed phase

To encapsulate compounds that are soluble in the dispersed phase, the conventional miniemulsion process is suitable. The compound has to be dissolved in the dispersed phase

before the homogenization step and still after the subsequent polymerization; the component is entrapped in the polymer nanoparticle. The final morphology of the polymer particle depends on the solubility of the active compound in the final polymer. A solid particle is formed, when the compound is homogeneously distributed in the polymer matrix. If the active compounds become insoluble in the final polymer, phase separation takes place which can lead to a core-shell structure by the distribution of smaller and larger domains in all over the matrix. The formation of capsules via miniemulsion will be described in the next chapter of capsule formation.

Many examples can be found for the encapsulation of active agent, soluble in the dispersed phase by several reactions during the miniemulsion process. Fluorescent dyes are one of the most used compounds in biomedical applications for labeling and monitoring purposes. Both hydrophobic and hydrophilic dyes can be encapsulated in polymer nanoparticles by the miniemulsion method. The hydrophobic fluorescent dye *N*-(2,6-diisopropylphenyl) perylene-3,4-dicarbonacidimide (PMI) was successfully incorporated into poly(methylmethacrylate) (PMMA), polystyrene (PS),[106] polyisoprene (PI), and PS-*co*-PI,[107] nanoparticles that were obtained by radical polymerization. Hydrophilic dyes with different molecular structures, namely reactive brilliant red K- 2BP (C.I. Reactive red 24), acid Fuchsin (C.I. Acid violet 19), and cationic brilliant red 5GN (RBR, AF, and CBR, have been successfully encapsulated into PS particles using the miniemulsion-in-miniemulsion or also called double miniemulsion method.[108] In this method, water droplets containing hydrophilic dyes were suspended in octane/styrene and miniemulsified in the presence of lipophilic emulsifiers to form a primary miniemulsion. After that, the primary emulsion was further dispersed in water and miniemulsified, followed by polymerization at elevated temperature. The encapsulation of the fluorescent dye sulforhodamine 101 (SR 101) was used to investigate the permeability of the poly(urethane/urea) shell which is formed via polyaddition at the interface in inverse miniemulsion.[109] Also hydrophobic metal complexes can be embedded in the matrix of polymer particles like platinum(II)acetylacetonate, indium(III)acetylacetonate, zinc(II)tetramethylheptadionate, zincphthalocyanine, and chromium(III)benzoylacetonate, respectively, with different loading capacities.[110] The volatile fragrance 1,2-dimethyl-1-phenyl-butyramide (DMPBA) was encapsulated in PMMA,

PS and copolymer nanocapsules for a long-time delivery of the fragrance at different temperatures.[111]

2.3.4.2 Encapsulation of active ingredients insoluble or solids material in the dispersed phase

Materials which are insoluble in the dispersed phase such as inorganic crystallites (e.g. titania, iron oxide, or amorphous nanostructures (e.g., silica), organic pigments such as carbon black, or insoluble dyes) have also been encapsulated by miniemulsion. In general, inorganic structures are not compatible with nonpolar organic liquids as monomers due to their hydrophilic character. Thus a surface modification for the compatibility by hydrophobization is needed and then the modified component can be dispersed in the monomer phase. In case of pigments or carbon-based materials - as they tend to aggregate due to their high specific surface area - it is difficult to disperse them in the monomer phase. To prevent aggregation, in the first step of the process, instead of directly dispersing the pigment or carbon-based material in the monomer, a dispersion of the pigment in water is generated using a non-ionic or ionic surfactant. This dispersion is then mixed with a miniemulsion, composed of the desired monomer in water and stabilized with the appropriate surfactant by ultrasonication. Subsequently, polymerization was carried out. This strategy was developed for carbon black[112] and then later used for the encapsulation of other organic pigments.[113] The encapsulation of magnetic particles like magnetite (Fe_3O_4) or magnemite (γ-Fe_2O_3) is interesting for biomedical applications. Even through the magnetic nanoparticles surface is hydrophilic, the coating with hydrophilic polymer in inverse miniemulsion is still essential.[114, 115] The most successfully incorporation of a high amount of magnetite into a hydrophobic polymer matrix applies oleic acid for hydrophobization of the magnetite surface. It is usually a three step process in direct miniemulsion. Magnetite nanoparticles are firstly precipitated from a ferrous/ferric chloride solution and then modified with oleic acid. In the second step, after the surface hydrophobization, magnetic nanoparticles are dispersed in octane and this dispersion is miniemulsified by ultrasound in water by using SDS as a surfactant. From the miniemulsion, octane is evaporated and then a stable dispersion of SDS-stabilized magnetite is obtained. The magnetite dispersion and a styrene miniemulsion can

then be mixed in the last step by co-sonication and magnetic polystyrene nanoparticles are obtained after radical polymerization.[116, 117]

2.3.5 Formation of nanocapsules via miniemulsion

Capsules are generally particles with a liquid (aqueous or organic) or a hollow core surrounded by a polymeric shell. Several techniques can be used to prepare capsules, such as the double emulsion technique, the layer-by-layer approach (with or without the use of sacrificial templates)[118, 119] and the miniemulsion process.[120, 121] The synthesis of capsules via miniemulsion polymerization has the advantage, in relation to the other methods, that it is possible to obtain capsules with sizes down to 100 nm in one single reaction step. For the formation of polymeric nanocapsules via miniemulsion, three general approaches which are presented in Figures 2.10 can be used: 1) phase separation by polymerization or solvent evaporation, 2) interfacial reaction, and 3) nanoprecipitation.
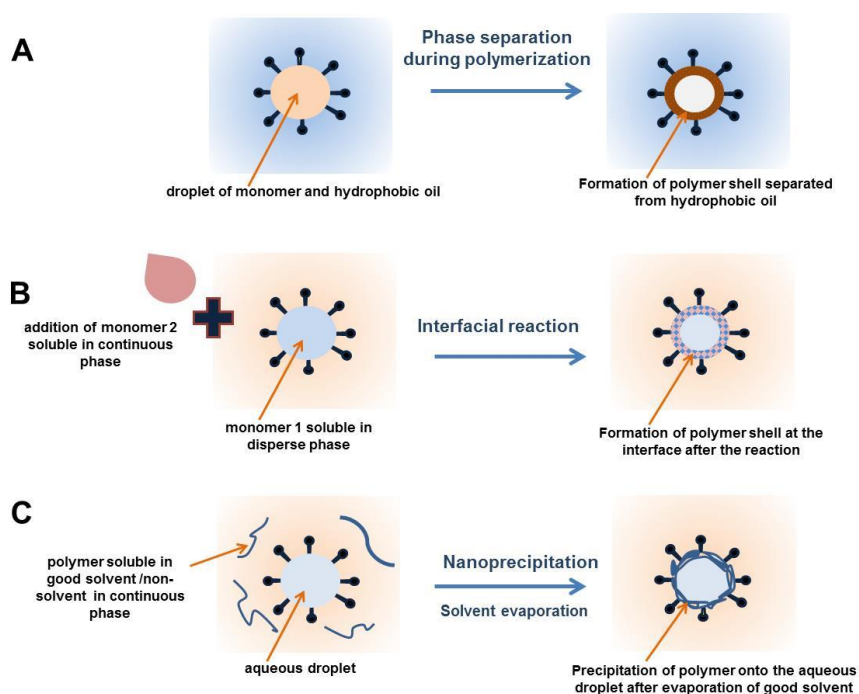
Figure 2.10 Three possibilities for the formation of polymeric nanocapsules via miniemulsion process; phase separation (A), interfacial reaction (B), and nanopricipitation (C).

Theoretical Background

The work of Torza and Mason[122] can predict the morphology of the equilibrium morphology based on thermodynamic considerations without the influence of kinetic factors. They studied two immiscible hydrophobic liquid drops, designated as phase 1 (oil$_1$) and 3 (oil$_2$), suspended in a third immiscible hydrophilic liquid, phase 2 (water). The resulting equilibrium morphology is predicted based on combination of the spreading coefficients from the tertiary system (i $\neq$ j $\neq$ k $=$ 1,2,3) which can be calculated from the interfacial tensions γ_{ij}. The spreading coefficients (S_i) are defined as:

$$S_i = \gamma_{jk} - (\gamma_{ij} + \gamma_{ik})$$

<div align="right">Equation 2.4</div>

Where γ is the interfacial tension (i, j, and k refer to the three phases).

Assuming that $\gamma_{12} > \gamma_{23}$ so that $S_1 < 0$, three different morphologies can be predicted (Figure 2.11). Complete engulfing (core/shell) occurs if $S_3 > 0$ and $S_2 < 0$. On the other hand, partial engulfing (acorn shape) will be preferred when $S_2 < 0$ and $S_3 < 0$.
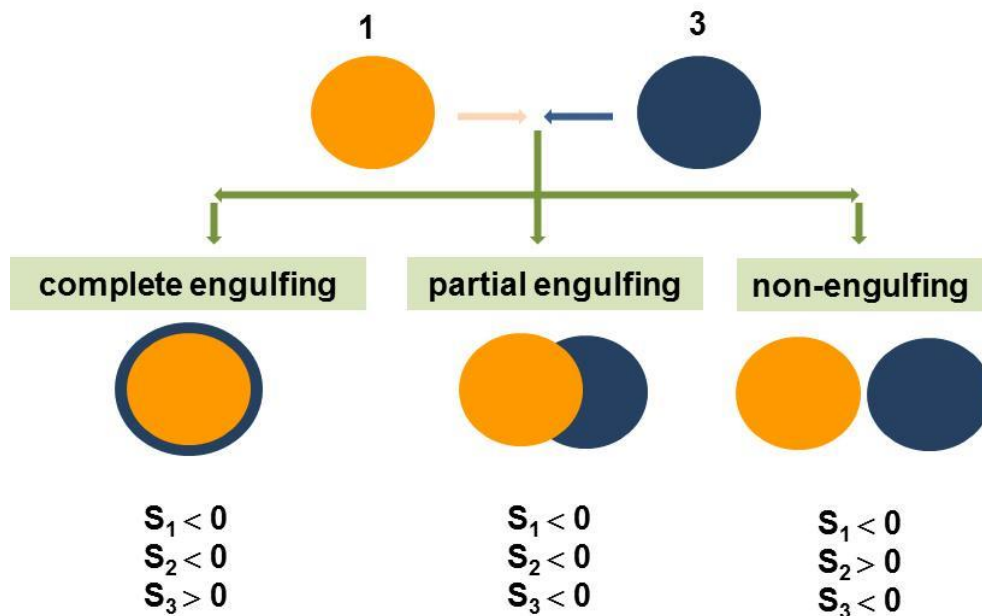
Figure 2.11 Equilibrium morphologies in a three-phase system. Phase 1, orange; phase 3, blue; phase 2 is the continuous phase.

This model provides a general idea of the resulting morphology of three immiscible liquid systems, but it is not always successfully applied for emulsion polymerizations, as surfactants, initiator etc. in the system may result in the deviation of a thermodynamic equilibrium.[123]

3. Results and Discussions

Results and Discussions

Outline

The first chapter (3.1) describes the use of lignin for the preparation of nanocarriers for the controlled release of both hydrophilic and hydrophobic cargo molecules. The synthesis and characterization of lignin capsules for hydrophilic substances prepared by the interfacial polyaddition in inverse miniemulsion process is described first. The encapsulation of the fluorescent hydrophilic dye sulforhodamine 101 (SR101) in lignin capsules is discussed exemplarily for an assessment of the enzymatic degradation of the lignin nanocapsules by laccase as a model enzyme and also by a mixed enzyme cocktail extracted from natural fungi (*chapter 3.1.1*). Next, the preparation of lignin nanocarriers suitable for delivery of hydrophobic substances is described (*chapter 3.1.2*); lignin was modified by the esterification with acrylic acid to increase the solubility of lignin in organic solvents and to allow crosslinking of the organic solution afterwards (*chapter 3.1.2.1*); then a combination of the miniemulsion and solvent evaporation process was performed to produce lignin nano- and microparticles with different morphologies (*chapter 3.1.2.2*). For these lignin particles, release studies have been performed by using 2-propylpyridine as a model active agent (*chapter 3.1.2.3*). Finally, the encapsulation of the antifungi drug (pyraclostrobin) for the treatment of the "Esca disease" of grapevine plants was established and its antifungal properties were examined both *in vitro* and *in planta* (*chapter 3.1.3*). In addition, chapter 3.1.4 presents the preparation of porous carbon with high surface area from lignin particles obtained by the miniemulsion process and subsequent carbonization. These structures can be used as bio-based adsorbents.

Chapter 3.2 summarizes a study of the uptake of polymer particles in young mung bean plants. First, magnetic polystyrene nanoparticles and fungicide-(pyraclostrobin) loaded lignin particles were incubated with mung bean seeds to investigate the uptake of the particles into the seeds and several parts of the mung bean plant after the germination and growth. The amount of iron and pyraclostrobin in several parts of plant was monitored by inductively coupled plasma (ICP) and high-performance liquid chromatography (HPLC) measurements, respectively (*chapter 3.2.1*). Next, the stability of the drug in the plant is investigated by monitored the content of pyraclostrobin after the injection of the encapsulated pyraclostrobin lignin particles into the plant (*chapter 3.2.2*).

Chapter 3.3 presents the kinetic investigations of the formation of glutathione-responsive nanocarriers via two competing "click" reactions at the interface in miniemulsion (thiol-maleimide addition and thiol-disulfide exchange). The two reactions were investigated by nuclear magnetic resonance (NMR) spectroscopy in solution and at the oil/water interface in a miniemulsion. Bucillamine with two thiol groups was selected as a model drug and monomer for the kinetic study. It can both react with 1,4-bis-(3-(2-pyridyldithio)propionamido) butane (BPB) or 1, 1′-(methylenedi-4,1-phenylene) bismaleimide.

3.1 Biodegradable lignin nanocontainers

This chapter covers the development of lignin as a carrier for controlled release of essential ingredients both hydrophilic and hydrophobic substances. As lignin is biodegradable and nontoxic, this platform can be widely applied as nanocontainers for the encapsulation of bioactive drugs, for example, to generate advanced agricultural applications or to encapsulate fertilizers or pesticides which was only studied on the macroscopic scale (i.e. blending) to date.[124-126] Different type of commercial lignin are applied to prepare lignin nanocapsules. Firstly, the encapsulation of a hydrophilic dye as a model of hydrophilic cargos and release upon an application of laccase enzyme from mushroom extraction are demonstrated. Furthermore, the modification of lignin is introduced by esterification for enhancing hydrophobic of lignin to prepare lignin nanocontainer for encapsulation of hydrophobic substances in direct miniemulsion process. Release of hydrophobic dye from lignin nanocontainer by laccase enzyme trigger and release profiles of its different morphologies are investigated. Moreover it is show that their use as fungicide carrier for Esca disease both in *vitro* and in *planta* and their application for carbon material as adsorbent are proven.

3.1.1 Lignin nanocapsules for hydrophilic substances

In this present chapter, the synthesis of a novel lignin nanocapsules carrier system for hydrophilic compounds and trigger release of encapsulated compounds upon the application of enzyme are described. In order to achieve an enzyme responsive lignin nanocapsules, crosslinking lignin shell were fabricated via a miniemulsion route. The process allows the facile encapsulation of hydrophilic compounds, as demonstrated for a model dye. Release of the encapsulated dye was achieved upon application of laccase from mushroom extraction. This chapter contains content of previously published paper. [127]
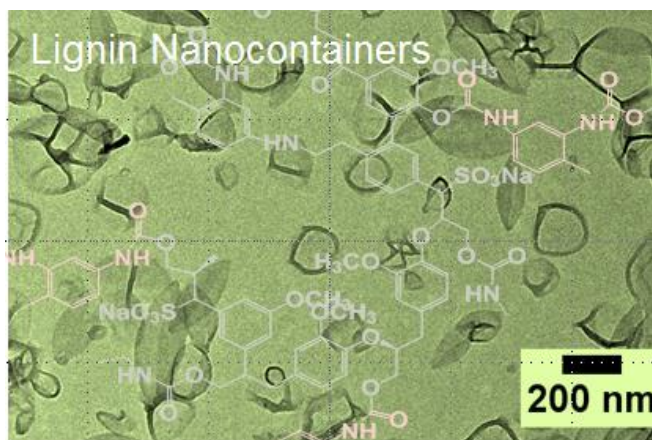
(Yiamsawas et al; RSC Adv. 2014, 4(23), 11661-11663, http://pubs.rsc.org/en/Content/ArticleLanding/2014/RA/c3ra47971d#!divAbstract - Reproduced by permission of The Royal Society of Chemistry)

3.1.1.1 Synthesis and characterization lignin capsules for hydrophilic substance

The main structural elements of lignin, a phenolic polymer, are the three basic structural elements (4-hydroxyphenyl, guaiacyl, and syringyl residues) which are connected via aromatic and aliphatic ether bonds that build up a hyperbranched, i.e. irregularly branched polymer. Because lignin has both phenolic and aliphatic hydroxyl groups, its further modification is obvious and was investigated in various works.[128, 129] In this work, the hydroxyl group has been also used as a functional group for the reaction.

A water-soluble lignin fraction was used to generate lignin-polyurea/polyurethane nanocapsules at the interface of stable water nanodroplets in an inverse miniemulsion. In an inverse miniemulsion the crosslinking polymerization of lignin was tailored to take place only at the interface of stable aqueous nanodroplets (acting as capsule templates) dispersed in an organic solvent. The reaction of toluene diisocyanate (TDI) with the lignin hydroxyl groups was used to generate a cross-linked shell surrounding a liquid aqueous core (Figure 3.1). With this protocol, potentially biodegradable nanocontainers with an aqueous core are obtained allowing the efficient encapsulation of hydrophilic substances as reported for other systems previously.[130, 131]
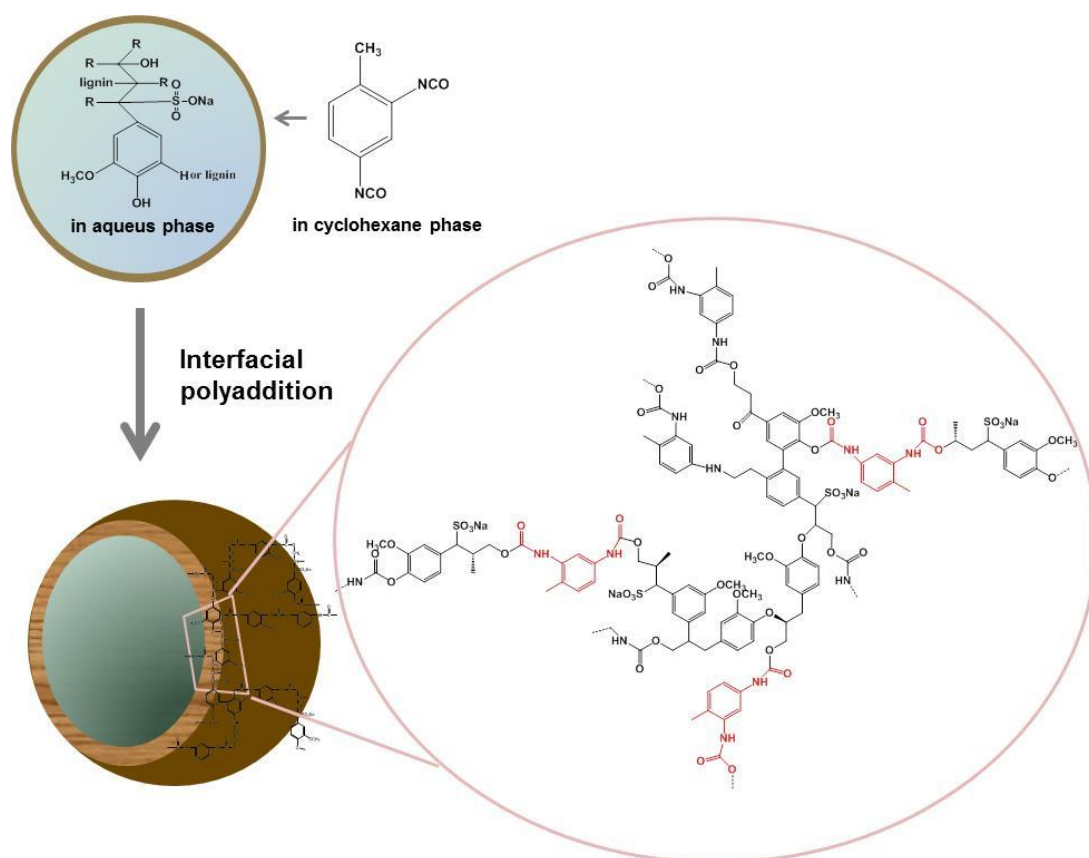
Figure 3.1 Synthetic protocol for the generation of lignin-polyurea/polyurethane nanocapsules at the interface in inverse miniemulsion. (Yiamsawas et al; RSC Adv. 2014, 4 (23), 11661-11663, http://pubs.rsc.org/en/Content/ArticleLanding/2014/RA/c3ra47971d#!divAbstract - Reproduced by permission of The Royal Society of Chemistry)

Lignosulfonic acid sodium salt or lignin was dissolved together with sodium chloride in Milli-Q water in order to generate the dispersed phase which was then mixed with cyclohexane containing the biocompatible surfactant polyglycerol polyricinoleate (PGPR). The pre-emulsion was stirred at room temperature and subsequently ultrasonicated in order to generate the stable miniemulsion. The polyaddition reaction at the interface of the miniemulsion nanodroplets was initiated after a solution of TDI in cyclohexane was added drop-wise to the previously formed miniemulsion. The reaction was kept at room temperature overnight in order to ensure complete consumption of the active species. The obtained lignin nanocapsule dispersion in cyclohexane was stable over a period of several months. The diameters of the capsules and the morphology were determined via dynamic light scattering (DLS), scanning and transmission electron microscopy (SEM and TEM),

respectively. The nanocapsules were then transferred into aqueous dispersion without the use of an additional surfactant due to the presence of sulfonic acid groups of the starting lignosulfonic acid producing (after dialysis) a surfactant free aqueous dispersion of the lignin nanocapsules. For lignin alkali (which does not carry additional ionic side groups) the same synthetic protocol was applied; however in this case a surfactant (SDS) had to be added to allow redispersion of the nanocapsules in water. The overall process for the preparation of lignin nanocapsules is shown in Figure 3.2.
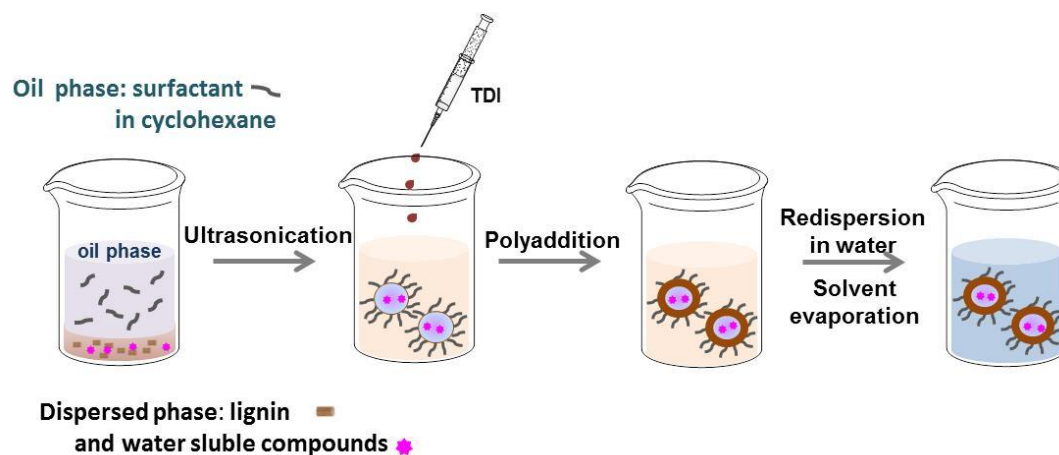
Figure 3.2 Miniemulsion and solvent-evaporation protocol used for the production of lignin nanocapsules followed by redispersion in water.

Since the isocyanate groups of TDI at the water/oil interface not only react with the hydroxyl group in the lignin molecules but can also be hydrolyzed by water to amine groups, urea linkages can be found in the capsule shell, and consequently poly(urea-urethane) cross-linked lignin nanocapsules are generated (Figure 3.1). From the Fourier transform infrared spectroscopy (FT-IR) spectra the presence of the urethane carbonyl bond at 1715 cm^{-1} and the urea carbonyl vibration at 1639 cm^{-1} were confirmed as presented in Figure 3.3. Moreover with increasing the amount of TDI in the reaction, the intensity of these vibrations increases indicating a higher degree of crosslinking within the nanocapsule shell. Further, from the FT-IR spectra, the ratio between urethane and urea bonds can be estimated by the peak area of the characteristic band of urethane/urea which decreased from 0.9 to 0.6 with increasing amount of TDI. This can be rationalized by a pronounced reaction of the isocyanate groups with water in the presence of a large excess of TDI resulting in urea

formation.[132, 133] All prepared nanocapsules are highly functional: in cyclohexane dispersion the presence of isocyanate groups on the capsule surface can also be detected (at 2272 cm^{-1}) which could be used to further functionalize the capsules from the outside. These reactive groups are hydrolyzed to amine groups when the nanocapsules are dispersed in water which could be also addressed in further reactions.
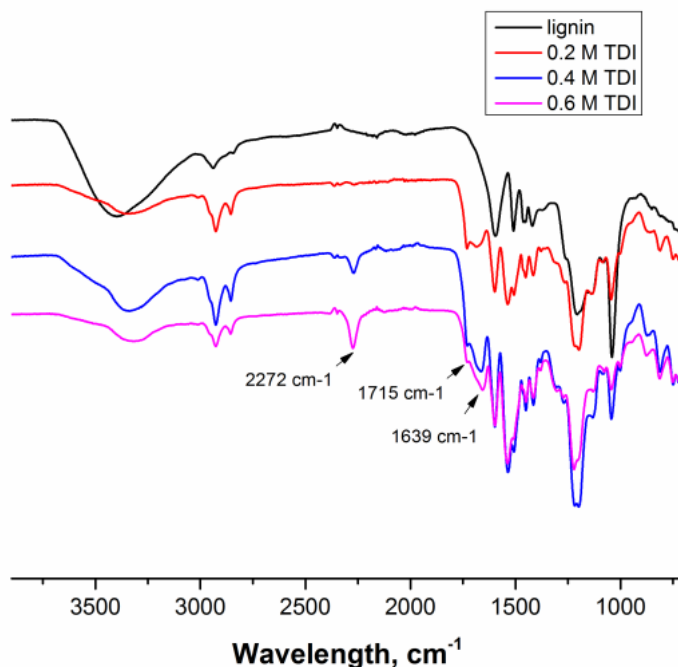
Figure 3.3 FT-IR spectra of lignin (top) and several lignin nanocapsules with varying amount of cross-linker from cyclohexane dispersion. (Yiamsawas et al; RSC Adv. 2014, 4(23), 11661-11663, http://pubs.rsc.org/en/Content/ArticleLanding/2014/RA/c3ra47971d#!divAbstract - Reproduced by permission of The Royal Society of Chemistry)

The cross-linked lignin nanocapsules exhibit diameters in the range of 162 to 220 nm and 311 to 390 in cyclohexane or water, respectively, as determined by DLS with varying amount of the cross-linker TDI (Table 3.1). The nanocapsules remained stable after being redispersed in water over a period of several weeks. Nevertheless the diameter of the nanocapsules in buffer solution is slightly larger than in cyclohexane probably due to swelling and some aggregation. To further confirm the morphology of the lignin nanocapsules, scanning and transmission electron microscopy techniques were performed as shown in Figure 3.4 for the cyclohexane dispersions. In all cases hollow capsule structures

were identified and their diameters correspond well to the result from dynamic light scattering. From the TEM images an average capsule wall thickness for all samples of 10-20 nm can be estimated (Figure 3.5).

Table 3.1 Size characterization of lignin nanocapsules.

#	lignin, mmol	TDI, mmol (mg)	diameter,[1] nm	diameter,[2] nm
1	0.002	0.28(50)	162±66	311±93
2	0.002	0.56(100)	185±87	333±72
3	0.002	0.84(150)	220±81	390±90

1: diameter determined by dynamic light scattering in cyclohexane
2: diameter determined by dynamic light scattering in water
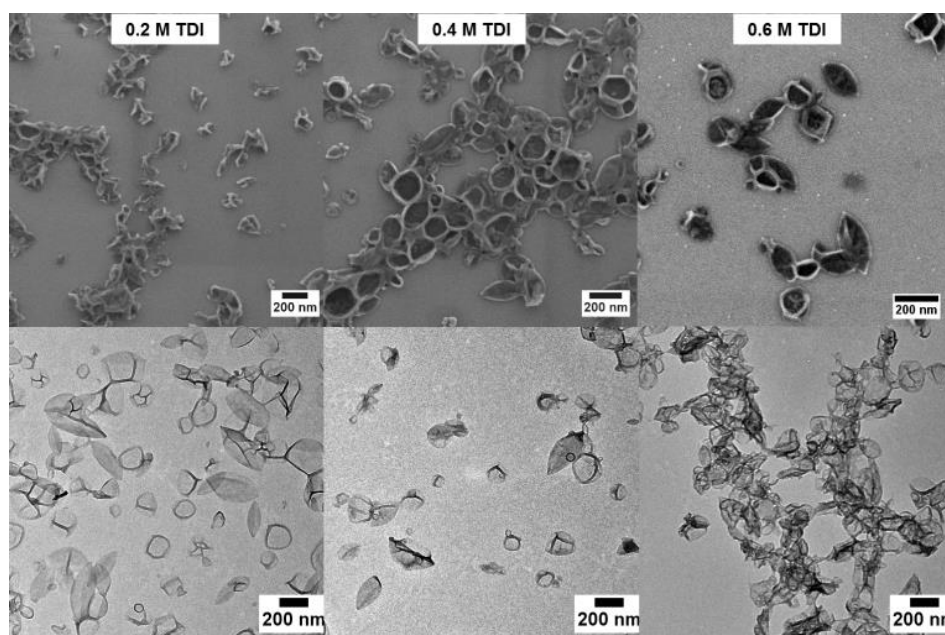
Figure 3.4 SEM (top) and TEM (bottom) images of several lignin nanocapsules with varying amount of cross-linker. (Yiamsawas et al; RSC Adv. 2014, 4(23), 11661-11663, http://pubs.rsc.org/en/Content/ArticleLanding/2014/RA/c3ra47971d#!divAbstract- Reproduced by permission of The Royal Society of Chemistry)
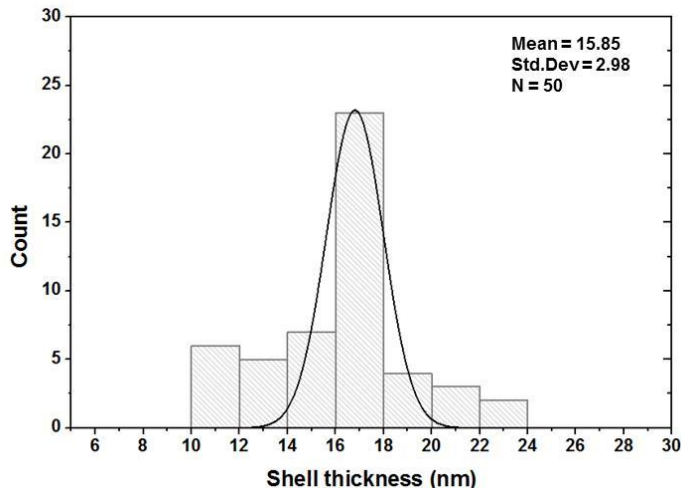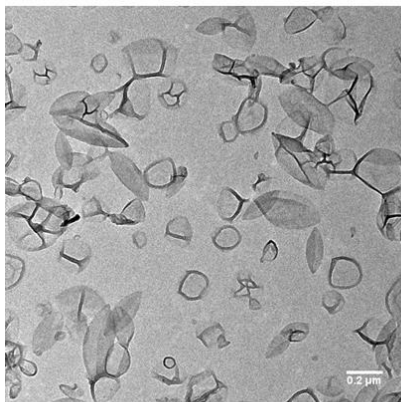
Figure 3.5 Estimation of the shell thickness of lignin nanocapsules from TEM.

3.1.1.2 Enzyme-triggered release of lignin capsules

Laccases are well-known enzymes present in the lignolitic systems of many fungi. Such enzymes are typically used for delignification, so in order to proof natural nanocapsules degradation, laccase is used as a natural model to degrade the lignin capsules. White rot fungi have been discussed in large detail as natural resources for laccases. In contrast to the lignolitic enzymes of these basidiomycetes, ascomycetes of the *Xylariaceae* family have not been intensively been studied. However, the presence of *Xylaria* species on decaying wood in almost all forests indicates an important role in the recycling of lignin.[134]

In order to investigate the biodegradability of the lignin nanocapsules, the hydrophilic fluorescent dye sulforhodamine (SR101) was encapsulated, which is released upon degradation of the capsule shell. The cleavage of the cross-linked lignin shell was studied by a laccase from the fungus *Xylaria sp*. IBWF-A55-2009. The scheme representative for the enzymatic cleavage of linin capsules is presented in Figure 3.6.
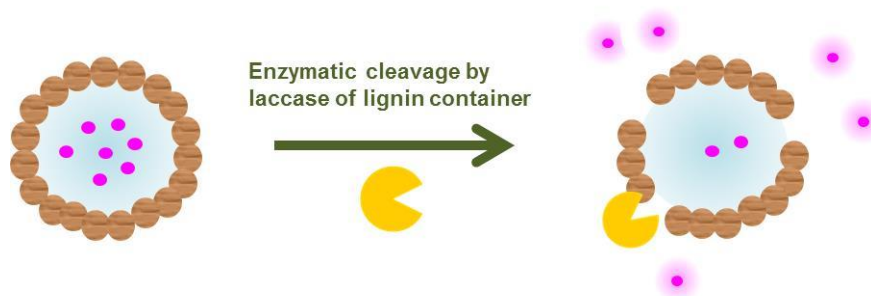
Figure 3.6 Scheme represent for the enzymatic cleavage of linin capsules.

Figure 3.7 shows the release of SR101 for the enzymatic cleavage by laccase (IBWF-A55-2009 Laccase) at 50 °C after incubation over a period of 24h at pH 3 and pH 7. At pH 3 and 50 °C, which are the optimum working conditions for this enzyme, a high amount of released SR101 was detected; however, also at neutral pH enzymatic release was proven to be effective. The enzyme extraction also proved to be efficient in cleaving the capsule shell and the released amount depends on the cross-linking density (Figure 3.8 & 3.9). This indicates that the lignin nanocapsules with higher degree of crosslinking have a denser network with polyurea-urethane bond are probably cleaved much slower by the enzyme.
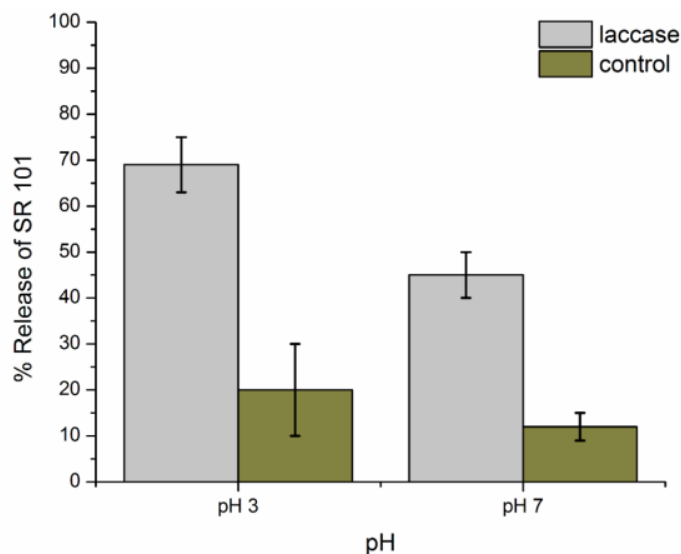
Figure 3.7 Release profile of the lignin nanocapsules prepared with 0.2 mM of TDI after degraded by *Xylaria sp.* IBWF A55-2009 laccase at 50 °C.
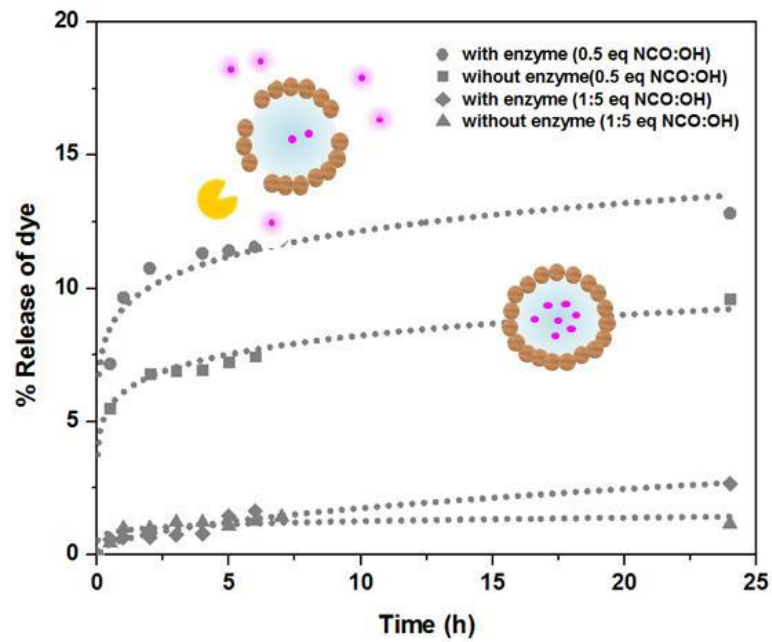
Figure 3.8 Release profiles of SR101 dyes from the crosslinked-lignin capsules after cleavage by enzyme cocktail at RT, pH 7.
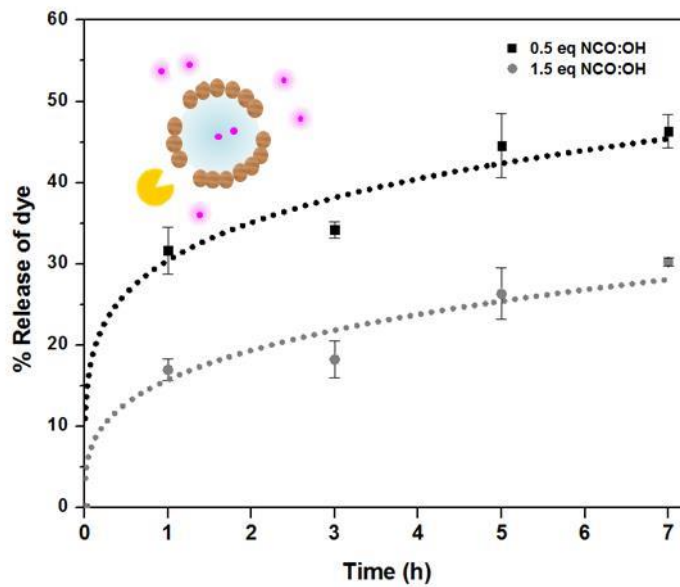
Figure 3.9 Release profile of SR101 dyes from the crosslinked-lignin capsules after cleavage by enzyme cocktail at 50 °C, pH 3.

In conclusion, the successful synthesis of hollow lignin nanocapsules with an aqueous core could be shown. They have been prepared by selective polyaddition at the interface of stable aqueous nanodroplets in an inverse miniemulsion. The reaction setup allows the efficient encapsulation of hydrophilic substances (drugs, fertilizers, pesticides) which was proved by the hydrophilic model compound (SR101). The obtained lignin nanocontainers showed diameters in the range of 150-200 nm and were stable in organic or aqueous dispersion over a period of several weeks-months. In addition, enzymatic degradation of the lignin nanocapsules has been performed by laccase as a model enzyme and also by a mixed enzyme cocktail extracted from natural fungi.

3.1.2 Lignin carriers for hydrophobic substances, its morphologies and release profiles

In the previous chapter, the synthesis of a novel lignin nanocapsules carrier system for hydrophilic compounds and the enzyme trigger release of the hydrophilic dyes from lignin nanocapsules were proven. In this chapter, an approach to generate lignin nanocarrier for hydrophobic compounds will be described. This route allows the formation of lignin nanocarrier with various morphologies (solid and porous nanoparticles and core-shell structures). These lignin nanocarriers can be loaded with hydrophobic substances, which is ideal for pesticides or antifungals as most of them are hydrophobic, making these nanoparticles ideal for drug delivery in plants. This route is based on miniemulsion polymerization in combination with solvent evaporation. In addition the nanoparticles were carbonized to produce biobased adsorbents which may be used for water purification for example. The nanocarriers exhibit a variable release profile, depending on the nanoscopic architecture. The synthesis starts with the modification of methacrylates allowing crosslinking by radical polymerization. After the attachment of methacrylates, lignin can be dissolved in organic solvents in a direct, i.e. oil-in-water, miniemulsion polymerization process combined with solvent

evaporation. Depending on the conditions, core-shell structures (with oil-core nanocapsules), solid nanoparticles, or porous nanostructures can be generated in a controllable way. In addition, loading of the nanocarriers with a model hydrophobic drug and different oils was studied. The core-shell structure formation was induced by internal phase separation between oil and lignin. Depending on the morphology of the nanocarriers, the barrier properties of the nanometer-sized lignin-membrane differs accordingly. Loose and dense nanocarriers have been achieved that allow release over time or enzymatically-triggered release of the cargo.

This section is applied for a patent with the title of "Lignin Biomaterial as Agricultural Drug Carrier" (EP16154480.4) and submitted for a scientific publication with the title of "Lignin Nanoparticles for Agricultural Drug Delivery and as Precursors for Bio-Based Adsorbents" (they will be published when this thesis is published).

3.1.2.1 Synthesis and characterization of methacrylated lignin

The synthesis of methacrylated lignin (MA-lignin) was conducted by esterification of the hydroxyl groups in lignin with methacrylic anhydride. FT-IR spectroscopy (Figure 3.10) and ^{1}H NMR spectroscopy were used to determine the successful incorporation of the methacrylate group to lignin. The formation of ester bond was confirmed by the vibrational band at 1710 cm^{-1} (-C=O). In addition, the broad hydroxyl group (-OH) band at 3000-3800 cm^{-1} was reduced significantly, an indication that high amount of hydroxyl groups of lignin have been reacted. Vinyl groups from methacrylates were further confirmed by ^{1}H NMR spectra by the broad resonances at between 6.5-5.5 ppm and diffusion-ordered NMR spectroscopy (^{1}H-DOSY NMR) is also confirmed the bonding between the methacrylate moiety and lignin. The diffusion coefficient for the signal between 6.5-5.5 ppm of =CH$_2$ is equal (ca 5.0 x10^{-11} m^2 s^{-1}) to that of lignin molecules as presented in Figure 3.11. Also gel permeation chromatography (GPC) analysis indicates the successful formation of MA-lignin (Figures S4 and S5); after attachment and purification of the methacrylates an apparent molecular weight of 16452 g·mol^{-1} with M_w/M_n=2.3.
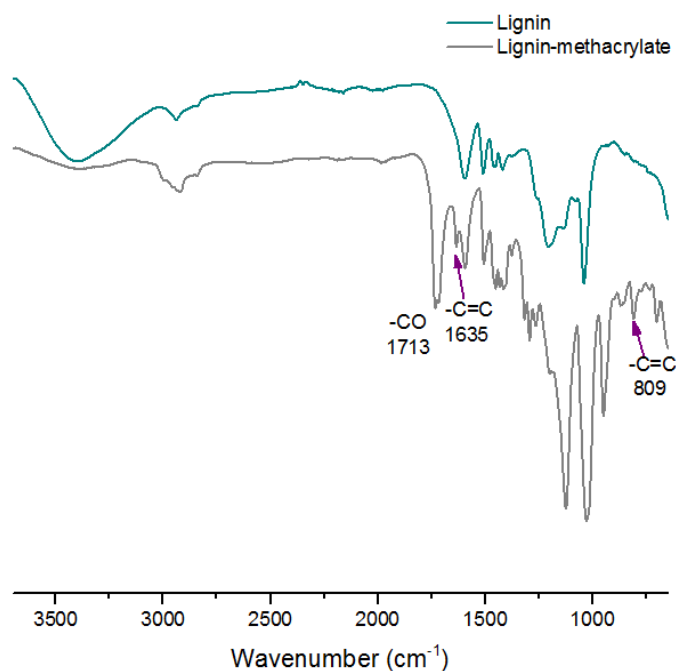
Figure 3.10 FTIR spectrum of lignin and MA-lignin.
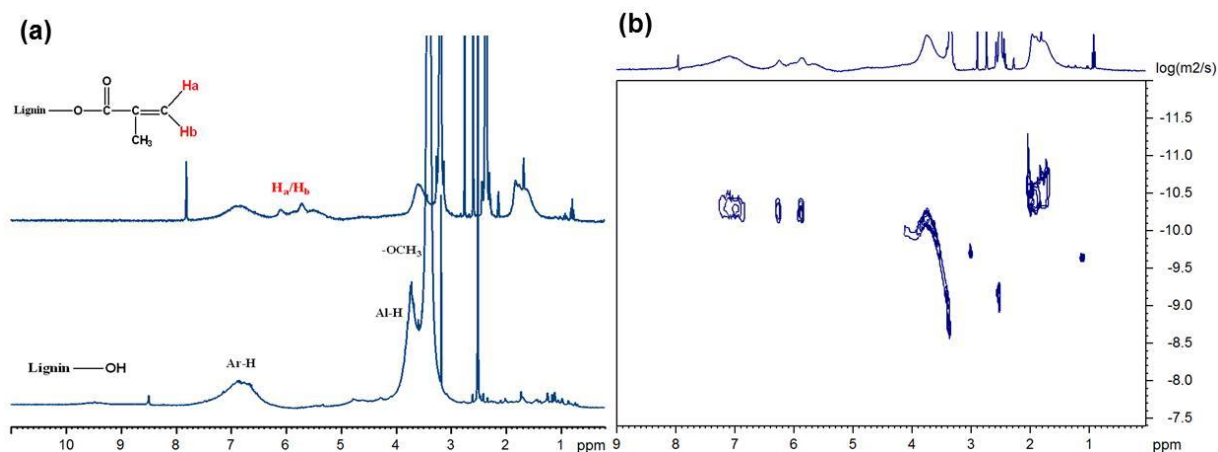
Figure 3.11 ^{1}H NMR spectra of lignin and methacrylate lignin (a) and ^{1}H-DOSY NMR of MA-lignin (b).

Successful transformation to MA-lignin was further confirmed by our X-ray photoelectron spectroscopy (XPS) result, as shown in Figure 3.12. The pristine lignin sample exhibits expected peaks located at ~284.1 eV, ~285.7 eV, and ~286.7 eV, these

photoemission signals come from carbon atoms existing in different chemical environment among the lignin molecule backbone: more specifically, with increasing binding energy the peaks were individually assigned to aromatic carbons (violet), aliphatic carbons (black), and carbon bonded near an oxygen atom (black). After esterification of the hydroxyl groups, another obvious peak appear at higher binding energy side (~288.3 eV, red), which can be unambiguously assigned to -COO- group, suggesting the successful formation of MA-lignin.
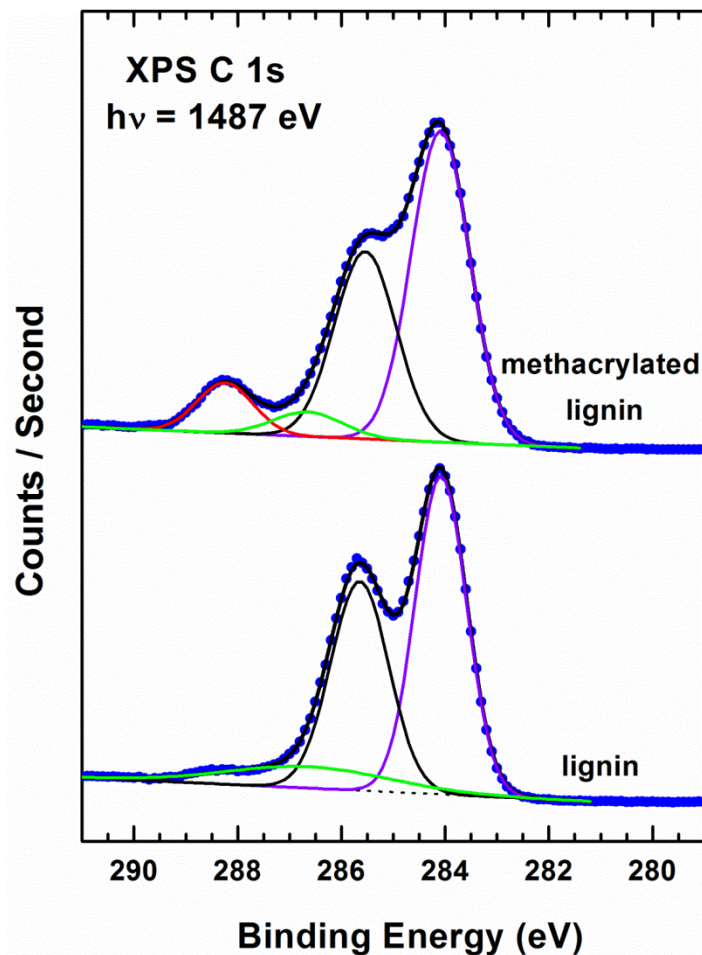
Figure 3.12 C 1s XP spectra of lignin and MA-lignin. The spectra were self-fitted with peaks assigned for individual components.

For further characterization of MA-lignin, the thermal properties were studied. From differential scanning calorimetry (DSC) (Figure 3.13) the glass transition temperature (T_g) of MA-lignin was determined to be ~16 °C (100 °C versus 82 °C) higher as compared to the

unmodified lignin, suggesting, correspondingly, the enhanced soft flexibility for modified lignin polymer (MA-lignin).
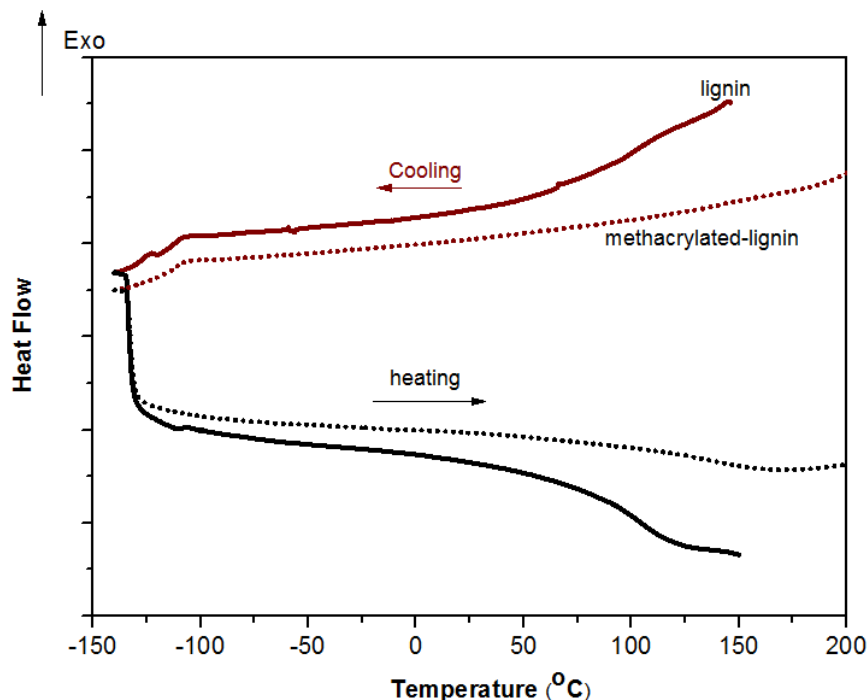
Figure 3.13 DSC thermograms of lignin and methacrylated lignin (solid line: lignin, dashed line: MA-lignin).

3.1.2.2 Formation of lignin nanocarrier for hydrophobic molecules

A stable oil-in-water miniemulsion (1:6 of oil:water) is prepared by dispersing a solution of MA-lignin together with hexadecane, olive oil or palm oil, dissolved in chloroform, in an aqueous solution containing a 2 wt% of surfactant compared to disperse phase (sodium dodecyl sulfate (SDS), Lutensol AT25, or lecithin). After ultrasonication, a stable miniemulsion was obtained and the crosslinking process was carried out by free radical. For the generation of core-shell structures by miniemulsion (with a liquid core and a solid shell) the addition of a hydrophobe is necessary that forms the liquid core after evaporation of a volatile solvent.[135-137] Different hydrophobes have been studied. Hexadecane

as the standard hydrophobe in oil-in-water miniemulsions was used which facilitates the encapsulation of oil-soluble drugs or dyes. As lignin is biodegradable, also olive or palm oil as the respective hydrophobes were used to generate fully biodegradable nanocarriers.

For the preparation of oil-core lignin-shell nanocapsules according to the combination of miniemulsion and solvent evaporation, the investigation of the solubility behavior of MA-lignin, the oily core (hexadecane) and the volatile solvent (chloroform) was performed. The resulting boundary curve in the ternary phase diagram of MA-lignin/hexadecane/chloroform separates the one-phase (I) and two-phase (II) region is shown in Figure 3.14. This curve provides information regarding the point where phase separation will appear. The composition of three components (percentage ratio of MA-lignin/hexadecane/chloroform; 10.5/3.5/85) which was used to prepare nanocapsules, was selected in the one-phase region far away from boundary curve.
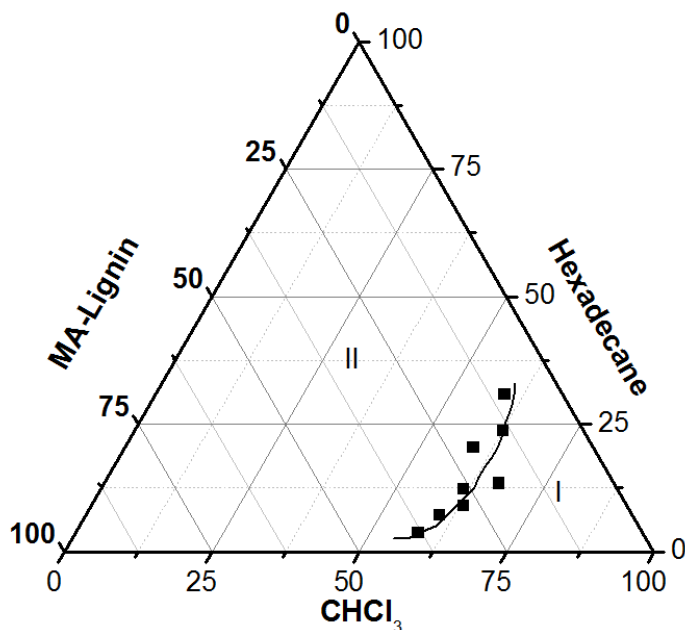
Figure 3.14 Ternary phase diagram for lignin-chloroform-hexadecane (I: one phase, II: two phase).

After solvent evaporation, the mean diameters of the lignin nanocarriers were determined by DLS for the system containing 10.5 wt% of MA-lignin in oil phase (Table 3.2). Three surfactants were applied for the stabilization of the nanodroplets in water (SDS,

Lutensol AT25 and lecithin). The use of Lutensol AT25 and lecithin led to large particles sizes with a broader size distribution, whereas the ionic surfactant SDS produced smaller particles sizes with lower size distributions at the same concentration (2 wt% to disperse phase). This can be explained by the fact the oil-water interfacial tension can be more decreased by using the ionic surfactant, which this phenomena induces smaller size of the droplets as listed in Table 3.2.

Table 3.2 Characterization data of hexadecane-filled lignin nanocarriers.

Surfactant	wt%[a]	diameter/ nm[b]	PDI[a]
SDS	1	996	0.45
SDS	2	417	0.26
SDS	3	246	0.20
Lutensol AT25	2	925	0.61
lecithin	2	806	0.36

a) compared to the dispersed phase.
b) determined by dynamic light scattering.

The interfacial tension plays an important role in the resulting morphology of the nanostructures that are generated. Such behavior has been intensively investigated by Torza and Mazon.[122] Regarding their work, interfacial thermodynamics was used to predict the morphology of emulsified droplets of two insoluble liquid oils dispersed in water in term of the spreading coefficient. The shape of the emulsion droplets depends upon the interfacial tension between the various different pairs of three phases (γ_{o1w}, γ_{o2w}, γ_{o1o2}). The necessary conditions to obtain core-shell structures with oil_1 surrounded by oil_2 derived from the following inequality equation as follow:

$$\gamma_{wo1} > \gamma_{wo2} + \gamma_{o1o2} \qquad \text{Equation 3.1}$$

When the inequality is reversed, acorn-shaped particles, which are two non-engulfed droplets attached to each other, are formed. This concept was later expanded by the Vincent group for microcapsules[135, 138] and the Landfester group for nanocapsules in miniemulsion,[130]

with one phase being eventually solid (polymer shell). According to the works of Vincent and coworkers, the core-shell structure from the solvent evaporation method is formed by phase separation of polymer within droplets of the emulsion, which involves several steps. Basically, an oil phase contained a mixture of the polymer (MA-lignin), a volatile, good-solvent (chloroform), and a nonvolatile poor-solvent (hexadecane). When the good solvent is removed (e.g. by evaporation), the composition in the oil droplets changes and the lignin phase separates as small droplets from the poor solvent within the emulsion nanodroplets. If the interfacial tension of the emulsion is balanced, the polymer droplet should then migrate and formed the shell at the oil/water interface (Figure 3.15).
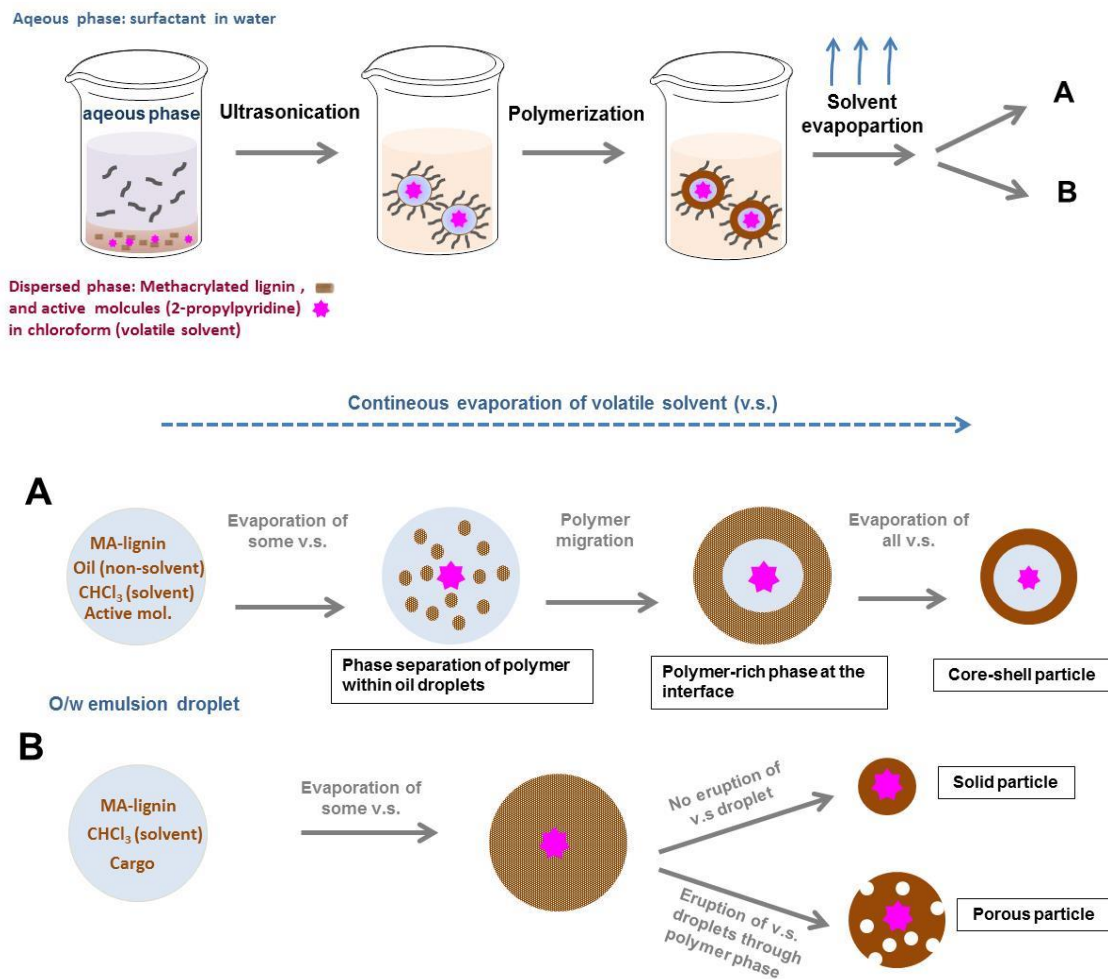
Figure 3.15 Preparation of lignin nanocarriers with variable morphologies by miniemulsion and a plausible explanation for structure formation.

Various combinations of surfactants and oils were used in the encapsulation experiments to investigate their individual effects on the structure of the lignin nanocarriers and their effect on the release behavior. The determined interfacial and surface tensions for the oil/MA-lignin system with different types of surfactants is shown in Table 3.3. Obviously, the surfactants display a broad range of influence on the interfacial tension at the oil/water interface and affect to the stability of the emulsion. Inspections of the values in Table 3.3, according to the previously mentioned inequality, show that the core-shell of hexadecane/MA-lignin or olive oil/MA-lignin systems will be not satisfied for all conditions since the oil-water interfacial tension was lower than the oil-polymer surface tension, and water-polymer surface tension.

Table 3.3 The interfacial tensions, contact angles calculated for the various systems.

Oil	Surfactant	wt% of surfactant to disperse phase	Θ_{op}	Θ_{wp}	γ_{ow}	γ_{op}	γ_{wp}
HD	SDS	1	< 3	34.9	6.0	21.5	12.7
HD	SDS	2	< 3	26.8	9.7	21.5	18.6
HD	SDS	2	< 3	23.4	4.7	21.5	22.6
HD	Lutensol AT25	2	< 3	38.8	7.87	21.5	14.5
HD	lecithin	2	< 3	58.7	19.0	21.5	17.4
Olive oil	SDS	2	20.7	26.8	1.5	19.0	18.6
Olive oil	Lutensol AT25	2	20.7	38.8	5.2	19.0	14.5
Olive oil	lecithin	2	20.7	58.7	15.3	19.0	17.4

Θ_{op} = Contact angle of oil on MA-lignin film obtained from optical contact angle,

Θ_{wp} = Contact angle of surfactant solution on MA-lignin film obtained from optical contact angle,

γ_{ow}= interfacial tension between oil and surfactant solution were measured by the spinning drop method using a spinning drop video tensiometer,

γ_{op}= interfacial tension between oil and MA-lignin film calculated by Young´s equation,

γ_{pw}= interfacial tension between surfactant solution and MA-lignin film calculated by Young´s equation.

First, the effect of different SDS concentrations on the morphology of the lignin nanocarriers after the crosslinking polymerization was investigated and visualized by TEM (Figure 3.16 upper images). The three different SDS concentrations produced core-shell and

capped structures with variable diameters (also compare Table 3.1). By contrast, in the system with a lower oil-water interfacial tension (i.e. higher surfactant concentration) more acorn-shaped objects are visible. If the oil in the core is changed from hexadecane to olive oil, while the surfactant remains constant, still core-shell structures, i.e. nanocapsules, can be obtained (Figure 3.16d).
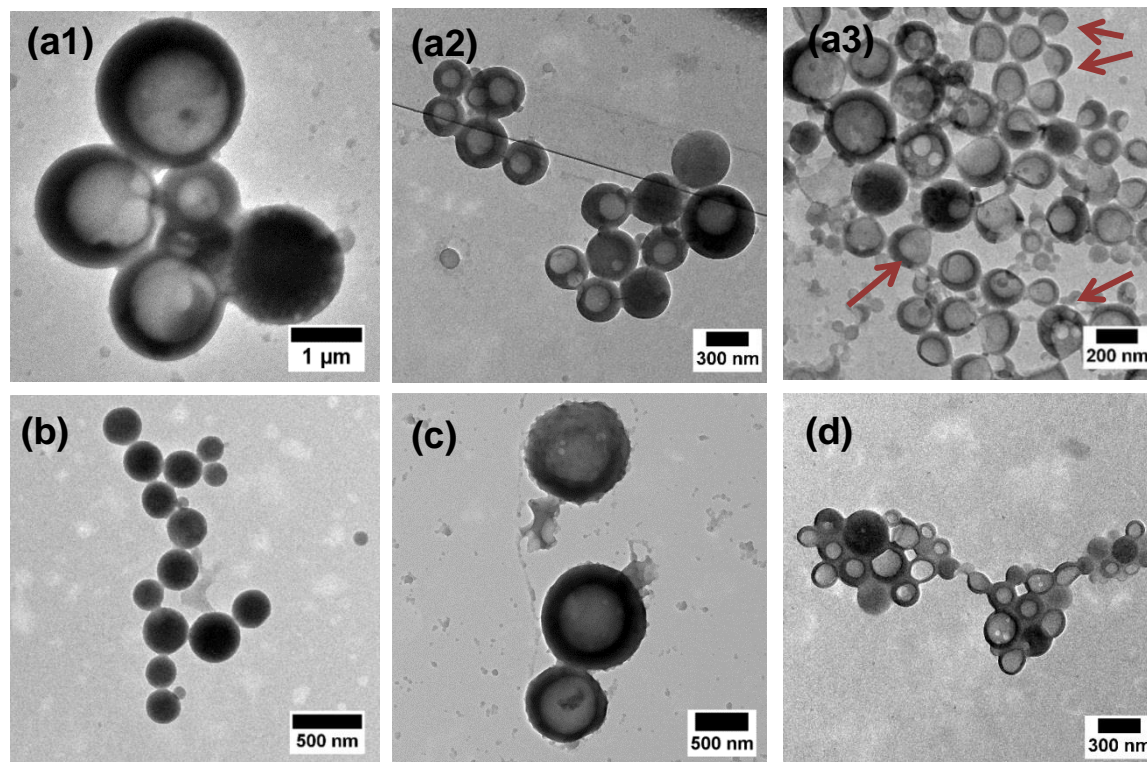
Figure 3.16 TEM images of hexadecane core - lignin shell nanocarriers stabilized with SDS at 1 wt% (a1), 2 wt% (a2), 3 wt% (a3), with 2 wt% of lecithin (b), with 2 wt% of Lutensol AT25 (c), and olive oil core–lignin shell with 3 wt% of SDS (d).

Furthermore, we noticed that the morphology of the lignin nanocarriers can be altered by changing the surfactant type: when lecithin was used, spherical nanoparticles were formed (Figure 3.16b) which did not correspond to the prediction of an acorn structure. In case of Lutensol AT25, also a core-shell morphology was generated (Figure 3.16c). However, most of them exhibited non-smooth surfaces with craters in the lignin shell (SEM: Figure 3.17). This might be explained by a mechanism from Lavergne and co-workers.[139] By using confocal fluorescence microscopy, they proposed that the craters are formed by the

penetration of the oil into polymer phase where it stabilizes water droplets. Obviously in their case, the nature of polymer and oil plays a more important role for the given process whereas the surfactant has a trivial influence. However it is difficult to find an explanation for the current forming process. In our case, to investigate the influence of the oil inside the droplets and the surfactant on the structure of the nanocarriers, the experiments without an oil core and without a surfactant were carried out. The presence of a hydrophobic and hydrophilic group makes lignin macromolecules diphilic, and therefore, it can be used to stabilize the miniemulsion directly and to omit an additional surfactant (i.e. acting as a "surfmer", i.e surfactant + monomer).[140, 141] However, self-lignin-stabilized emulsion from our system could not obtained with good stability.
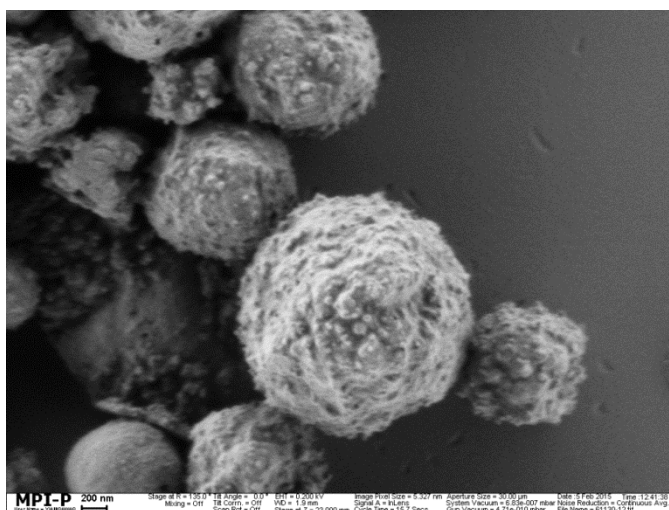
Figure 3.17 SEM image of oil-core lignin shell capsules with Lutensol AT25 as the surfactant.

If SDS is used as a surfactant and no oil is added during the preparation in the organic phase, the TEM images show the formation of spherical nanoparticles with a broad size distribution and mean particle diameters of ca. 250 nm (Figure 3.17a). Particles prepared using Lutensol AT25 as emulsifier are very polydisperse and larger in diameter, up to ca. 2-3 µm. Also aggregation occurred and the dispersion shows a poor colloidal stability. However, the produced nanocarriers exhibit an extraordinary porous structure with high surface areas. Nanoscopic holes in the particle and on the surface as a highly porous structure are detected

by SEM and TEM (TEM: Figure 3.18 b, c; SEM: Figure 3.18d). It seems that the solvent loss through the larger particles occurred by the eruption of solvent droplet through the polymer phase. This leads to the formation of multiple voids in the nanocarriers as seen the proposed mechanism in Figure 3.15.
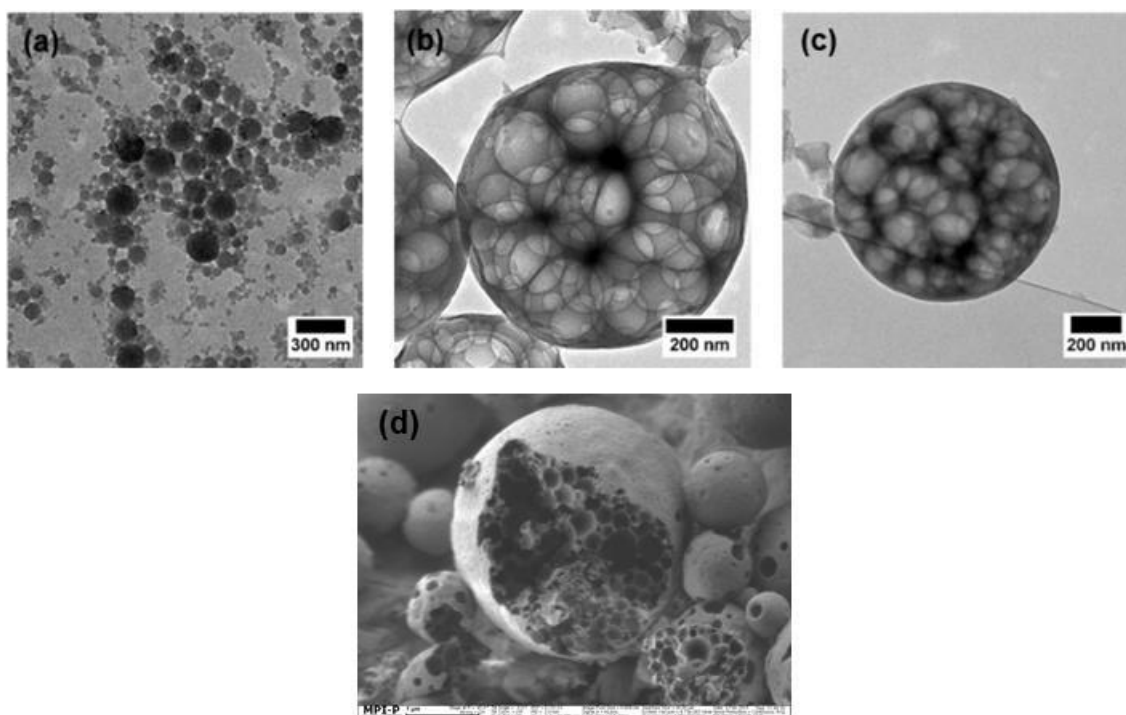
Figure 3.18 TEM images of lignin nanocarriers without the addition of oil or hexadecane and different surfactants: SDS (a), Lutensol AT25 (b) and without surfactant (c) and SEM image of porous lignin nanocarriers with Lutensol AT25 as the surfactant (d).

3.1.2.3 Release profiles of lignin nanocarriers

The loading of hydrophobic molecules inside the oily core of the lignin nanocarriers is interesting for future applications, for example in drug delivery in agricultural applications, as laccase present in plants may degrade the nanocarriers and thus release the drug.[127] As a model compound, a small molecule, i.e. 2-propylpyridine, was encapsulated into the nanocarriers. It was dissolved in chloroform with the oil and MA-lignin during the pre-emulsion process. In case of the lignin nanoparticles (analogues to the ones shown in Figure 3.18a), 2-propylpyridine was added in the chloroform phase to MA-lignin, but without the

addition of a hydrophobic oil. The polymerization of the lignin was carried out by the addition of azobisisobutyronitrile (AIBN) as radical initiator in the oil phase with subsequent ultrasonication. The effect of the lignin particle morphologies on the release profile of 2-propylpyridine, was studied as shown in Figure 3.19. It is obvious that a small amount of cargo (ca. 10%) is released from the solid lignin nanoparticles (Figure 3.19a, ■). This makes them promising candidates for a controlled and stimuli-responsive release after the addition of an enzyme capable of cleaving lignin (see below). A higher release was detected in the case of the porous structures (Figure 3.19a, ●). This is probably because of some open pores in the structure and an overall thinner lignin layer compared to the nanocapsules with an oil core. However, nanocapsules (with a liquid oily core) prepared from miniemulsions containing MA-lignin and hexadecane or olive oil as an internal phase show a release of 10-35% within 24 h. The release however, levels off after that period (Figure 3.19a, ▲ and ◆). This clearly indicates a certain barrier property of lignin and lignin nanomembranes for low molecular weight compounds.[142] 2-Propylpyridine is a rather small molecule and can be regarded as a benchmark test for the density. All drugs that are commonly used for example in agriculture (antifungals or herbicides) are larger molecules that probably would be released slower. However, the different morphologies of the lignin nanocarriers allow a controlled (and rather low) release over time by diffusion.

Furthermore, the release of the cargo from the lignin nanocarriers can be increased in the presence of an enzyme capable of degrading lignin. The cleavage of the lignin shell was achieved by the enzyme laccase as shown in Figure 3.19b. The core-shell particles show a higher amount of 2-propylpyridine in aqueous phase. After the addition of laccase, both nanocarriers show a high release of 2-propylpyridine which is much higher than the diffusive release from the same systems. These results prove that laccase is capable of cleaving the crosslinked lignin shell of nanoparticles, and thus allow an enzymatically triggered release of a hydrophobic cargo. It further indicates that the triggered release of the cargo also depends on the morphology and can be related to the partition coefficient of the active ingredients between the oil core and the polymer shell (lignin). More than 20% of 2-propylpyridine retained in the lignin shell. It is clear that 2-propylpyridine and lignin have some specific interaction retarding the diffusion rate.
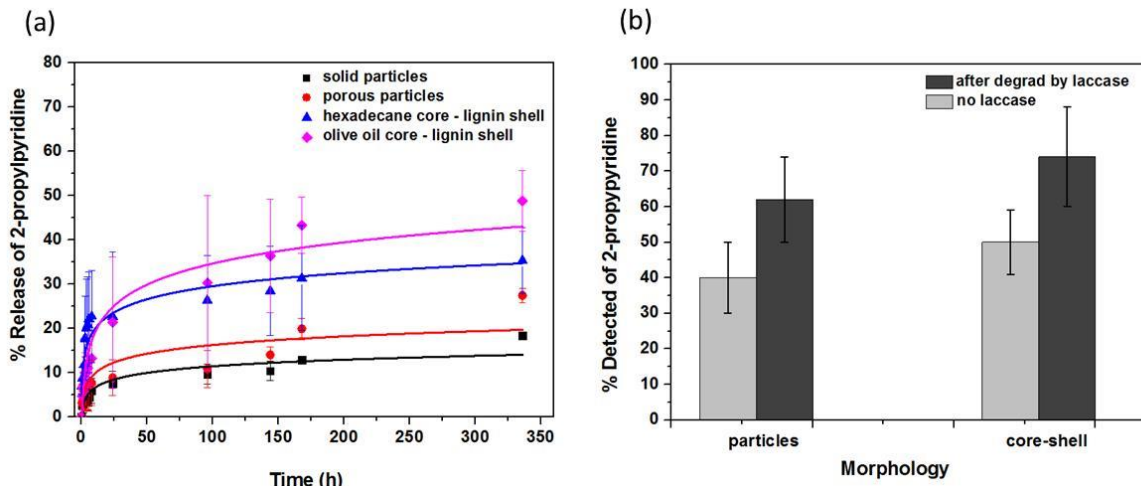
Figure 3.19 a) Release profile of 2-propylpyridine from lignin nanocarriers (no oil and SDS (solid nanoparticles, compare Figure 3.18a) (■)), olive oil, SDS (nanocapsules, compare Figure 3.16d (◆) hexadecane, SDS (nanocapsules compare Figure 3.16 a2) (▲) no oil and Lutensol AT25 (porous nanocarriers, Figure 3.18b) (●). b) Detected percentage of 2-propylpyridine from lignin nanoparticles in aqueous phase before and after cleavage by laccase.

In summary, lignin: a highly functional building block from nature was success modified through esterification of the hydroxyl groups with methacrylic anhydride. Then lignin nanocarriers with different morphologies (solid nanoparticles, core-shell structures, porous nanoparticles) were produced by a combination of miniemulsion polymerization and a solvent evaporation process. A UV-active cargo is used as a hydrophobic drug model to investigate the release behavior of the lignin nanocarriers depending on their morphology. The addition of the enzyme laccase degrades lignin and strongly enhances the release from the lignin nanocarriers, thus rendering these structures as highly interesting for future biodegradable drug delivery vehicles for agricultural applications.

3.1.3 Potential application of lignin carrier for Esca disease of grapevine

The following work has been conducted together with Prof. Eckhard Thines and Dr. Jochen Fischer (Institute of Biotechnology and Drug Research in Kaiserslautern). In order to prove the potential application of lignin nanocarrier for drug delivery in plant, the fungicide encapsulated lignin nanoparticles are applied to treat Esca-infected grapevine plants.

This section is registered for a patent in a title of "Lignin Biomaterial as Agricultural Drug Carrier" (EP16154480.4) and in preparation for a scientific publication submission in a title of "Targeted drug delivery with lignin nanoparticles cure Esca-infected wine plants".

The Esca disease is one of the most destructive infections in Europe and California for the woody parts of grapevines (*Vitis vinifera L.*).[143-145] The first historical knowledge of the disease was made in Roman times and this is also the reason for its Latin name, which means "cinder", because the dying plant parts are dry and burn easily.[146] In literature, the term 'grapevine trunk diseases' is used inconsistently and refers to a number of different diseases of pathogenic fungi inhabiting and deteriorating the wooden organs of grapevine. The most destructive among these diseases are called esca and young vine decline ('young Esca'). The latter arise in recently planted vineyards whereas the other establish in plantations older than seven years. [144, 147, 148] At this point of knowledge the disease is spread all over southern Europe and the western parts of the United States of America (USA). But since the temperatures in Central Europe during hot summers are rising the disease propagates in Germany and Northern France as well as Italy and Spain.[149] The symptoms, which can be seen on the leaves, are necrotic yellow-brownish spots around the leaf veins. The grapes often get brown spots and subsequently dry. These symptoms are often observed in California and Italy.[150] When the trunk of the vine is cut and opened, diverse necrosis is often observed. For example black circles or brown sports, as well as already dried wood can be seen.[151] Since Esca is a trunk disease with separated sites of production and impact of the

phytotoxic substances it is almost impossible to treat the infected plant. Sometimes spraying the plants with sodium-arsenide had some effect.[152] But since arsenide compounds have been banned in Europe, new treatments for grapevine trunk diseases are demanded.

In the last decade scientists all over the world tried to gain their knowledge on Esca disease. First efforts were made by the description of two major phytotoxic compounds, produced by *Phaeoacremonium aleophilum (Pal)* and *Phaeomoniella Chlamydospora (Pch)* were isolated and characterized.[153, 154] Furthermore, Bruno et al.[155] gained the knowledge on the interaction of the host plant and the pathogenic fungi involved. But those conclusions could not provide any solutions of healing for already infected plants. Many scientists searched for solutions to prevent an infection of grapevine plants.[156] The treatment of grapevine cuttings with hot water lead to some positive results, especially since none of the chemical or biological treatments caused a similar reduction in *Phaeomoniella* and *Phaeoacremonium* infection in the treated rootstocks.[157, 158] But even since the hot water treatment and spraying biological control agents on grapevine cuttings in combination with differing nursery management strategies, vineyard management and pruning wound protection methods could ensure the production of high-quality grapevines with low levels of infection; these methods are not suitable to cure infected plants.[159] If all efforts on protecting the pruning wounds of uninfected plants are rootless and the pathogens entered the trunk no curing method so far is known.[148, 160] Darrieutort and Lecomte[161] made first injection tests but in their trials, the injections did not cure the mature vines. In their study propiconazole, difenoconazole and 2-hydroxy-benzoïc acid were injected into the infected plants. However, the disappointing data recorded were quite similar to those from other experiments that have recently been reported.[162] One of the difficulty in curing the plant and defeat the tracheomycotic pathogens is to deliver an amount fungicide suitable to antagonize the pathogenic fungi close enough to the mycelium. Therefore a hydrophobic substance would be recommended. This substance would be able to diffuse easily through the vascular system of the host plant. Contrariwise that substance could not accumulate closely related to the pathogen; hence the amount of fungicide that needs to be injected into the plant would be too high. Then again a hydrophobic fungicide would not diffuse through the vascular system und would precipitate next to the injection side. To date, no curative treatment for Esca has been reported.

As a biodegradable polymer, lignin is a promising material for the preparation of drug delivery vehicles for fungal diseases. As shown previously, lignin nanocarriers can be degraded by laccases, an enzyme secreted by various fungi.[127]

In this thesis, a Trojan horse has developed for the first curative treatment of wine plants against Esca. The hydrophobic fungicide pyraclostrobin was encapsulated by a combination of miniemulsion polymerization and solvent evaporation into lignin nanoparticles. The resulting aqueous nanoparticle dispersion was studied *in vitro* and *in planta* for the activity against Esca. After injection of the lignin nanoparticles into the grapevine plants, the lignin nanoparticles are probably degraded by secreted laccase and the drug can act against Esca. The symptoms of Esca were reduced and all plants did not exhibit symptoms after a year in the field. This is the first report to treat Esca-infected grapevine plants in an early state of infection cycle which may be further extended to other trunk diseases.

3.1.3.1 Preparation and optimization of lignin nanoparticles for fungicide encapsulation

In order to allow the encapsulation of the hydrophobic fungicide, similar approach of the chapter 3.1.2 was applied. Firstly esterification of lignin with methacrylic anhydride was performed and followed by Michael reaction in a combination of miniemulsion and solvent evaporation to from lignin nanoparticles. MA-lignin was dissolved together with hexadecane and fungicide in chloroform to generate the dispersed phase which was then mixed with the aqueous phase containing the surfactant. SDS (anionic surfactant), Lutensol AT25 (nonionic surfactant) and lecithin were used to generate the emulsions. The pre-emulsion was stirred at room temperature and subsequently ultrasonicated in order to generate the stable miniemulsion. The Michael reaction was initiated after a solution of 2,2´(ethylenedioxy)bis(ethalamine) was added and heated at 50 °C to the previously formed miniemulsion.

In this study 2,2´(ethylenedioxy)bis(ethalamine) molecules which can dissolve both in aqueous and chloroform phase are selected as a crosslinking agent. Two possible routes for crosslinking lignin particles by adding the diamine molecules in disperse phase before or

after ultrasonication were investigated. It was found that adding diamine molecules to the aqueous phase after forming the droplet prior to heat the reaction gave the greatest stability of the emulsion.

Cross-linked lignin was obtained by diamine molecules in the aqueous phase diffused into the droplet of MA-lignin and reacted with double bond of MA-lignin. After completed reaction, the reaction vessel was kept open at room temperature overnight in order to ensure complete evaporation of chloroform leaving the aqueous dispersion of lignin nanoparticles.

The surfactant, the fungicide-loading content and the encapsulation efficiency play important role in the antifungal activity. In order to optimize the formation condition of the emulsion and fungicide loading efficiency, several types of the parameters were varied in the experiment. The miniemulsion conditions and some data results are summarized in Table 3.4. The diameter of the cross-linked lignin particles was in the range of 250-700 nm as observed by DLS. The use of non-ionic surfactant Lutensol AT25 and lecithin led to larger particles sizes with a broad size distribution, whereas smaller particles can be obtained from the ionic surfactant SDS at the same concentration (2 wt%). TEM was also used to investigate the morphology of fungicide-loaded lignin particles as show in Figure 3.20. TEM images showed individual particles with a well-define spherical which were prepared with three different types of surfactant.

Firstly, the influence of the weight ratio of MA-lignin:chloroform in the miniemulsion droplet on the particle size of unloaded-fungicide lignin particles was investigated. It was found that when the weight ratio of MA-lignin:chloroform was increased from 1:10 to 1:6, the particles size raised from about 266 to 352 nm. It can be explained by an increase in the viscosity of the dispersed phase (lignin solution) making more difficult its dispersion. A homogeneous system can be obtained in both cases with around 0.3 of polydispersity index.

In the next step, pyraclostrobin as a hydrophobic fungicide was added to the disperse phase in the pre-emulsion step to encapsulate in the crosslinked-lignin particles. The influence of the feed mass ratio (MA-lignin to fungicide) and surfactant type and concentration on the fungicide-loaded lignin particles size was observed. The result in the Table 3.4 shows that the particles size gradually increased from 266 nm to 314 nm when pyraclostrobin was added into the system however the particles size did not significantly

change with increasing the pyraclostrobin at 2 wt% of surfactant (SDS) to disperse phase. However the particle size of the pyraclostrobin-loaded lignin particles was obviously influenced by the SDS concentration, as the SDS amount was increased, the particles decreased in size. In addition, when the surfactant type was changed from anionic to nonionic surfactant (Lutensol AT25) and natural biodegradable surfactant (lecithin) an increase of the pyraclostrobin-loaded-lignin particles size was found in both cases. In general, an ionic surfactant could be used more efficiently than nonionic surfactant to synthesize small particles.[163]

Table 3.4 Effect of fungicide to lignin on the size distribution, fungicide-loading content (LC) and encapsulation efficiency (EE).

Fungicide : MA-lignin wt ratio	MA-lignin :CHCl$_3$ wt ratio	Surfactant[a] (wt%)	Diameter[b] (nm)	PDI	%LC	%EE
-	1:6	SDS (2)	266	0.346	-	-
-	1:3	SDS (2)	352	0.329	-	-
1:20	1:6	SDS (2)	314	0.217	3.9	94.0
1:10	1:6	SDS (2)	334	0.378	8.6	94.1
1:5	1:6	SDS (2)	310	0.422	15.1	97.9
1:20	1:6	SDS (1)	511	0.408	4.5	98.7
1:20	1:6	SDS (3)	220	0.354	2.1	64.0
1:20	1:6	Lutensol AT25(2)	641	0.289	4.5	99.7
1:20	1:6	Lecithin (2)	645	0.389	3.5	98.1

a)   compared to the dispersed phase.
b)   determined by dynamic light scattering.
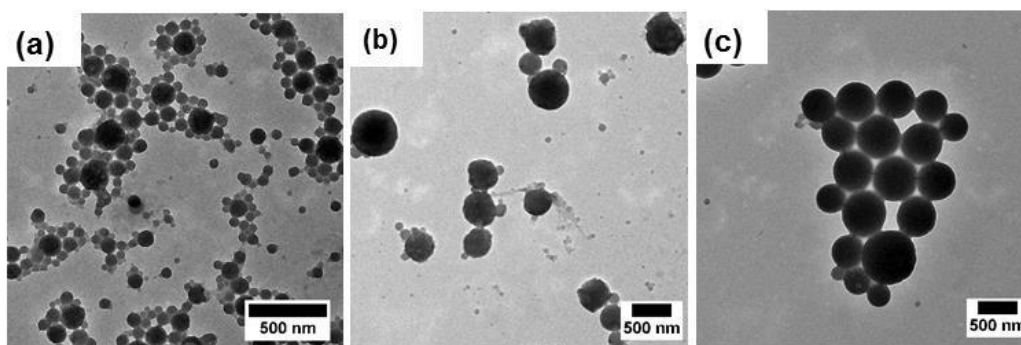
Figure 3.20 TEM images of lignin particles in different stabilized system; SDS (a), Lutensol AT25 (b) and lecithin (c).

Since the stability of the particles is an important aspect to consider, the particles sizes had been observed over a time period of one month. There was no significantly change in the size of all samples during this time. In order to check the morphology stability of the particle after drying, the dispersion was freeze-dried then dispersed in water. No apparent morphological changes were observed after re-dispersion, unloaded-fungicide lignin particles remained spherical shape however the re-dispersion of particles.

From the formulations in Table 3.4, the fungicide encapsulation efficiency is relatively high in the range of about 60-99%. Even at 15% of fungicide loading content, more than 97% of encapsulation efficiency was obtained. The concentration of surfactant significantly influenced on the encapsulation efficiency of pyraclostrobin. The encapsulation efficiency decreased from 99 to 64% by increasing the SDS content from 0.5 to 2.0 mg·ml^{-1}. When the concentration of surfactant in the system increases, there is a high possibility to have free fungicide inside the micelle during the formation of the pre-emulsion before the cross-linking reaction. The free fungicides do not corporate in the matrix of cross-linking linin particle so it can be detected with a higher concentration of surfactant. Not only the effect of surfactant concentration on the fungicide encapsulation efficiency be studied but also the surfactant type. Both the anionic (SDS) and nonionic (Lutensol AT25) surfactant including the natural surfactant (lecithin) led to high encapsulation efficiency.

From the above mentioned results it is indicated that cross-linked lignin particles can be efficiently be stabilized by both anionic and nonionic surfactants. For further experimental

studies, the effect of the surfactant on the antifungal activity in the lab and field tests had been continue studied in both lab and field test.

3.1.3.2 *In vitro* and *in planta* antifungal test

First *in vitro* tests at the laboratory using 96-well plates were tested to determine the concentration of lignin particles filled with fungicide needed for an efficient inhibition of spore germination and growth inhibition of the Esca-associated fungi. Furthermore the tests should verify whether the fungi had the capability to lyse the lignin coat and set the encapsulated fungicide free. The emission of fungicide should afterwards inhibit the growth of the plant pathogens *Pal* and *Pch*. The conditions of the samples for the antifungal test are presented in Table 3.5.

Table 3.5 Data of the lignin nanoparticles used for antifungal test.

Entry #	% Disperse phase	Surfactant (wt%)[a]	Size (nm)	solid content (wt%)	Fungicide (wt%)[b]
66	14	Lutensol AT25 (2)	139	1.5	-
72	14	SDS (2)	147	1.5	-
77	14	SDS (2)	1000	1.5	3
78	14	SDS (2)	660	1.5	7
79	7	SDS (2)	162	1.0	7
80	7	SDS (2)	277	1.0	20
81	14	Lutensol AT25 (2)	136	1.5	3
82	14	Lutensol AT25 (2)	119	1.5	7
83	7	Lutensol AT25 (2)	167	1.0	7
84	7	Lutensol AT25 (2)	168	1.0	15

Mass ratio of MA-lignin:CHCl$_3$ keep constant at 1:10
a)   compared to disperse phase.
b)   calculated per lignin particle (assumed density of lignin =1 g/cm^3).

As can be seen in Figure 3.21, the fungi sporulation in the medium mixed with antibiotic-free nanoparticles. The growth (and thereby the optical density) of the mycelium is for the lignin particles (SDS as emulsifier: no.66 and Lutensol as emulsifier: no.72 at 2 wt% to disperse phase) even better than for the negative control (medium without particles). The growth rates of *Pch* and *Pal* differ only slightly for the particles stabilized by SDS or Lutensol AT25. In the case of lignin particles filled with the fungicide pyroclostrobin (25 $\mu g \cdot ml^{-1}$) and stabilized by Lutensol AT25, *Pal* is less sensitive to the nanoparticles than *Pch*. The lignin particles filled with the fungicide and stabilized by SDS showed a stronger effect on growth inhibition than for particles stabilized with Lutensol AT25. Furthermore, the lignin particles stabilized with SDS have almost the same germination inhibiting rate as the positive control. This indicated that SDS is partly contributing to the growth inhibition of the fungi.
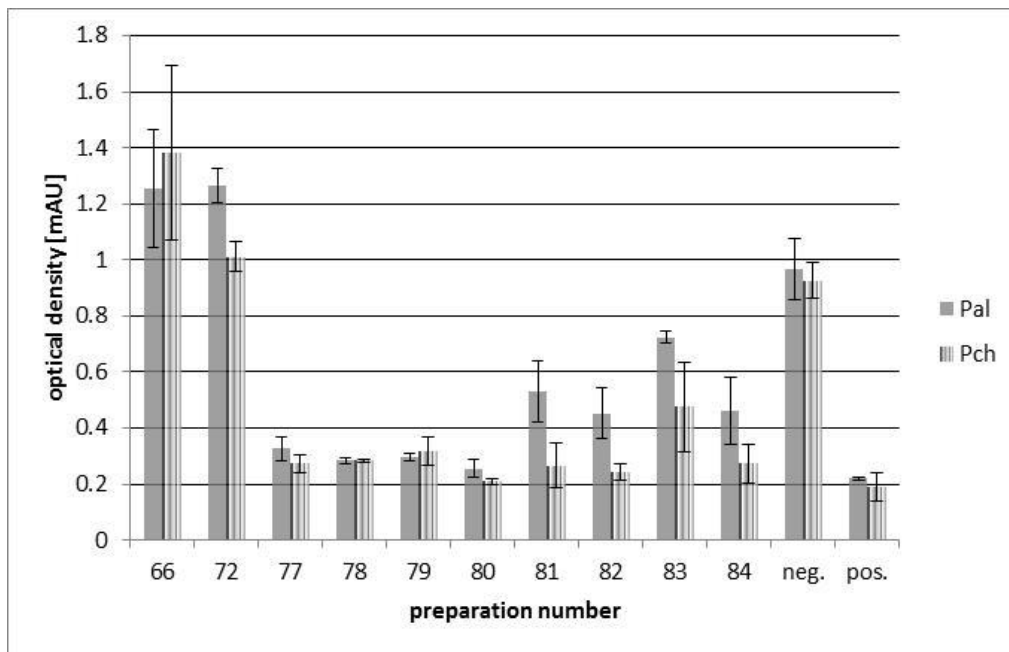
Figure 3.21 Microplate assay: spore germination and growth inhibition test on *Pa. aleophilum* (*Pal*) and *Pm. chlamydospora* (*Pch*), standard deviation n=12, neg. (negative control, sample with spores and without lignin particles); pos. (positive control, sample with 50 $\mu g \cdot ml^{-1}$ glufosinate-ammonium).

After the verification for the activity of the nanoparticles in vitro, the first tests in a vineyard were conducted together with Dr. Jochen Fischer (Institute of Biotechnology and Drug Research in Kaiserslautern). 3 ml of lignin nanoparticles dispersions were injected into grapevine plants showing early stage Esca symptoms as shown in Figure 3.22. The vineyard with all treated and untreated plants as well as the timeframe when the experiment was controlled and documented passed through summer time in 2014 starting from beginning of July 2014. Treated plants were randomly selected from the vineyard. Finally the treated plant with fungicide filled lignin particles reduced the severe effects of the Esca infection during the summer time. While the Esca symptoms increased on plants only treated with unloaded lignin particles showed only one out of eight plants after three month more distinct necrosis than at the beginning of our treatment. From this field test, it indicates that the lignin nanoparticles are attractive carriers for fungicide in agricultural applications.

In conclusion, the first curative treatment for Esca-infected grapevine plants was demonstrated. Lignin nanocarriers loaded with drug have been prepared via a Michael addition in miniemulsion with variable diameters (200-700 nm) and adjustable drug loading. The lignin nanoparticle dispersion was injected into the inflected grape plants. The injected plants were observed one year. As Esca secretes laccase, the nanocarrier can be degraded in planta and successfully releases the drug from the lignin carrier to cure the infected plant. This allows for the first time a targeted drug delivery in planta with specific enzymatic opening at the place of action to cure Esca.

Figure 3.22 Grapevine plant showing early stage Esca symptoms and injection of lignin particles dispersion after two weeks.

3.1.4 Potential application of lignin as bio-resource for carbon nanoparticles

In previous chapter, the targeted drug delivery of lignin nanocarrier is proven. Due to high carbon content of lignin resources, carbon material from the carbonization of lignin nanoparticles with porous structure is further investigated targeting for other applications reported in this chapter. The N_2 adsorption-desorption isotherms are used to study the effect of carbonization on the microstructure and surface area of the carbon material from the lignin nanoparticles. The specific objectives included evaluating: (1) thermal stability, (2) the physical and adsorption properties of carbonized lignin particles in term of the pore structure, surface chemistry and (3) methylene blue absorption capability by comparing the carbonized lignin material. In order to

3.1.4.1 Thermal stability

Firstly, thermal decomposition characteristics of lignin, MA-lignin and lignin particles with porous structure (prepared by a combination of miniemulsion and solvent evaporation with Luthensol AT25 as stabilizer in chapter 3.1.2) were investigated by thermogravimetric analysis TGA (weight loss of samples in relation to the temperature of thermal degradation) at a constant heating rate of 10 °C·min^{-1}. The degradation profile of lignin, MA-lignin, and lignin particles from miniemulsion are shown in Figure 3.23. The percentages of residual char at different temperatures were obtained from TGA (Table 3.6). The amount of char residue during thermogravimetric analysis under nitrogen decreased after the esterification of lignin and lignin nanoparticles formation. The main weight loss was in the broad range of 300-500 °C temperature. The percent yield of char was slightly decreased after 600 °C. In general, carbonization is a complex reaction process composed of elimination of volatile matters and structure reengineering within the remaining product.[164] For this reason, it was assumed that the carbonization temperature range of 300–500 °C was

not adopted in the experiment because major decomposition reactions occurred in this temperature region.

Table 3.6 Thermal decomposition characteristics.

Entry	Char residual (wt%)		
	300 °C	**600 °C**	**800 °C**
lignin	91	56	50
MA-lignin	97	52	44
lignin particles	96	36	33
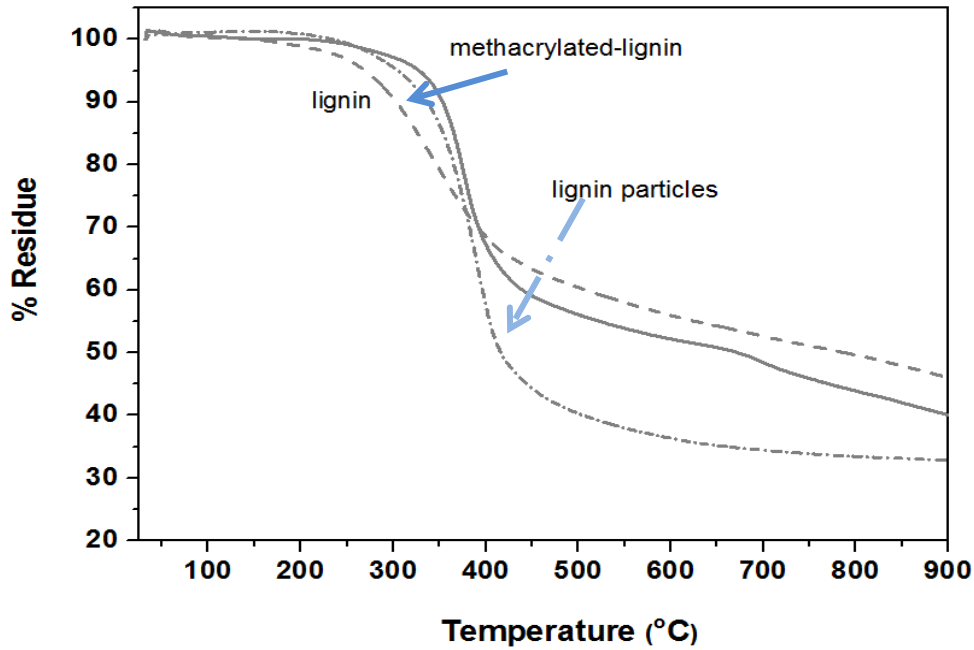
Figure 3.23 TGA of lignin and methacrylated-lignin under N_2 gas.

3.1.4.2 Characterizations of pore structure and surface chemistry of the carbon samples

The carbonization process was carried at 600 °C and 800 °C for 1 h in order to completely eliminate all volatile organic compounds. TEM were used to investigate the morphology of the carbon particles from lignin porous particles. The micro porous structure of the lignin particles has deformed to small fine carbon particles when the carbonization temperature was increased from 600 to 800 °C, as shown in TEM images (Figure 3.24).
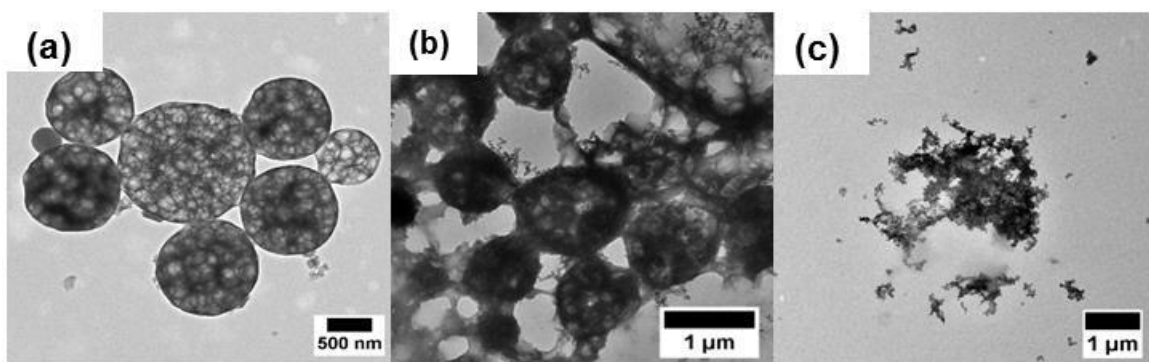
Figure 3.24 TEM images of lignin porous particles (a) before and (b)after carbonization at 600 °C , and (c)800 °C.

N_2 adsorption as determined by the Brunauer–Emmett–Teller theory (BET-N_2) and X-ray photoelectron spectroscopy (XPS) were applied to further understand physical and surface chemical properties of the carbons particles. Figure 3.25 illustrates the N_2 adsorption-desorption isotherms and pore sizes distributions of various samples obtained under different carbonization temperatures. As clearly seen, the lignin sample before and after carbonization, as well as lignin porous particles before carbonization (L49) exhibit all low adsorption capacities. By contrast, carbonized lignin porous particles at 600 °C (L49-600) and 800 °C (L49-800) display dramatically enhanced adsorption capacities, in particular at the low pressure region, indicating the presence of micropores inside; the characteristics hysteresis loop from L49-800 exhibits maximum adsorption capacity, suggesting probably the

embedded mesoporous structure. The BET surface area and pore size structures of the various samples are summarized in Table 3.7. Correspondingly, lignin porous particles after carbonization at 800 °C show the maximum BET surface area and micropore volume at 552 $m^2 \cdot g^{-1}$ and 0.274 $cm^3 \cdot g^{-1}$, respectively.
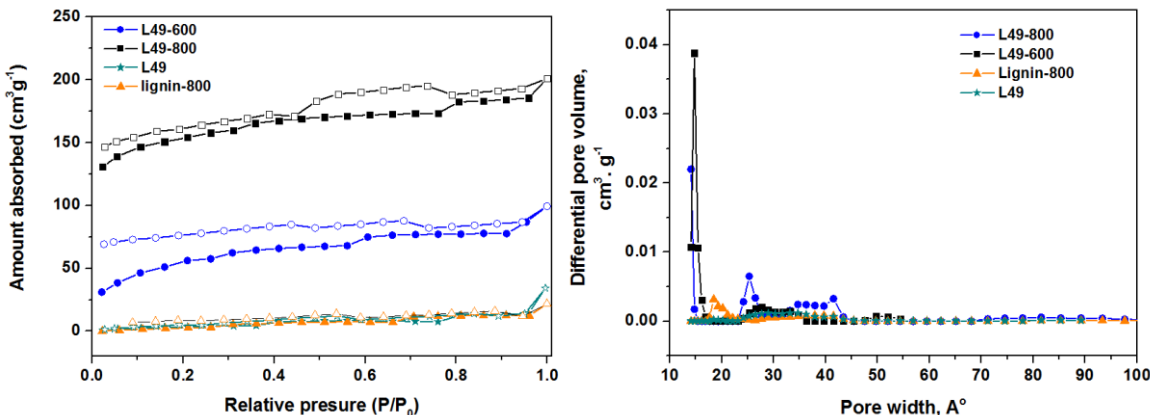
Figure 3.25 (left) Nitrogen adsorption (full symbols) and desorption (empty symbols) isotherms, and (right) pore size distribution of lignin porous particles before (▲) and after carbonization at 600 °C (●) and 800 °C (■) and lignin after carbonization at 800 °C (★).

Table 3.7 Pore structures parameter of lignin porous particles before and after carbonization at 600 °C, 800 °C, and lignin after carbonization at 800 °C.

Entry - Temperature	Surface area - BET $(m^2 \cdot g^{-1})$	Pore volume $(cm^3 \cdot g^{-1})$	Pore width $(Aver, A^0)$
lignin	5	0.017	16.5
L49	15	0.020	34.7
lignin-600°C	29	0.023	18.5
L49-600°C	202	0.123	14.7
L49-800°C	552	0.274	14.8

XPS can help to gain more molecular-level understanding in the carbonization of the lignin porous particles. As clearly seen in Table 3.8, after carbonization on lignin particles at 600 °C, and 800 °C, the oxygen atomic composition decreases from ~21.6% first to 17.2%,

and further even to ~8%, while a similar decreasing trend is also observed for pristine lignin before and after carbonization treatment. The relative decrease of the oxygen composition after carbonization can also be clearly identified in the survey and C 1s XP spectra in Figure 3.26: as seen in survey spectra (Figure 3.26 b), the C correlated photoemission peak becomes more intense (versus oxygen) for lignin particles after carbonization at 600 °C, and 800 °C. Correspondingly in C 1s spectra (Figure 3.26 d), the spectra weight for the oxidized carbon component (green) decreases dramatically after carbonization, while in the carbon material states, the dominant spectra contribution most probably comes from graphite (violet) with correlated binding energy at ~284.2eV. Very interestingly, it should be noted that the XPS-derived decrease of the oxygen atomic composition upon carbonization is not only occasional case, but presumably provides one "molecular-level" mechanism in this carbonization process: In MA-lignin (see Figure 5.3), the oxygen atoms mainly exist in the linking agent for further cross-linked lignin particles, their sacrificial lose upon carbonization clearly suggests the break of lignin polymer backbone, thus leading to the deformed lignin particles, as observed in TEM images (Figure 3-24). In addition, the breakdown of the lignin backbone can also explain the much increased adsorption capacities for carbonized lignin particles observed in BET-N_2 adsorption measurement (Figure 3.25 and Table 3.7), where larger BET surface area and micropores were formed by the backbone breaking of lignin particles.
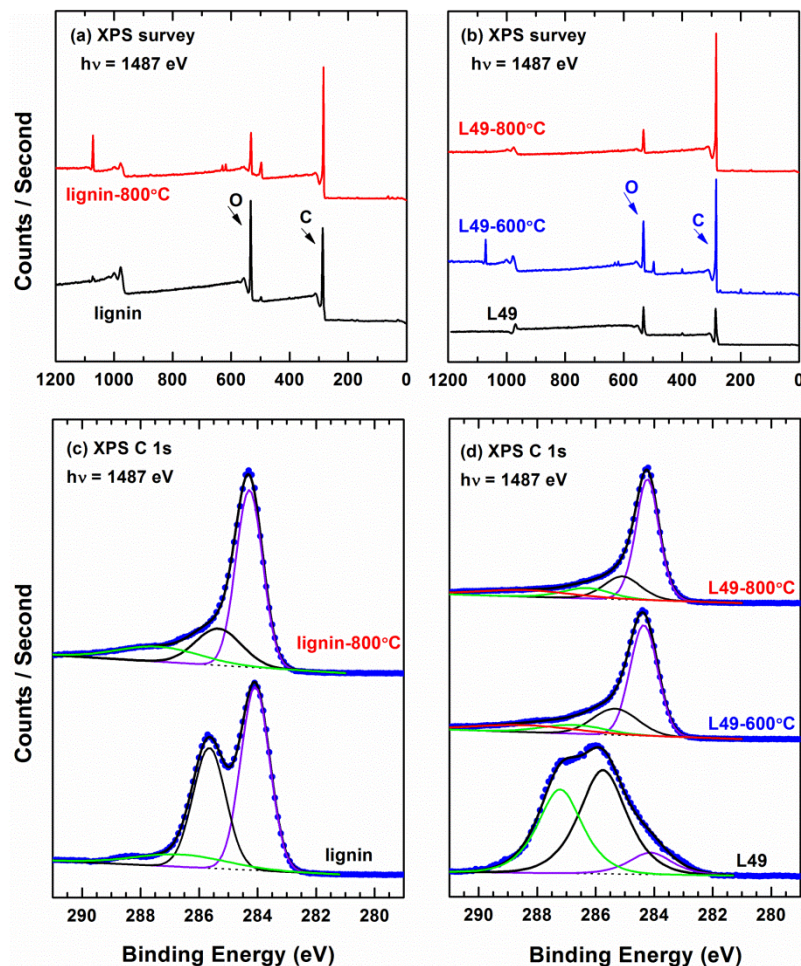
Figure 3.26 Survey (a, b) and C 1s (c, d) XP spectra of lignin and porous lignin particles before and after carbonization. The C 1s spectra were self-fitted with peaks assigned for individual carbon components: violet, sp_2 carbon, graphite; black, aliphatic carbon; green and red, oxidized carbon.

3.1.4.3 Adsorption of methylene blue dye on obtained carbon samples

The kinetic adsorption and adsorption ability of carbon particles from L49-800 had been compared with lignin raw material after carbonization at 800 °C by using methylene as a model of dye adsorbed. It was found that the kinetic adsorption of carbon particles from porous lignin particles has an adsorption rate faster and an adsorption capacity higher than lignin as seen in Figure 3.27. These results indicated that lignin particles from miniemulsion have a high potential to act as a precursor for carbon material.
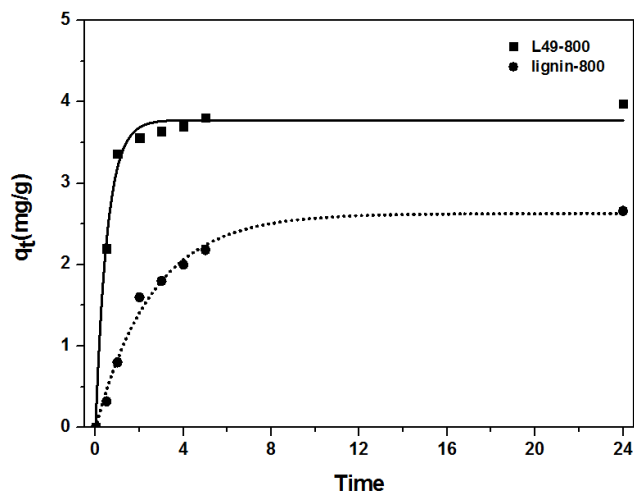
Figure 3.27 Kinetic adsorption of methylene blue for carbon from lignin (■) and lignin particles (L49-800) (●) after carbonization at 800 °C ; C_0 20 mg·l^{-1} at 25 °C.

3.1.5 Conclusion

Different approaches have been established to prepare enzymatically cleavable lignin nanoparticles, which can be loaded with hydrophilic and hydrophobic compounds.

The hollow lignin nanocontainers with an aqueous core have been firstly prepared by interfacial polyaddition in inverse miniemulsion. The cross-linked lignin nanocontainers can be loaded with hydrophilic substances which can be released by an enzymatic trigger from natural plant extracts revealing them as potential nanocontainers for agricultural applications.

Furthermore, lignin nanocarriers of variable morphology have been prepared by the combination of miniemulsion polymerization with a solvent-evaporation/ phase separation protocol. Solid nanoparticles, core-shell structures with a liquid core (hexadecane, plant oils) and a solid lignin shell, or highly porous lignin nanocarriers have been prepared. All systems were loaded with a hydrophobic cargo and it was found that the release behavior strongly depends on the morphology of the nanocarriers (with the solid nanoparticles exhibiting the slowest release, while the core-shell structures can be loaded with high amounts of lipids/fats). The addition of the enzyme laccase degrades lignin and strongly enhances the

release from the lignin nanocarriers, thus rendering these structures as highly interesting for future biodegradable drug delivery vehicles for agricultural applications.

This platform was further applied for fungicide encapsulation for treatment of Esca-infected grapevine plants. As Esca secretes laccase, the nanocarrier can be degraded *in planta* ("auto-enzymatic trigger") and thus releases the drug from the lignin carrier. This allows for the first time a targeted drug delivery in planta with specific enzymatic opening at the place of action to cure Esca.

In addition to drug delivery, the porous lignin nanoparticles were also carbonized. The resulting carbon particles exhibited a high surface area of 552 $m^2 \cdot g^{-1}$ and showed efficient adsorption of methylene blue.

These results prove that the abundant biopolymer lignin can be used as an efficient reagent for the preparation of nanoparticles with variable morphology that can be applied in agriculture as biodegradable drug carrier or as adsorbent after carbonization.

3.2 Uptake polymer nanoparticles in plants

This thesis focuses mainly on using lignin nanoparticles as carrier in agricultural applications. This section shows the influence of polymer nanoparticles on the plant (mung bean) growth and their transportation and distribution in the plant cell. The polystyrene encapsulated magnetic nanoparticles and lignin particles were used in the experiments.

This chapter is currently being prepared for the submission as scientific publication with the title "Nanoparticles as a Delivery Vehicle for Plants". It will be published when this thesis is published.

3.2.1 Influence of the nanoparticles on the germination and growth of mung beans

The development of agricultural technology has currently changed to a modern trend technology for supporting the rapid increase in farm productivity. Among the latest technology, nanotechnology takes predominated position in agriculture and food production.[165] At present, the main attractive of research in nanotechnology is in the field of electronics,[2] energy[3] and medicine.[4] Experiences gained from these fields of nanotechnology promote also a change in agriculture. Nanotechnology allows broad advance in agricultural research and development[166] such as genetic improvement of plants,[167] early detection of pathogens and contaminants in food products,[165] smart delivery systems for agrochemicals like fertilizers and pesticides[168] and delivery of genes and drug molecules to specific sites at the cellular level.[169, 170] These smart systems deliver active molecules in a controlled and specific manner to the target site similar to drug delivery in mammals.[171-173] The reports on the uptake mechanism and application of the nanoparticles as a delivery vehicle in the mammalian system and knowledge on uptake pathway, sub-cellular localization has increased dramatically in the last decade.[174-178] In contrast, only few reports have been published for nanoparticle uptake in plants mainly dealing with unwanted uptake, i.e. by

pollution. Some works have reported the uptake, translocation, and accumulation of nanoparticles in plant for example Zhu et al. demonstrated the absorption of iron oxide nanoparticles by pumpkin plants[179] and Dan and coworkers reported the uptake and accumulation of gold nanoparticles by tomato.[180] However, there remain numerous unresolved issues with respect to understanding their potential effects on plants and the environment including plant cell uptake, which should be systematically examined before application of these nanoparticles. Especially drug delivery in plants mediated by nanoparticles is a rather neglected field in literature.

In this study, magnetite nanoparticles coated with polystyrene PS-FeNPs from the work of Bannwarth et al.[181] and lignin particles LN-NPs (Figure 3.28) were chosen to investigate the effect of two different types of polymer nanoparticle on plant growth. Finally the penetration and movement of the nanoparticles were analyzed in specific part of the pant. The properties both nanoparticles are given in Table 3.8.
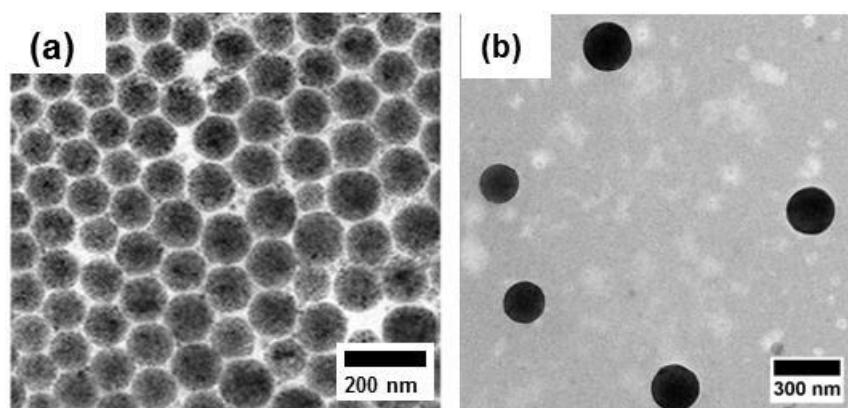
Figure 3.28 TEM image of polystyrene particles with encapsulated iron oxide (a), lignin particles (b).

The mung bean was selected as a model plant due to reliable and easy germination. The PS-FeNPs were chosen because of its biological compatibility, stability, and its potential use due to the magnetic stimulus.[181] Moreover, the iron can be quantified for example by atomic absorption (AA)[182] or inductively coupled plasma (ICP)[183] after the digestion of the biomass. Electron microscopy methodologies can also be used to localize the metal nanoparticles inside the plant.[184] In addition to the PS-FeNPs, biodegradable lignin

nanoparticles were also studied with respect to the uptake and the effect on the plant, since lignin is an attractive material for the smart delivery in agriculture as it is enzymatically degradable.[127] Different methods were used to monitor the uptake and distribution of the LN-NPs into the plant: an UV-active fungicide (pyroclostrobin) was loaded into the lignin nanocarrier (compare experimental) and quantified HPLC of parts of the plant.

Table 3.8 Data of the nanoparticles used for uptake study.

Sapmle	Surfactant	Sized (nm) from DLS	Solid content (wt%)
PS-FeNPs	SDS	124±49	1.4
LN-NPs	SDS	160±57	1.0

To test the influence of polystyrene coated magnetic nanoparticles and lignin particles on germination and development of crop seedlings, The bean seeds were incubated with the nanoparticle dispersions during the germination, growth and further development of the plant (until 7 days). Similar size of mung bean seeds were chosen after 2 days of germination and incubated with different concentrations of the dispersion of PS-FeNPs, LN-NPs, and pure water as control. After incubation at 30 °C for 5 days in a dark warm place, the mung bean sprouts were harvested. The root elongation was significantly inhibited by PS-FeNPs at both concentrations (1.4 and 2.8 mg·ml^{-1}) after the germination step for 2 days, compared to the pure-water treated group as shown in Figure 3.29 (a) and for 5 days in Figure 3.29 (b). Exposure to LN-NPs treatment had not significantly impact on stem elongation as compared to unexposed water control.

The stem length was carefully measured and recorded as shown in Figure 3.30. After 5 days of incubation and growth, incubated in 1.4 and 2.8 mg·ml^{-1} of the PS-FeNPs, the growth was reduced by 21% (from 63 to 50 cm) and 47% (from 63 to 32 cm) respectively, relative to the control incubated in water. In the case of LN-NPs at higher concentration (5 mg·ml^{-1}) it showed a slightly decrease stem length even through lignin known as a non-toxic material and biocompatible.

Figure 3.29 Photos of mung bean seeding incubated in water, 1.4 and 2.8 mg·ml^{-1} of the polystyrene encapsulated iron oxide nanoparticles (from left to right) after 2 days (a) and 5 days (b).
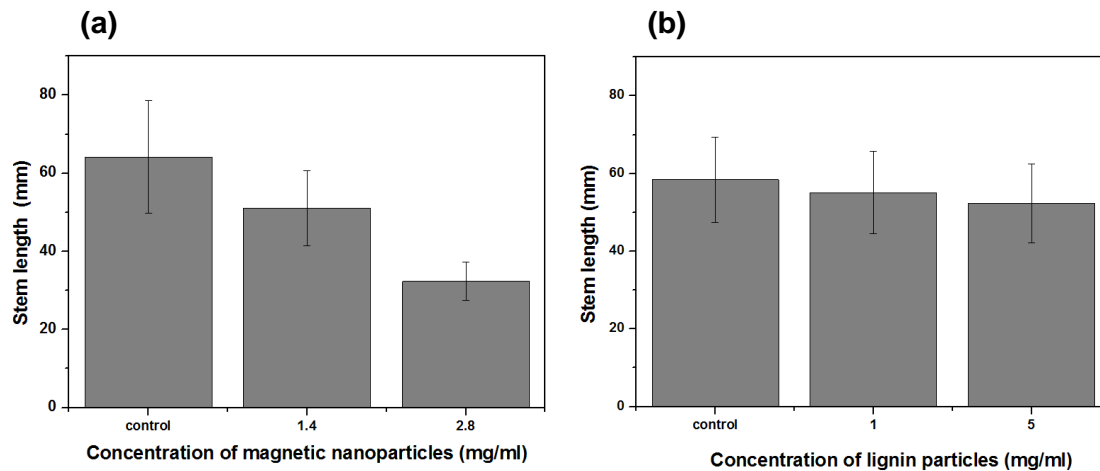
Figure 3-30. Stem length of mung bean in the presence of water (control), 1.4 and 2.8 mg·ml^{-1} magnetic nanoparticles (a), water (control) 1 and 5 mg·ml^{-1} lignin nanoparticles after 5 days of the nanoparticles exposure (b).

In addition, to further monitor the plant seed germination, the level of moisture in the bean sprouts was measured by weighing before and after freeze drying. Seeds contacted to both nanoparticles had no significant change level of water in the sprout. This fact indicates that magnetite and lignin nanoparticles could not affect the water uptake of mung beans during germination step.

At the end of experiment, the different parts of the mung bean sprouts were freeze dried, ground to small pieces, and digested by with HNO_3 and H_2O_2 method for determination the iron amount in the young plant. An accumulation of the nanoparticles were clearly detected by the magnetite content via ICP measurement which decreased in order root > cotyledon > leaf $\geq$ stem (Fig. 3.31). These results indicate that the polymer nanoparticles filled with magnetite in the range of 100-500 nm can penetrate into the mung beans; however the majority of the nanoparticles remain in the root of the plant. The result of the nanoparticles penetration was confirmed by work from Peng J. et al.[185] They used confocal imaging to prove the penetration of rare-earth upconversion nanophosphors to the thick seed coat and were taken up into seeds. From these results, it indicated that nanoparticles can penetrate through the seed coat or opening of the seed coat during its germination and then finally take up and accumulate inside seeds.
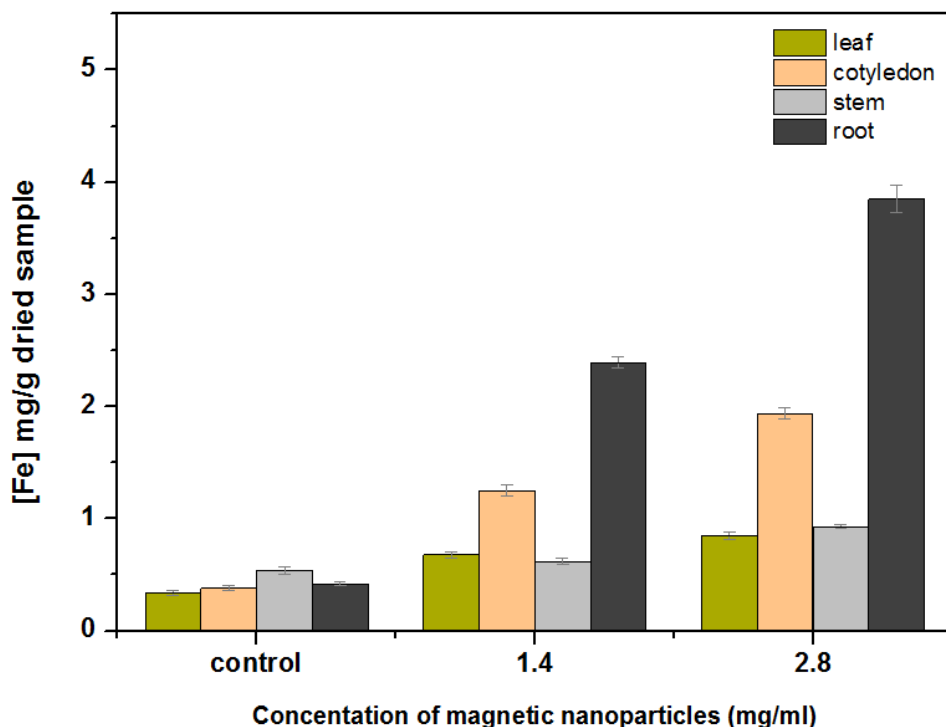
Figure 3.31 The concentration of Fe in separated part of mung bean sprouts after expose to magnetite coated polystyrene for 5 days.

3.2.2 Uptake and distribute of the nanoparticles in plant

To investigate the transportations and accumulation of the nanoparticles in plants, a penetration of the PS-FeNPs and LN-NPs was introduced by the incubation (by root system) and injection (to stem or truck system) method as shown in Figure 3.32. Mung bean plants were grown *in vitro* by hydroponic system. When the plants developed the second leaves pairs, the PS-FeNPs were applied to the plants by the incubation method with 2 ml of the nanoparticles at 2.8 mg·ml^{-1} and watered with 1 ml of water every day. Firstly we questioned that the nanoparticles can be taken by the root system and reach a vascular cylinder. Samples of the roots and leaves were collected after 14 days of the incubation with PS-FeNPs. It was found that the Fe content in root expose to 5.5 mg·g^{-1} dry tissue which is 5 times higher than in stem and leaf (Figure 3-33).
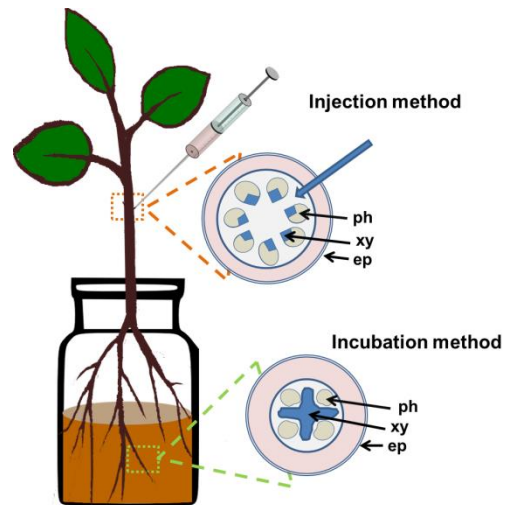
Figure 3.32 Scheme of the nanoparticles application to the plant cell. Diagram showing cross section of the roots where the nanoparticles were absorbed by incubation method and cross section of stem showing the point where the nanoparticles were applied by injection method. ep, Epidermis; xy, xylem vessels; ph, phloem vessels.
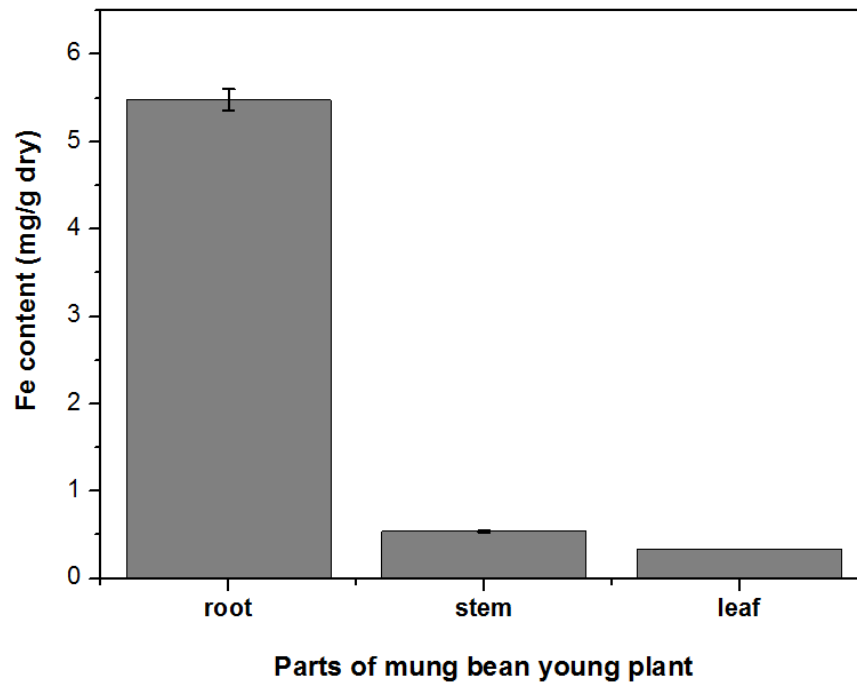
Figure 3.33 The concentration of Fe in separated part of mung bean plant after incubation with magnetite coated polystyrene nanoparticles for 14 days.

Figure 3.34 shows as further confirmation the presence of PS-FeNPs in root and leaf cells. It shows clearly the accumulation of the magnetite nanoparticles in the cross section of root and leaf tissue. The nanoparticles appeared freely to be aggregated and surrounded with intracellular components in the cytoplasm of root cell, although the conditions employed for sample fixation were not optimized for membrane preservation. By the sample preparation for the TEM, the leaf cell collapsed so it could not see clearly where the nanoparticles located whether inside or outside of the cytoplasm of the leaf cell. Concurrently, the elemental composition of the dark regions in the cells was analyzed by energy dispersive X-ray spectrometer (EDX) (Figure 3.35) and confirmed the presence of the Fe in the leaf. These results indicated that the incubation of the root in the nanoparticles dispersion provide a probability to get the nanoparticles into the root and transport them to the leaves system.
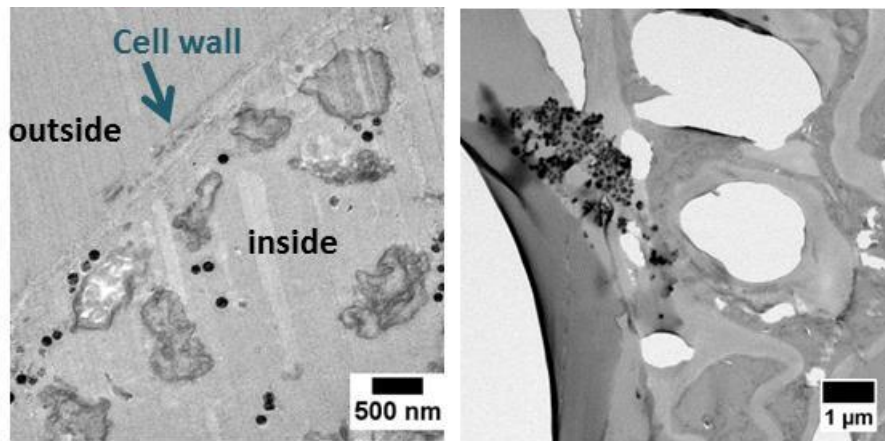
Figure 3.34 TEM images of the root (right) and leaf (left) cross section (some damage from cutting and beaming process shown as white holes) of the mung bean plant after incubation with the magnetite coated polystyrene nanoparticles for 14 days.
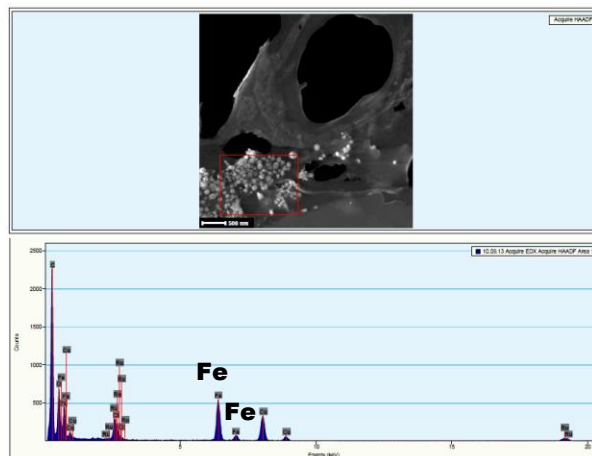
Figure 3.35 TEM-EDX measurement with of leaf mung bean cross section.

From previous work there are several mechanisms that have been explained the uptake of the nanoparticles in plants, however which nanoparticles and which conditions are important to enhance the uptake of the living plants is still unclear.[186] Unlike animal cell, plant cell are surrounded by extra barrier, called the cell wall, which has a pore diameter in the rage of 5-20 nm and determines its sieving properties.[187] Thus nanoparticles or nanoparticle aggregates with a size smaller than that of the largest pore could enter the cell wall and reach the plasma membrane.[188] A range of 100-300 nm of both nanoparticles was applied in this study which is larger than the pore diameter of the cell wall. This might indicate that the permeability of the cell wall can be enhanced during the interaction with nanoparticles resulting in the enlargement of pores or the induction of new pores for the entry of the nanoparticles and reaching the membrane. Nanoparticles can also enter plant cells by binding to carrier protein through aquaporins or ion channels. With regard to a pathway of the uptake nanoparticles to cells, previous work from Wang [189, 190] demonstrated clearly an endocytosis as one of the transmembrane pathway for CuO nanoparticles uptake in plant.

A further analysis was performed to confirm the presence of lignin biodegradable nanoparticles. The LNPs were applied to the plants by the incubation method with the LNPS dispersion at 5 mg·ml^{-1} concentration. Separated part of mung bean plant were determined its content of pyraclostrobin fungicide. HPLC quantification proved the existence of fungicide pyraclostrobin filled lignin particles as show in Figure 3.36. By an incubation method through root system the highest content of fungicide found in the root and followed by stem

and leaf. This result confirmed our results for the penetration of the LNPs nanoparticle to the root and translocation throughout the vascular system to the stem and finally leaves as our result from the penetration of PS-FeNPs in the previous discussion.
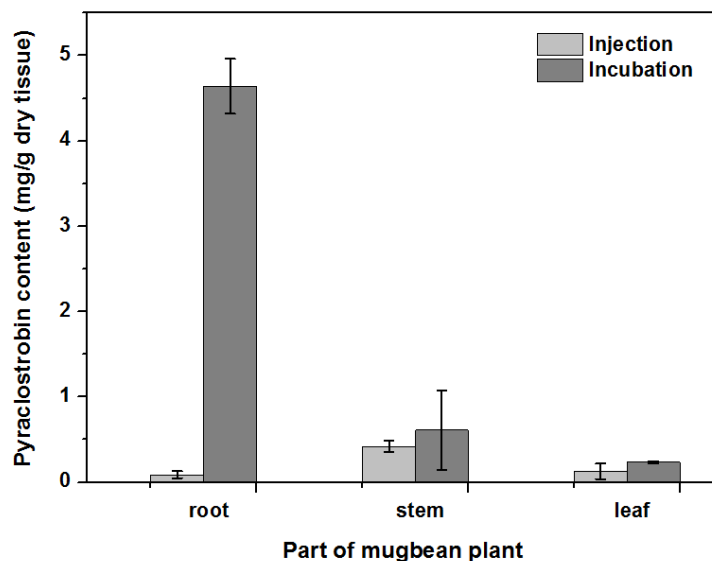
Figure 3.36 The content of pyraclostrobin fungicide in the tissue of the mung bean plants with different applications of lignin nanoparticles.

For some of the potential applications of lignin nanoparticles in plants, such as diseases control and genetic engineering, the localization of lignin nanoparticles in shoot organs is of interest as well. The LNPs (1 ml of 1 wt% solid content LNPs dispersion) were injected into the stem of mung bean plant (the second leaves pair growth stage). After two week, the content of pyraclostrobin was still found more in the stem tissue than in other tissues. However even the plant was injected at the stem part, the pyraclostrobin was also detected in the root tissue as shown in Figure 3.36. This result indicates that the fungicide can transport throughout vascular vessels inside the whole plant. Nevertheless, we cannot confirm that fungicide translocate as released molecules or in form of fungicide filled lignin nanoparticles. However since lignin nanoparticles can penetrate and bring active molecules into plant cells, it shows a potential to use lignin nanoparticles as a delivery vehicle for agrochemicals. Also the low transport in the plant is beneficial, as the drug remains in the root, hindering pathogens to enter the plant. In addition the low amount of nanoparticles

found in the leaf (and probably in fruits) makes this strategy interesting for future treatment of plant diseases.

Finally the effect of the application of nanoparticles on the subsequent growth of the plants was investigated. Some treated and untreated plants were kept under controlled conditions. There were no apparent differences between plants subjected to the treatment and the control plants, which indicated that treatment with nanoparticles did not impact a toxicological effect on plant growth.

3.2.3 Conclusion

Magnetite coated polystyrene and lignin nanoparticles interact with living plants: they can be taken up by the roots or can be injected into the stem. Different positions of mung beans have been investigated for nanoparticle amounts. To the best of our knowledge, this is the first report on the study of biodegradable polymeric nanoparticles in planta. In summary, most nanoparticles are found in the root however, some nanoparticles were transported to leaves probably via the xylem. Interestingly, they could be translocated from leaves back to roots via phloem in vascular transportation of plant after injection into the stem. Preliminary studies indicated that lignin nanoparticles did not show a pronounced effect to the germination step of the mung bean seeds, while the polystyrene encapsulated magnetite nanoparticles reduce the growth. The uptake in the plants' root could be a beneficial strategy for the treatment of plant diseases with drug-loaded nanoparticles hindering pathogens entering the plant via the roots.

3.3   Glutathione responsive nanocarriers

In previous chapter (3.1), laccase enzyme responsive nanocapsules from lignin were successfully prepared by polyaddition at the droplet interface in inverse miniemulsion process. One of the advantages of miniemulsion route to prepare capsules is that many reactions can be carried in the process as described in the theory chapter. Thus a capsules formation via click reactions at the interface of the droplet and kinetic of the reactions for glutathione responsive nanocarriers is presented in this chapter.

This chapter is submitted for a publication. (Yiamsawas D, Wagner M, Landfester K, Wurm FR. Competing and Simultaneous Click Reactions at the Interface and in Solution)

The synthesis of nanoscale biocompatible carriers that are able to release encapsulated material within an intracellular environment in a controlled way still remains a challenge. Disulfide linkages have emerged as an alternative route to fabricate cleavable carriers for drug delivery. Degradation of the carrier through reduction of the disulfide bond is triggered by the presence of glutathione (GSH)-a thiol containing tripeptide. Due to the difference in extracellular and intracellular concentration of GSH (2–20 μmol $\cdot$l^{-1} vs 1^{-10} mmol$\cdot$l^{-1}), degradation mainly takes place in the cytoplasm, thus enabling release of the material exclusively inside the cell. Many kinds of methods have been used to introduce the disulfide moiety to the vehicle shell. Recently, the formation of glutathione responsive vehicles was achieved through the interfacial thiol–disulfide exchange reaction between dithiol DNA oligonucleotides (20 bases) and disulfide groups of a comonomer 1,4-bis (3-(2-pyridyldithio)propionamido)-butane (BPB).[191] However the kinetics of competing for both reactions has not been investigated in detail. In this section the kinetics of the thiol–disulfide exchange and the thiol-maleimide "click" will be presented both in solution and at the interface.

3.3.1 Competing and simultaneous click reactions at the interface and in solution for glutathione responsive material

Chemistry for biomedical applications requires modular and specific reactions under mild, aqueous conditions. The thiol-ene reaction is an attractive approach for bioapplications, as it can follow ''click'' characteristics and is inert to most functional groups in biomolecules, but can also selectively be used to address cysteine residues for example.[192, 193] The thiol-ene reaction has been used for dendrimer synthesis,[194] nanoparticle modification,[195] or polymer post modification.[196] Thiol-ene reactions can proceed via a Michael-type addition (catalyzed by acids, bases,[197] or nucleophiles[192, 198]) or by a radical pathway[199, 200] and they can be conducted in polar solvents such as water, alcohols, or dimethylformamide (DMF).[201] The main highlight of this reaction is a wide range of suitable substrates, including activated and non-activated olefins, as well as multiply-substituted double bonds.[193, 202] However, all thiol-ene reactions lead to stable thioether linkages. The combination with another efficient reaction that allows the introduction of cleavable dithiol bonds would be attractive for the design of drug-polymer conjugates or biodegradable nanocarriers. The thiol-disulfide exchange reaction[203, 204] (due to the reversible cleavage and formation of a new covalent S-S bond) is a powerful tool to be combined with thiol-ene reactions. A recent report from our group demonstrated the successful synthesis of biocompatible DNA-based nanocarriers through the interfacial thiol-disulfide exchange and interfacial click of thiol-ene reactions in inverse miniemulsion.[205] This strategy allowed the combination of an efficient polyaddition and polycondensation with the cleavability of S-S-bonds in biological environment, however, the kinetics of the two concurrent reactions remain unclear. As both, the thiol–disulfide exchange and the thiol-maleimide "click", require the same intermediate, i.e. the thiolate anion, their reactions kinetics are essential to understand in concurrent reactions. The thiol-maleimide reaction requires the initial formation of the thiolate anion[206, 207] (Figure 3.37). The mechanism of thiol-disulfide exchange also involves the initial ionization of the thiol to thiolate anion. To the best of our knowledge, there is no report the kinetic study of the two competitive "click" reactions -thiol-maleimide addition and thiol-disulfide exchange.
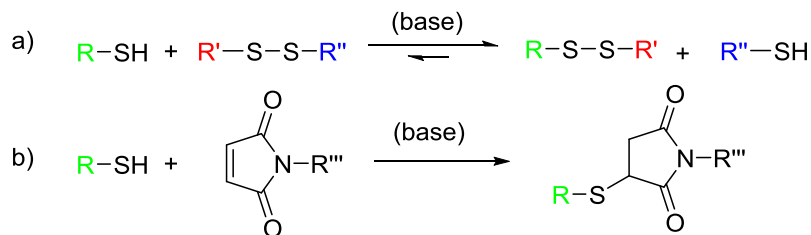
Figure 3.37 a) Thiol-disulfide exchange reaction (with R'' as a good leaving group, e.g. pyridine-2-thiol); b) Thiol-maleimide reaction (nucleophilic addition).

In this study, difunctional molecules were used, i.e. a difunctional pyridyldisulfide (**1**), a dimaleimide (**2**), and a dithiol (**3**) to investigate the concurrent polyaddition/-condensation of the three monomers. The kinetics of the two reactions were studied both in solution and in a water-in-oil miniemulsion. Bucillamine (**2**) with two thiol groups (pKa values 8.39 and 10.22) is selected as a model drug and monomer for the kinetic study. It can both react as a B_2-monomer with 1,4-bis-(3-(2-pyridyldithio)propionamido) butane (BPB, **1**) or 1, 1′-(methylenedi-4,1-phenylene) bismaleimide (**2**) as the respective A_2-monomers (Figure 3.38). Since two thiols of monomer 3 have a different reactivity also the final products include additional structural isomers. First, we investigated the reaction kinetics of both reactions separately in solution. Then, the reactions were investigated in an oil-in-water miniemulsion (i.e. in the presence of a surfactant) with stable aqueous nanodroplets containing **2** and a continuous chloroform phase containing **1** and **3**; the reaction takes place at the water-oil interface of the (Figure 3.39).
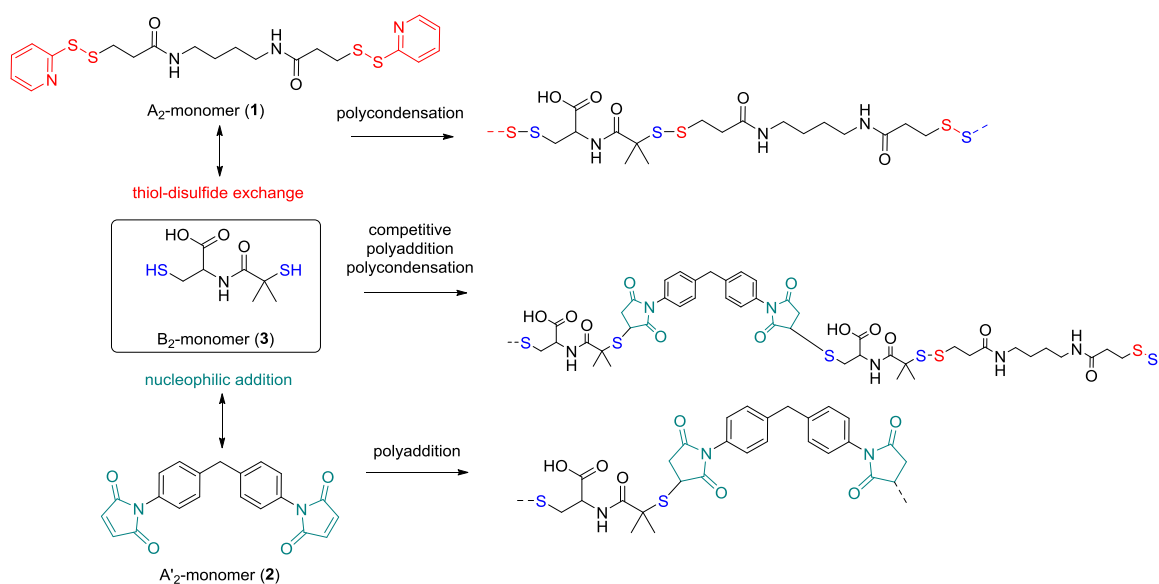
Figure 3.38 Structures of the three difunctional monomers used in this study (A$_2$-monomer: 1,4-bis-(3-(2-pyridyldithio)propionamido) butane (**1**); A'$_2$-monomer: 1,1′-(methylenedi-4,1-phenylene) bismaleimide (**2**); B$_2$-monomer: bucillamine (**3**)) and their reaction pathways.
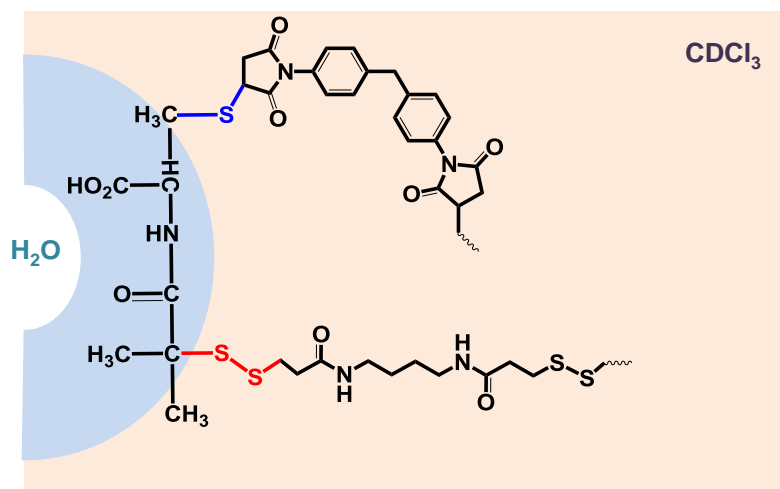
Figure 3.39 Scheme competitive click reactions between A2 and A'2 with B2 at the interface of a droplet.

3.3.1.1 Kinetics evaluation

In this study, we exploit the advantages of real-time NMR spectroscopy which is a well-established method for monitoring reaction kinetics. The use of ^{1}H NMR spectroscopy to study real time polymerization both in solution and inverse

miniemulsion polymerization has been previously successful reported from our group for both chain and step growth polymerization.[208, 209] Herein, the *in situ* kinetic measurements of dual the thiol–disulfide exchange and thiol-maleimide reactions were measured over a period of 600 min. All reactions in solution were carried out in deuterated tetrahydrofuran (THF-*d8*) and in inverse miniemulsion in chloroform-*d* (CDCl$_3$-*d*) as a continuous phase and deuterium oxide (D$_2$O) as the dispersed phase. Triethylamine (TEA) was used as a basic catalyst. The reactions were carried out with a delay time of approximately 5 min between each spectral acquisition. In typical reaction, 2 eq. of bucillamine, 1 eq. maleimide, and 1 eq. disulfide were added into the NMR tube containing 0.75 ml of deuterated solvent. The evolution of the integral of specific protons of each reactant was followed over time and compared to an inert internal standard (0.13 ppm from hexamethylcyclo trisiloxane). The maleimide resonance of **2** at 6.9 ppm was monitored for the thiol-maleimide and the resonances of the pyridine ring of **1** (at 8.4 ppm) were monitored for the thiol-disulfide interchange, respectively. Figure 3.40 presents an overlay of ^{1}H NMR spectra for ^{1}H NMR spectra of dual reaction thiol-disulfide interchange and thiol-maleimide click reaction in solution and in miniemulsion. The results of the consumption of disulfide and maleimide by the integration over time are plotted in Figure 3.41.

In thiol-disulfide interchange reactions, a thiol is exchanged with a reactive disulfide, resulting in the formation of a new disulfide by the release of pyridine-2-thiol. This reaction reacts as a nucleophilic displacement, the thiol nucleophile (thiolate anion) attacking the electrophilic disulfide. The rate of this reaction is dependent on the nucleophilicity of the thiol (RSH – note: in the case of 2 both thiols have a slightly different nucleophilicity which was not considered in all reactions). As a nucleophilic addition, also the thiol-maleimide addition depends on the nucleophilicity.
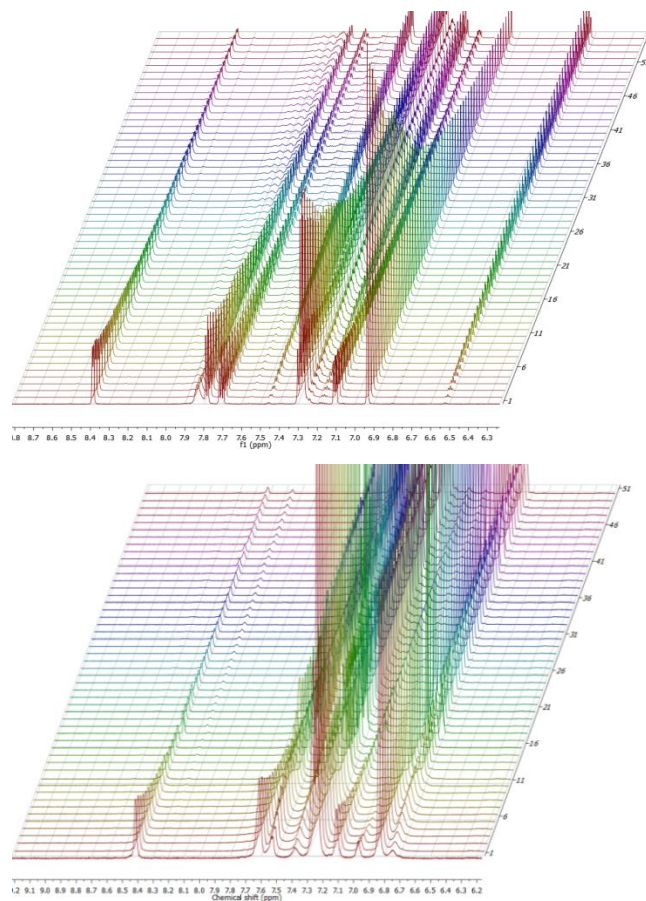
Figure 3.40 Overlay of ^{1}H NMR spectra of the two competitive reactions: thiol-disulfide exchange and thiol-maleimide click reaction in THF-d_8 (upper) and in miniemulsion (lower) at 700 MHz, 283 K.
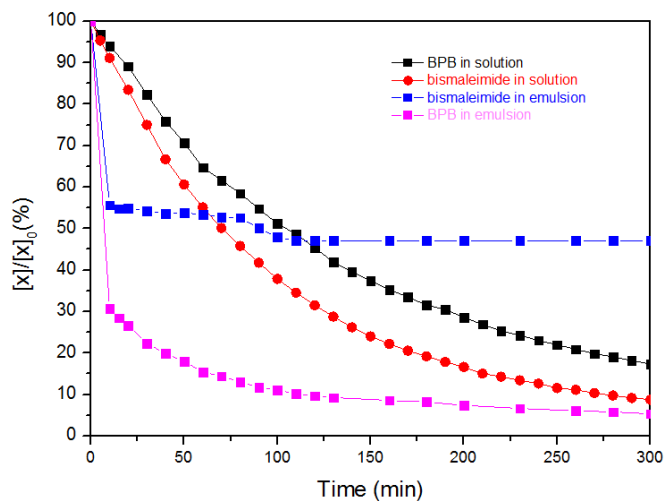
Figure 3.41 Comparison of kinetic profiles for the simultaneous reactions of thio-disulfide interchange and thiol-maleimide in solution and miniemulsion system.

3.3.1.2 Effect of base catalyst

As an additional factor, different base (TEA) concentrations were examined in the solution system. It was found that both kinetic profiles prove the significant effect of TEA promoting the thiol-maleimide reaction. In contrast, the thiol-disulfide exchange reaction proceeds already without the addition of the catalyst with very fast reaction kinetics in THF (at 298 K). The consumption of 1 reached more than 90% after five minutes at ambient temperature (298K) which was too fast to be measured by NMR (due to time losses for locking and shimming). An increase of the reaction rate of thiol-maleimide was observed as the TEA concentration in the reaction was increased at 298 K both in solution (THF) and in miniemulsion as shown in Figure 3.42. However, the reduction of the temperature to 283K and the addition of 2 eq TEA in solution, allowed bringing both reaction kinetics closer to each other as show in Figure 3.43.
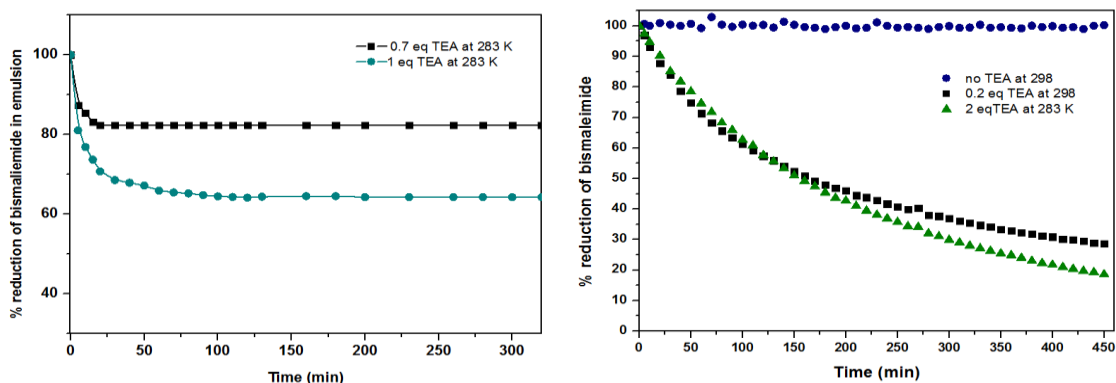
Figure 3.42 Real-time ^{1}H NMR measurements of the thiol-maleimide reaction in solution with different amounts of TEA as catalyst, (right) measured in THF, [3]=[2]= 0.013 mol·l^{-1}) and in miniemulsion (left, 283 K).
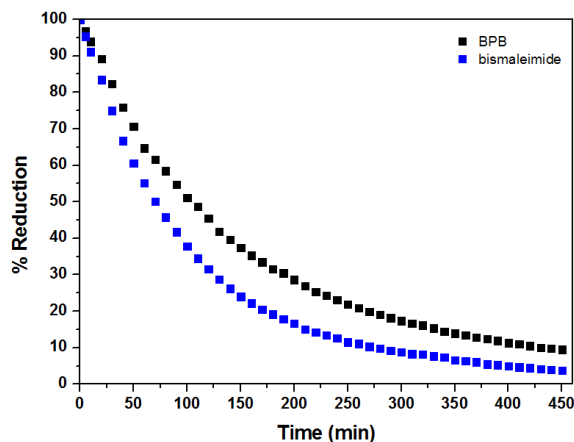
Figure 3.43 Real-time ^{1}H NMR measurements of for the simultaneous reactions of thio-disulfide interchange and thiol-maleimide with 2 eq. of TEA in solution at 283 K.

To determine the reaction order of both reactions, the different reaction rate equations for first-, and second order reactions can be considered as following:

$$\frac{dx}{dt} = k(x)^n$$

$$\ln[x]_t = -k_1 t + \ln[x]_0 \quad , n=1; \text{ first-order reaction}$$

$$\frac{1}{[x]_t} = -k_2 t + \frac{1}{[x]_0} \quad , n=2; \text{ second-order reaction}$$

Based on the equations of the rate law, linear plot fitted the best for the first hour to the second-order in the solution system for both thiol-maleimide reaction and the thiol–disulfide exchange. When rate constants (k_2) of the thiol-maleimide reaction were examined as a function of the catalyst concentration, an increase of the rate was observed as the TEA concentration in the reaction was increased. The summarized value can be observed in Table 3.9. The reaction between **2** and **3** was accelerated from 0 to 0.0066 min^{-1}·mol^{-1}·l^{-1} as the amount of TEA was increased from 0 to 0.2 eq. at 298 K. For lower temperatures (283 K), a very similar reaction kinetics was achieved when the amount of TEA was increased to 1 eq. When the same reaction was performed in inverse miniemulsion at 283 K (0.10 ml D$_2$O and 0.65 ml chloroform, conc 2= 0.056 mol·l^{-1}, conc 3 = 0.011 mol·l^{-1}) the initial reaction speed for different TEA concentrations is increased by a factor of ca. 4 , however, after a certain period of time the bismaleimide concentration remained constant. This might be due to the

formation of an insoluble polymer-membrane at the interface of the droplets, i.e. the formation of nanocapsules as seen in Figure 3.44, which terminates the polyaddition.

In the miniemulsion, also for the competitive reactions, a drastic increase of the reaction kinetics can be observed (0.65 ml CDCl$_3$, 0.1 ml water and with 1:1 eq.of TEA:monomer 3 in aqueous phase.). Also very obvious is the much faster thiol-disulfide exchange leading to almost full conversion of 1, while again the slower reaction kinetics of the thiol-maleimide addition leads to incomplete consumption of 2 as the polymer membrane probably hinders the reaction to go to completion. More than 70% reduction of 1 was observed in the first 10 min, after that the rate decreased, but the reaction still continues. In the case of thiol-maleimide reaction, the rate of reaction seems to be very similar to the thiol-disulfide exchange for the first 10 min. As in contrast to solution polycondensations/-additions, the interfacial reaction setup is rather independent of the monomer stoichiometry to generate polymeric material, the formation of a polymer membrane is very likely, leaving unreacted 2 and 3 (acting as cargo) behind, while the nanocapsule wall is mainly formed from the polycondensation product of 1 and 3, with several units stemming from the polyaddition product of 2 and 3 (Figure 3.44 shows the TEM image of the nanocapsules obtained from this process).

Table 3.9 Kinetic rate constants (k) and linear fitting values (R) describing the kinetics of thiol-disulfide interchange and thiol-maleimide click reaction.

Kinetic order	Rate constant	Thiol-disulfide @283 K	Thiol-maleimide		Dual	
			0.2 eq TEA @ 298 K	1 eq TEA @283 K	Disulfide @283 K	Maleimide @283 K
	Solution					
1	**k_1 (min^{-1})**	0.0105	0.00556	0.00485	**0.00721**	**0.01006**
	R	0.972	0.997	0.997	**0.99445**	**0.99861**
2	**k_2 (min^{-1} mol^{-1} l)**	**0.01534**	**0.00657**	**0.00561**	0.00892	0.01359
	R	**0.9917**	**0.99841**	**0.99869**	0.98238	0.98912
	Miniemulsion					
1	**k_1 (min^{-1})**	0.02402	-	0.01939	0.08092	0.03623
	R	0.9959	-	0.77874	0.63287	0.42648
2	**k_2 (min^{-1} mol^{-1} l)**	**0.03127**	-	**0.02278**	0.07048	0.04974
	R	**0.9969**	-	**0.81509**	0.62503	0.4939
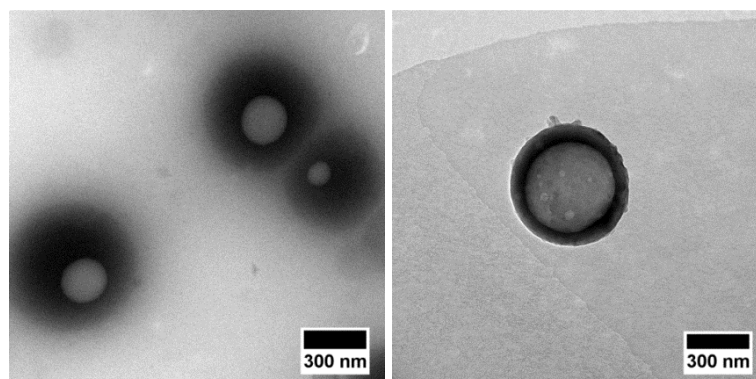
Figure 3.44 TEM images of the reaction products obtained by thiol-maleimide reaction (left) and two competitive reactions (right).

3.3.1.3 Characterization of the polymer structure

The evolution of the molecular weight for the dual reaction in solution and emulsion was followed by GPC. It was found that the final products for the competitive "click" polyaddition/condensation is lower for the solution setup (oligomers with 1,500 $g \cdot mol^{-1}$) than for the miniemulsion setup (4,600 $g \cdot mol^{-1}$).

The results of the total correlation spectroscopy (TOCSY) and ^{1}H NMR experiment for product of dual reactions in miniemulsion, are shown in Figure 3.45 where the proton resonances that are coupled to each other are outlined with a box drawn around them; two sets of coupled resonances were identified (a and b), each corresponding to a benzene ring. The aromatic protons from bismaleimide are presented the coupling signal at 7.18 and 7.36 ppm which is identified as box (a) in Figure 3.45 (upper). However, there are signals of byproduct (pyridine-2-thiol and pyridine-2-thione) from thiol-disulfide exchange reaction. The 4 signals (6.75, 7.28, 7.42 and 7.65 ppm) in the aromatic area correlate with each other. From the integration, the two other resonances at 7.78 and 7.91 ppm assign to N-H from bucillamine and disulfide molecules, respectively which slightly move to low magnetic field after the reaction.

The morphology of nanocapsules from the inverse miniemulsion process was confirmed by transmission electron microscopy with diameters of 570±100 nm determined by dynamic light scattering after redispersing the nanocapsules in 0.1 wt% aqueous SDS solution. These results confirmed the successful simultaneous dual reactions both in solution and emulsion and the formation of polymeric nanocarriers by the two competitive click reactions.
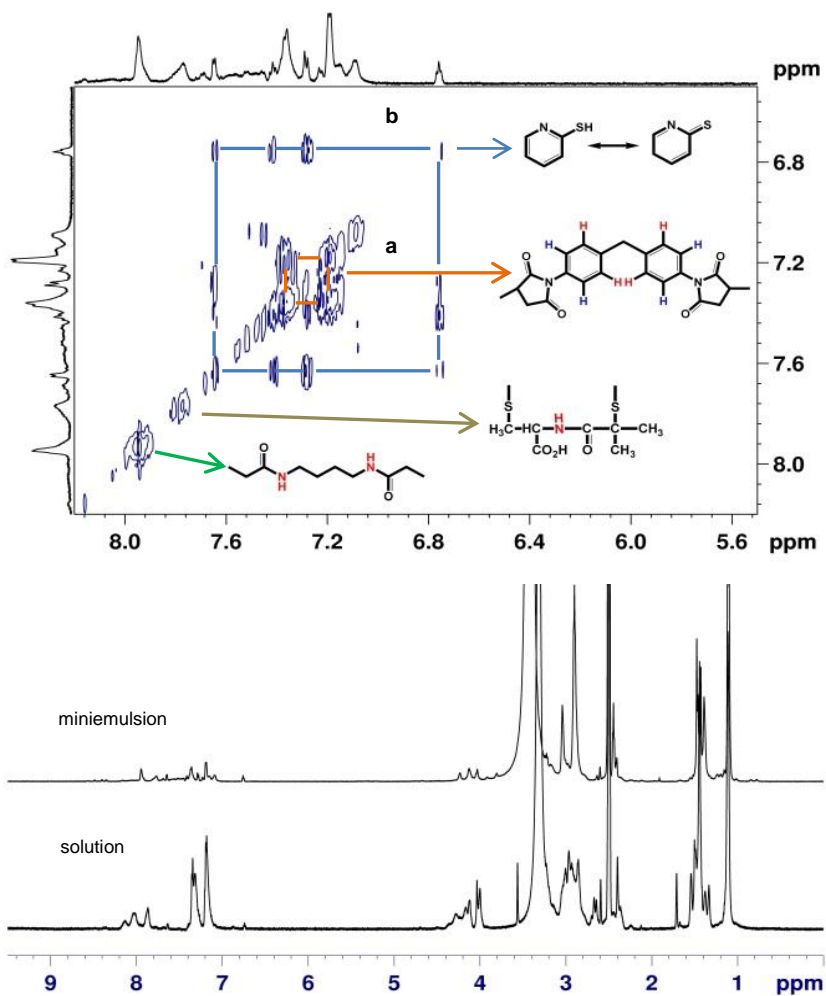
Figure 3.45 (Upper) TOSCY NMR (700 MHz) measurement (^{1}H-^{1}H correlation) of the product from dual reaction in miniemulsion at 283 K in DMSO-d6 and (lower) ^{1}H NMR spectra of the product from dual reaction in solution and miniemulsion process in DMSO-d_6.
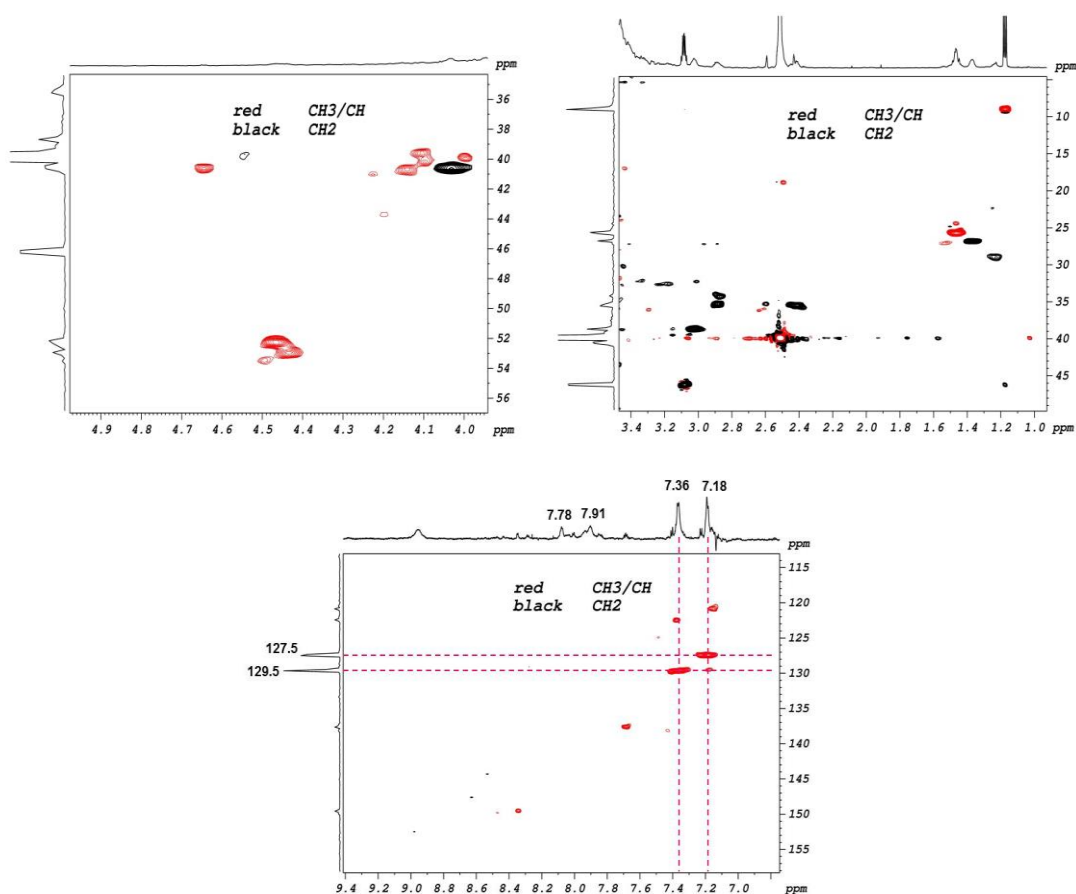
Figure 3.46 2D ^{1}H,^{13}C-HSQC of the product from dual reaction in miniemulsion in (700 MHz, DMSO-d$_6$, 298K).

3.3.1.4. Cleavage by glutathione

To investigate the degradation of final product of dual reaction by glutathione, ^{1}H diffusion-ordered NMR spectroscopy (DOSY) ^{1}H-NMR analysis was performed. From ^{1}H-DOSY NMR the degradation of the capsules by disulfide (S-S) bond cleavage of glutathione is finally proven as shown in Figure 3.47. The diffusion coefficient for the signal between 7-5 ppm and 2 ppm of final product increased which indicated some smaller molecules after the degradation. In addition, the degradation of the capsules by disulfide (S-S) bond cleavage of glutathione is proven by investigation the release of dye after cleavage of capsules by glutathione. The hydrophilic fluorescent dye sulforhodamine (SR101) was encapsulated,

which is released upon degradation of the capsule shell. Figure 3.48 shows a higher release (~70%) of SR101 for the cleavage by glutathione at room temperature after incubation over a period of 7 h at pH 7 compared to the control sample (~60%). This indicated that the formation of glutathione responsive capsules was successfully carried via the simultaneous dual reactions of maleimide-thiol-disulfide reaction in miniemulsion process
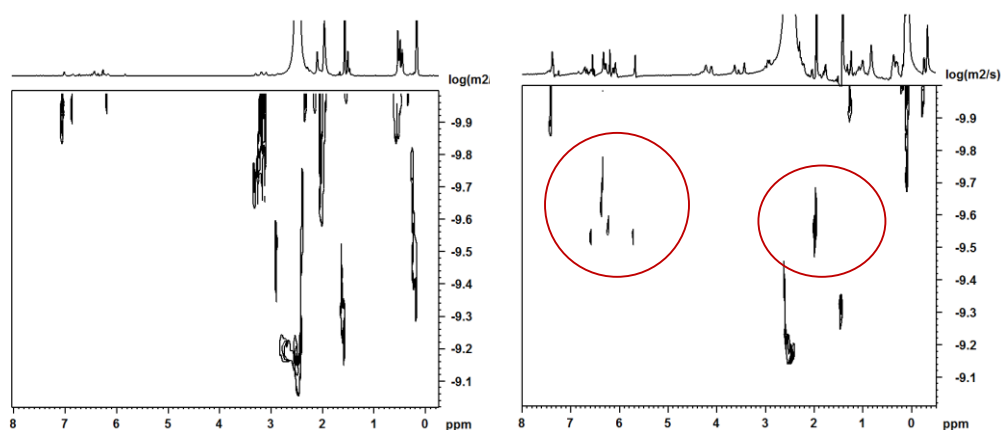
Figure 3.47 DOSY-^{1}H NMR (700 MHz) measurement of the product from dual reaction in miniemulsion at 283 K before (left) and after (right) cleavage by glutathione process in DMSO-d$_6$.
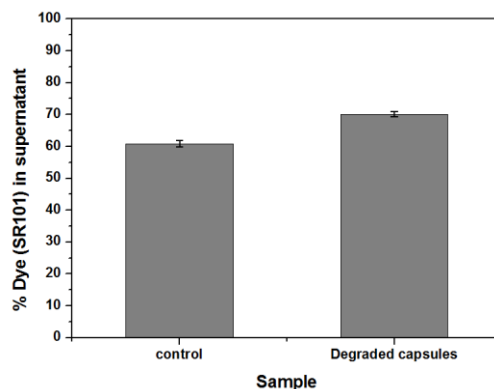
Figure 3.48 Percentage of SR101 dyes in supernatant from glutathione responsive capsules after cleavage by glutathione for 7 h, room temperature at pH 7.

3.3.2 Conclusions

In summary, real-time ^{1}H NMR spectroscopy revealed a new insight into two competitive "click" reactions for the formation of polymeric nanocarriers. The competitive nucleophilic addition of a dithiol (**3**) with a dimaleimide (**2**) and the dithiol-exchange reaction with (**1**) was studied. The dithiol-exchange follows the faster reaction kinetics under the investigated conditions. However, the concurrent thiol-maleimide addition could be accelerated by the addition of trimethylamine as a basic catalyst, allowing a copolymerization of all three monomers both in solution and at the interface of an inverse miniemulsion. The interfacial polymerization leads to higher molecular weights and exhibits faster reaction kinetics and does not need exact monomer stoichiometry. The competitive reaction at the interface produces polymeric nanocarriers with cleavable disulfide bonds synthesized via a selective chemistry. These materials may be useful drug carriers that are encapsulated in the nanocarrier or polymerized in the shell of the nanocarrier which can be released under biological conditions due to reduction of the S-S-bonds.

3.3.3 Supporting Information

The selection of ^{1}H NMR spectra and kinetic plots from chapter 3.3.
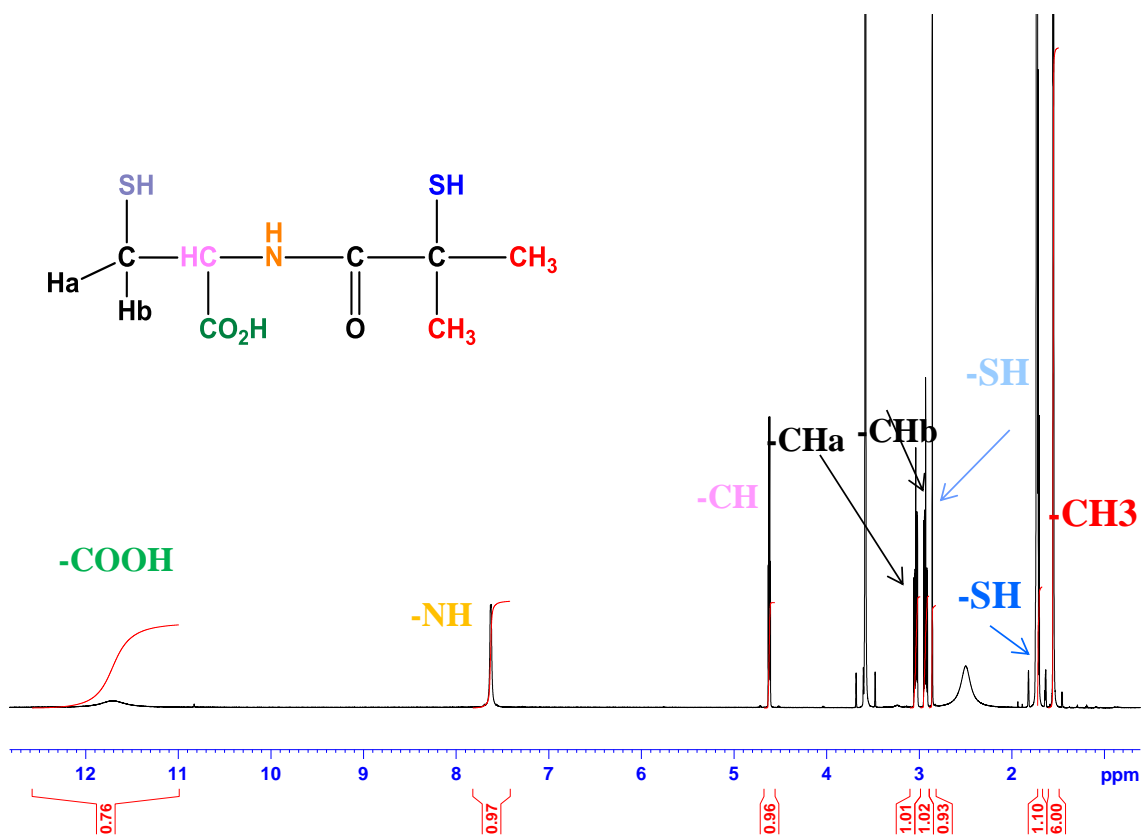
Figure S.1 ^{1}H NMR spectrum of bucillamine in THF-d_8 (700 MHz, 298 K)
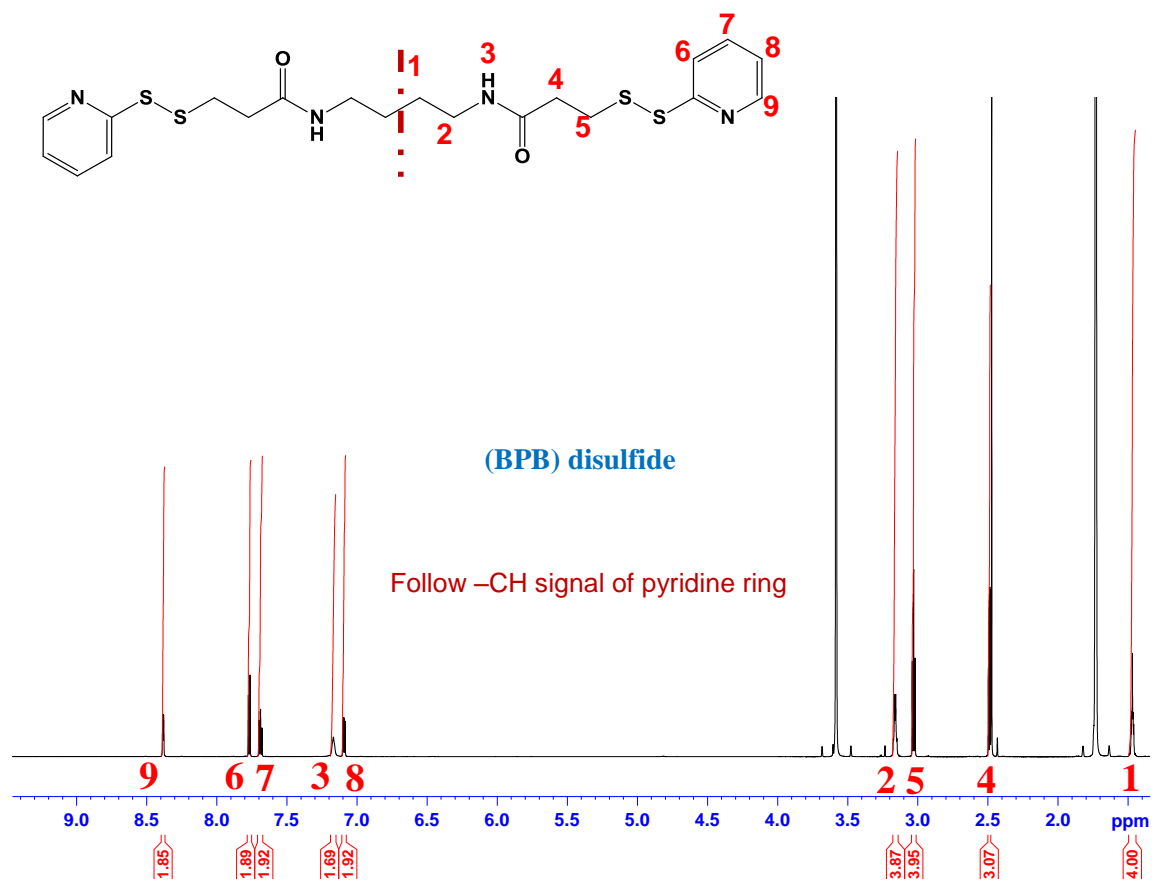
Figure S.2 ¹H NMR spectrum of 1,4 bis (3-(2-pyridyldithio)propionamido) butane (BPB) in THF-*d8* (700 MHz, 298 K).
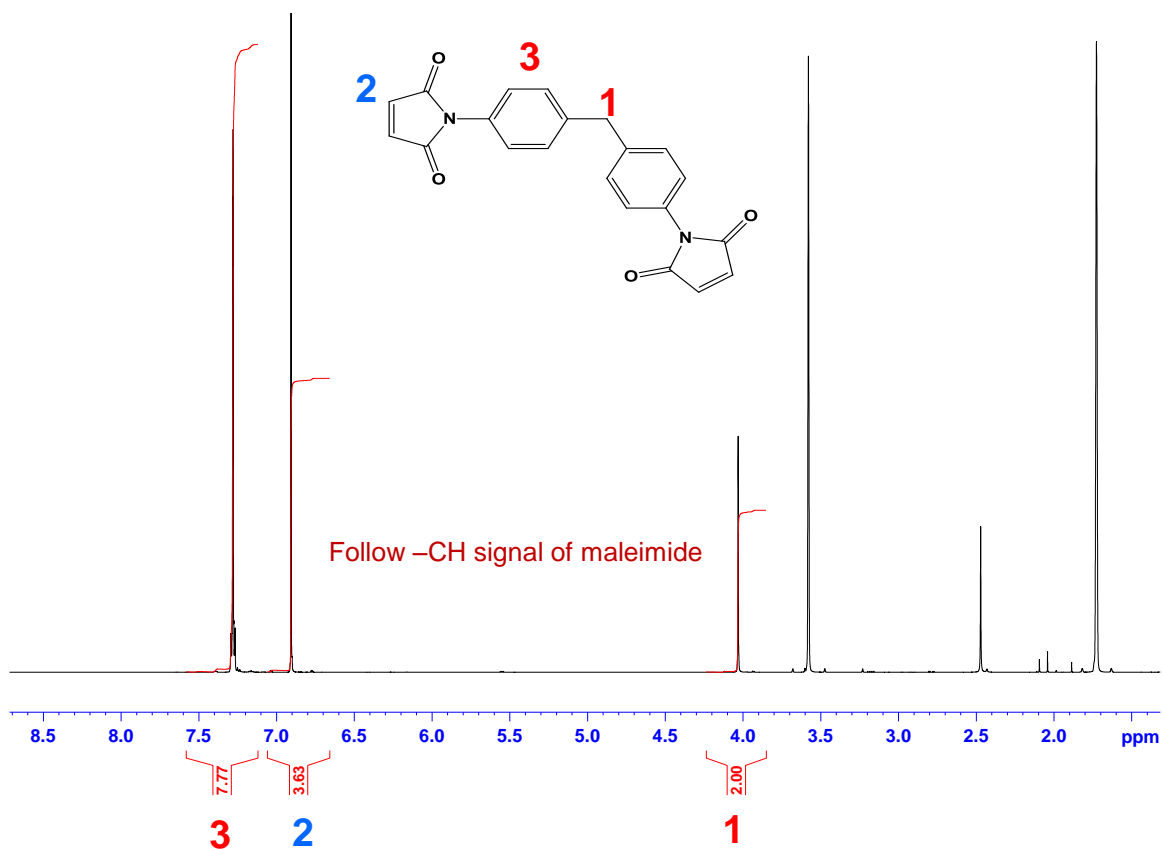
Figure S.3 ^{1}H NMR spectrum of 1,1′-(methylenedi-4,1-phenylene) bismaleimide in THF-d_8 (700 MHz, 298 K).

-CH signal in pyridyl ring decreased
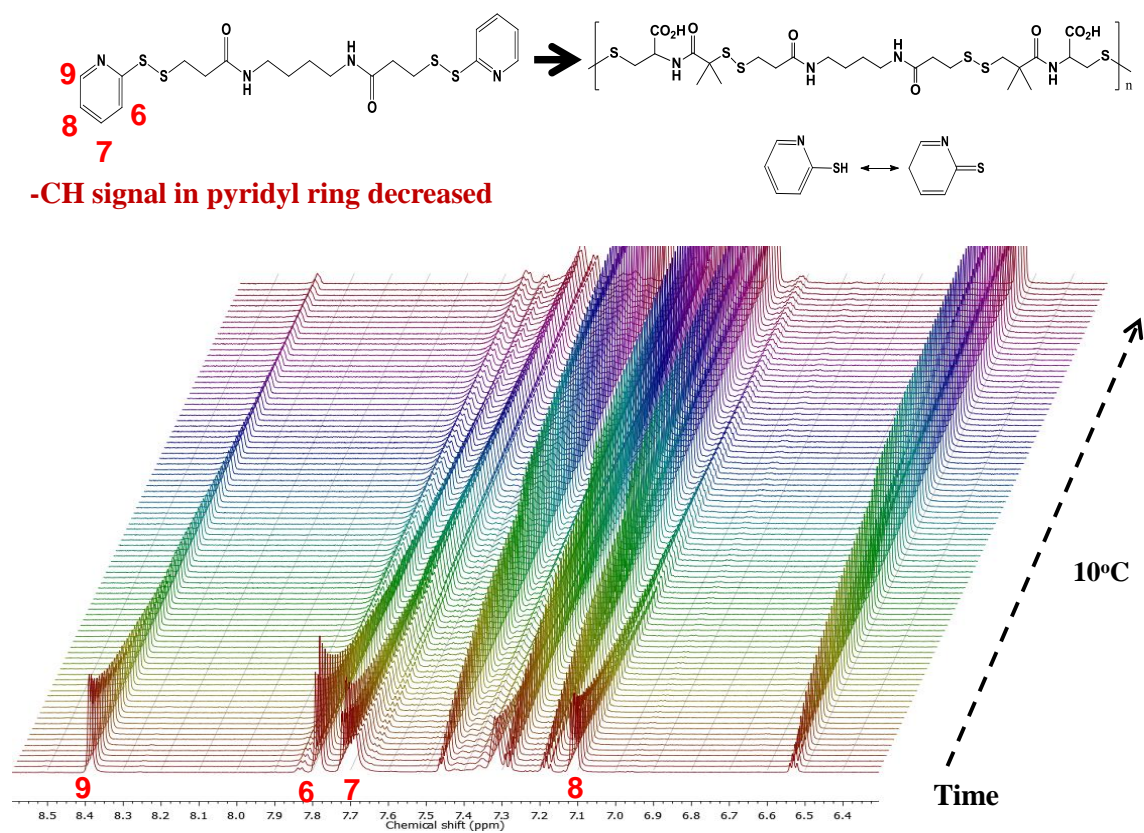
Figure S.4 Overlay of ^{1}H NMR spectra of dithiol-disulfide interchange reaction in THF-d_8 (700 MHz at 283 K).
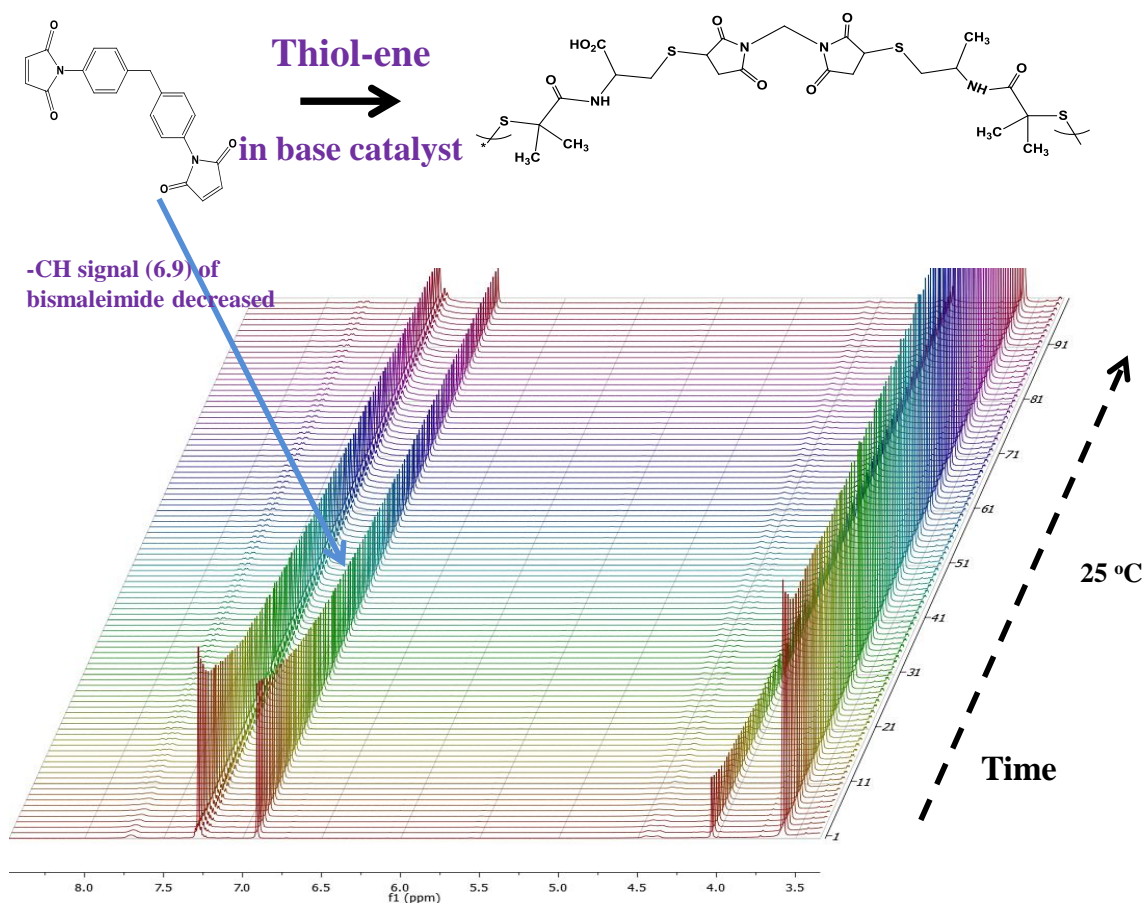
Figure S.5 Overlay of ¹H NMR spectra of thiol-maleimide click reaction in THF-d_8 (700 MHz at 298 K).
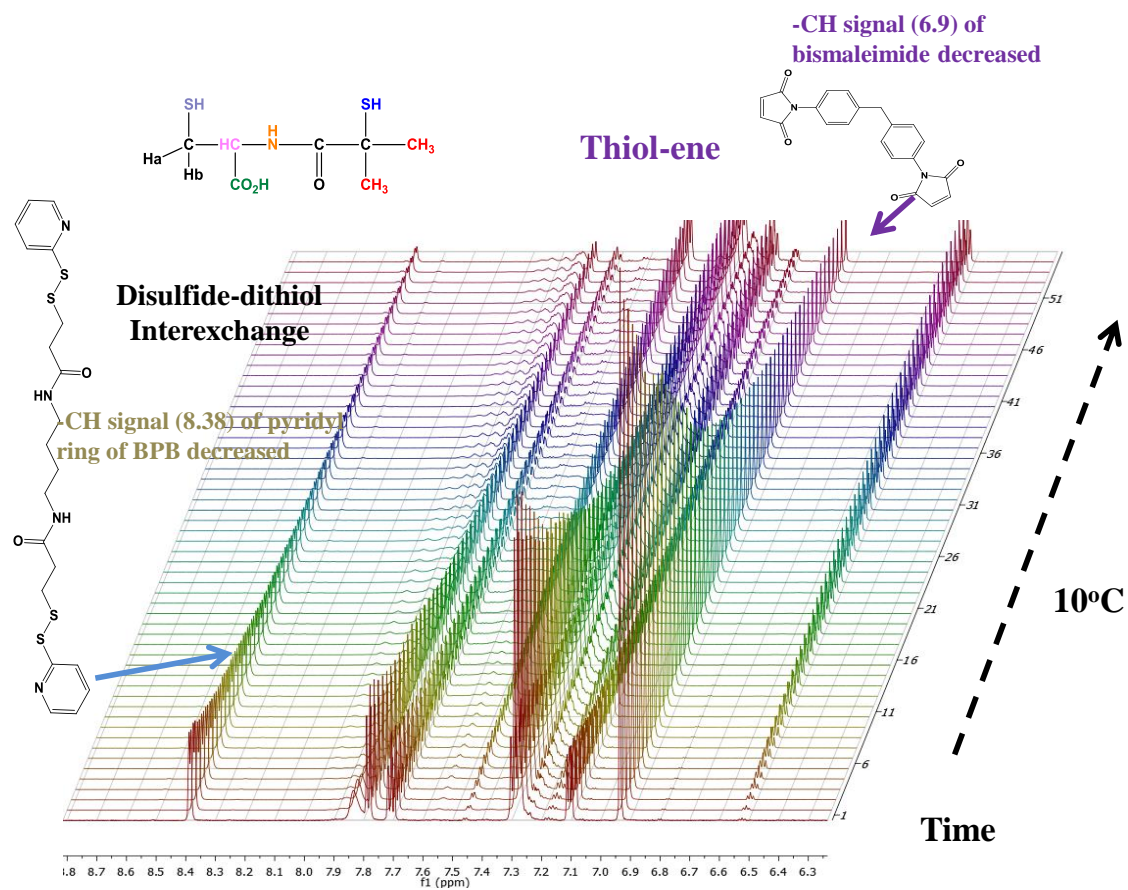
Figure S.6 Overlay of ¹H NMR spectra of dual reaction thiol-disulfide interchange and thiol-maleimide click reaction in THF-d_8 (700 MHz at 283 K).
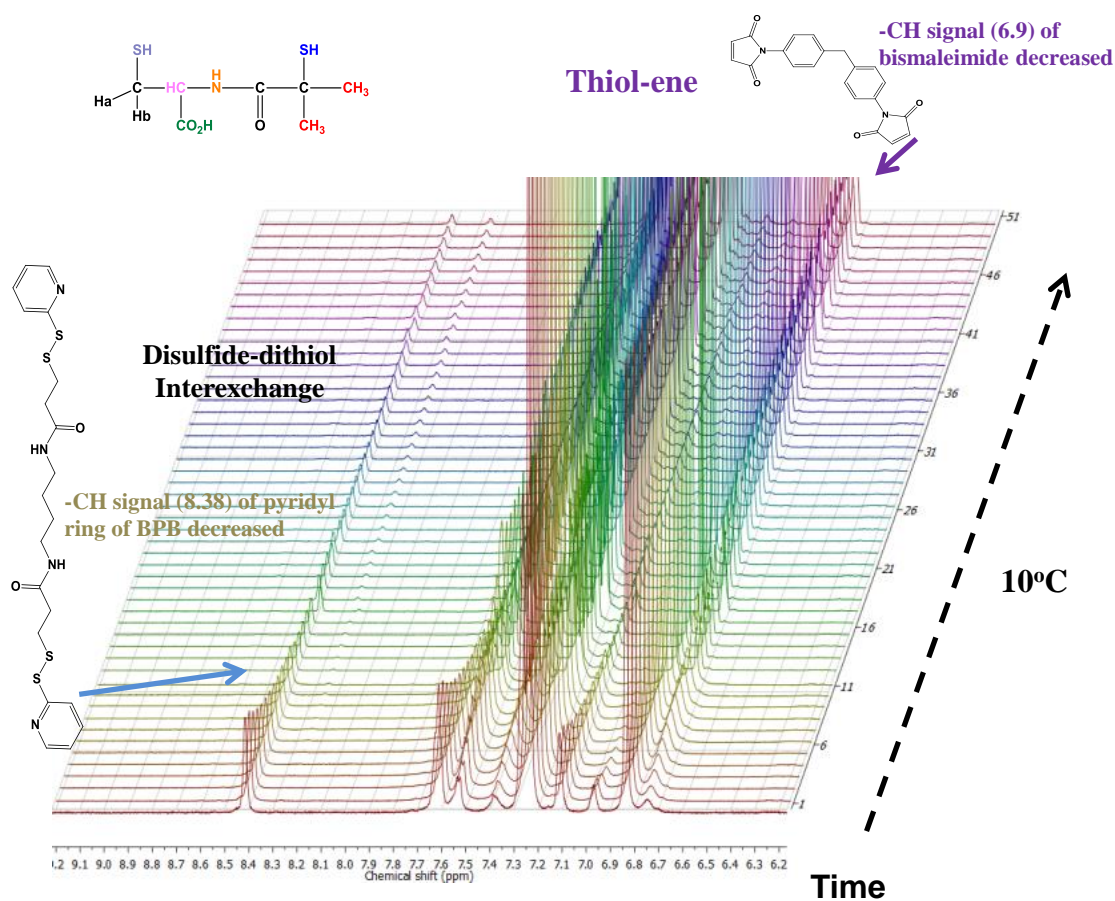
Figure S.7 Overlay of ^{1}H NMR spectra of dual reaction thiol-disulfide interchange and thiol-maleimide click reaction in miniemulsion (700 MHz at 283 K).

(a)

(b)
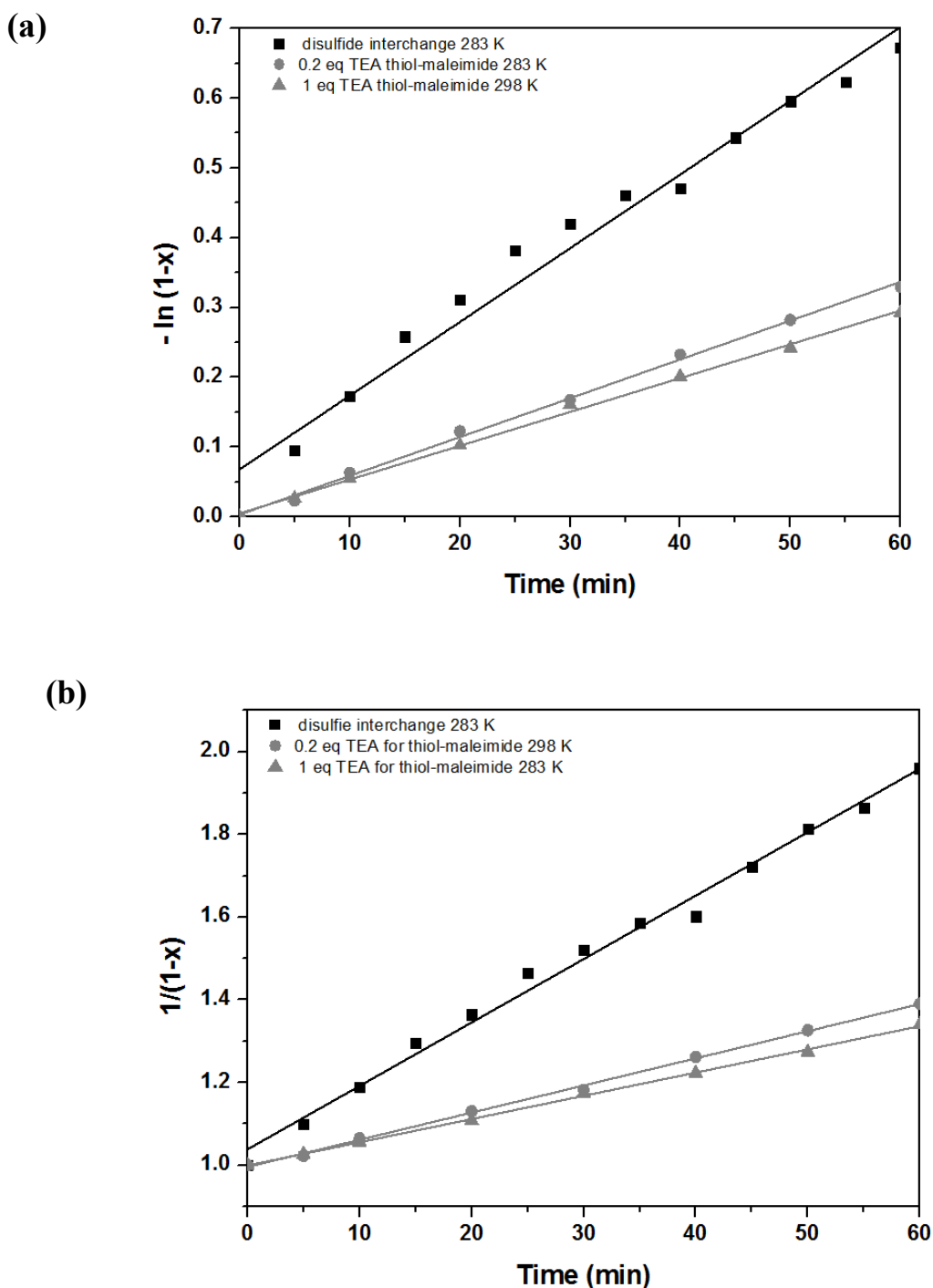
Figure S.8 Pseudo-first (a), second (b) order reaction kinetics for the first hour of thiol-disulfide interchange and thiol-maleimide click reaction in THF-d_8 by ^{1}H NMR spectroscopy.

(a)

(b)
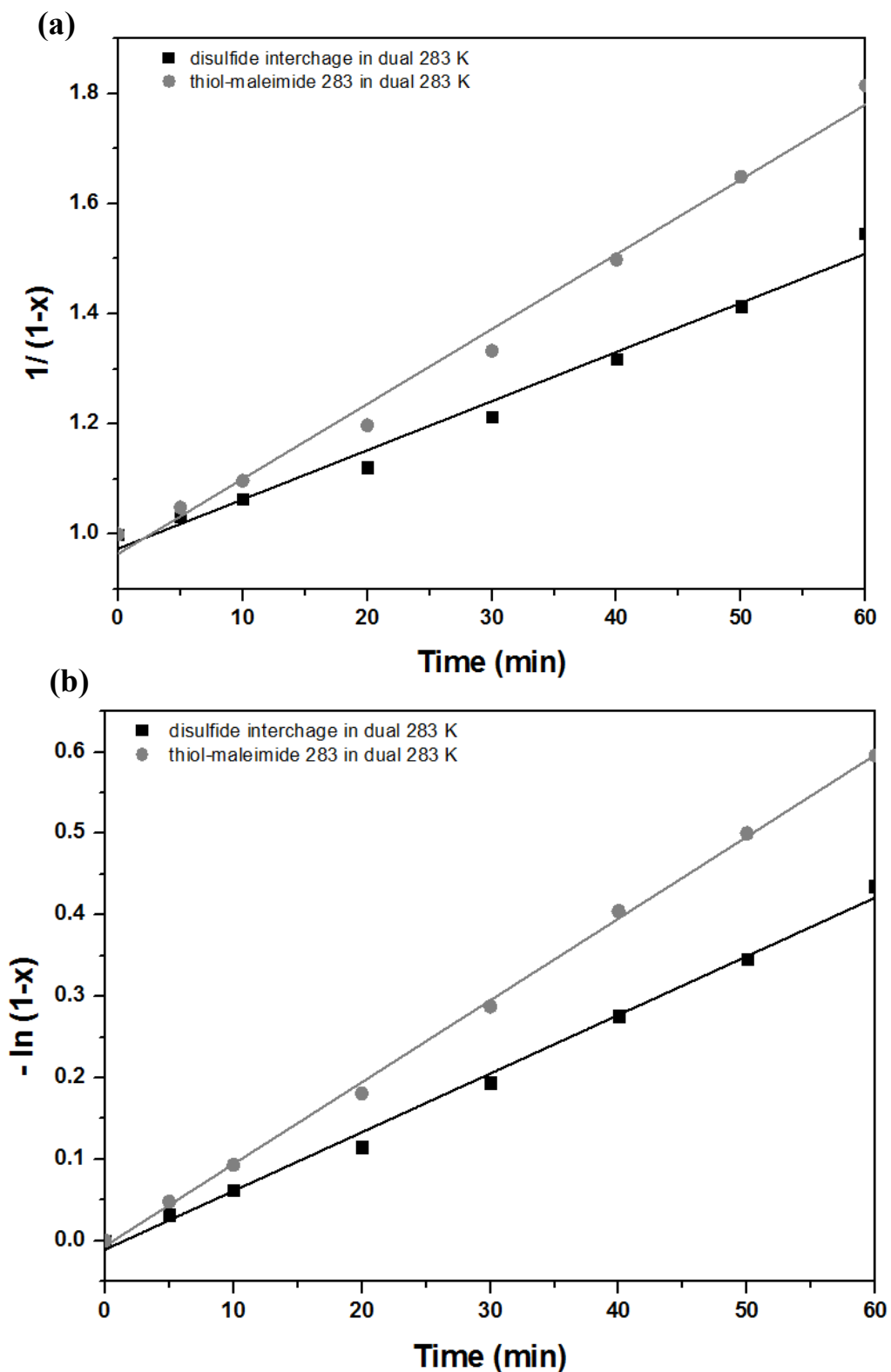
Figure S.9 Pseudo-first (a), second (b) order reaction kinetics for the first hour of dual reactions thiol-disulfide interchange and thiol-maleimide click reaction at 1 eq. of TEA, 283 K in THF-d_8 by ^{1}H NMR spectroscopy.

4. Conclusions and Perspectives

Conclusions and Outlook

A short summary of the reached achievements as well as outlooks is given in this chapter.

In chapter 3.1, the synthesis of hollow lignin nanocapsules with an aqueous core had been prepared by selective polyaddition at the interface of stable aqueous nanodroplets in an inverse miniemulsion. The obtained lignin nanocapsules showed diameters in the range of 150-200 nm. The enzymatic degradation of the nanocapsules had been proven by laccase as a model enzyme and also by a mixed enzyme cocktail extracted from natural fungi. In addition, lignin nanocarriers (from solid nanoparticles, core-shell and porous nanoparticles) were produced by a combination of miniemulsion polymerization and a solvent evaporation process. Hydrophobic substances can be load and release from these systems. The presence of laccase enzyme showed enhances the release from the lignin nanocarriers and the release behavior strongly depends on the morphology of the nanocarriers. Not only enzymatic trigger release for drug delivery application was studied in this work but also carbon material from porous lignin particles for waste water treatment application. Carbon form lignin particles showed higher surface area than carbon from lignin and high efficiency for methylene blue adsorption.

Next chapter, the effect of biodegradable lignin nanoparticles and magnetite coated polystyrene nanoparticles on the plant development of mung beans and their biodistribution is studied *in planta*. Magnetite coated polystyrene nanoparticles influenced the growth of the root and the stem development during seeding, while the lignin particles did not have an effect. Both nanoparticles with diameter more than 100 nm can penetrate the epidermis of the root tissue, accumulated in root cells and can transport through the vascular cylinder to leaves.

The last chapter presented the capsules formation of polymeric nanocarriers by two simultaneous "click" reactions(thiol-maleimide addition and thiol-disulfide exchange). The kinetics of two simultaneous "click" reactions were investigated by NMR spectroscopy in homogeneous solution and at the oil/water interface of an inverse miniemulsion. For the polyaddition/-condensation of difunctional reagents it was found that the thiol-disulfide exchange is faster than the thiol-maleimide reaction. The addition of a basic catalyst influences the copolymerization behavior of the competitive "click" reactions.

The thesis presents the first examples of lignin used as a building block for the preparation of biodegradable nanoparticles and capsules. These nanocarriers can be designed either for hydrophilic or hydrophobic cargos and their nanostructure can be adjusted to tune the release kinetics. The enzymatic trigger allows the release of pesticides, fungicides, etc. based on the renewable resource lignin as carrier material for future applications in agriculture.

As a biodegradable polymer, lignin is a promising material for the preparation of drug delivery vehicles for fungal diseases. The development of a platform to treat Esca-infected grapevine plants in an early state of infection cycle has been successfully demonstrated in this thesis which could be further extended to other trunk diseases and other release systems either for fertilizers or pesticides control release. Moreover, the development carbon material with high surface area by carbonization of porous lignin nanoparticles is another potential of the nanocarriers developed in this thesis apart from drug delivery. It is a confirmation for the versatile tool of our protocol to be applied in many applications.

For drug delivery application in plants, the accumulation and transportation profiles of nanoparticles has to be concerned in term of an efficient distribution and toxicity to the plant tissues. In this thesis, lignin nanoparticles and their distribution through the plant (mung bean as a model) were proven. These results confirmed that lignin, as a biopolymer has a high potential for drug delivery in agriculture. However the toxicity of the nanoparticles on the plant depends certainly on species of the plants thus the verity of the investigated plants is important.

This thesis has also explored the reactivity of two competing "click" reactions both in solution and at the interface of a miniemulsion: the Michael addition between thiols and maleimides and the thiol-exchange reaction were studied for the generation of nanocarriers. With the reactive thiol groups this platform could be also applied for the generation of lignin nanocarriers from sulfur-containing lignin fractions, which could be further modification to become glutathione responsive based-lignin carriers.

Lignin can be considered as enzyme responsive material or smart material. Actually, it can be further innovated on developing lignin into a multi response material such as light responsive, temperature-sensitive, hydrogels or even in nanofibers form. It is promising that lignin based smart materials would be more design and perform in the future.

Conclusions

In addition, other biomass materials such as starch, cellulose, chitosan and collagen are currently well known and used in biomedical application. These biomaterials show excellent bioactivity and biocompatibility. The bomass materials currently accepted the use as carriers for drug or gene delivery, scaffolds for tissue engineering and patches for wound healing. A lot of researches have been published based on these biopolymers. In contrary, few researches have studied the possibility of utilization lignin as biomedical materials. The studies carried out are quite limited to the cytotoxicity evaluation of lignin in some of human cell types. Lignin with biodegradability, antibacterial properties and antioxidant activity is a promising candidate to serve as biomaterials for reducing the stress and inflammation generated by implantation and could also be applied in other pharmaceutical and cosmetic products.

Indeed, renewable lignin-based materials display a bright future to replace petroleum-based materials. Lignin shows many advantages; however its variety and complex structures might obstruct lignin utilization for the scale-up from laboratory to industry. To overcome this limitation, the understanding of the physics and chemistry of the natural lignin together with the development of lignin purification is necessity. With the progress of modification chemistry and the development of processing techniques, lignin will become a promising renewable resource for high performance materials in the near future.

5. Experimental Part

5.1 Lignin biodegradable carrier for controlled release

5.1.1 Lignin capsules for hydrophilic substances

Materials and Method

Lignosulfonic acid sodium salt (molecular weight Mw: 50,000 g·mol^{-1}) and 2,4-toluene diisocyanate (TDI), sulforhodamine 101 (SR101) and solvents were purchased from Sigma-Aldrich. Polyglycerol polyricinoleate (PGPR) was obtained from Danisco and used as surfactant. All chemicals were used without further purification.

The *Coprinus cinereus* laccase used within this study was purified from submerged cultures of the fungus by chromatographic methods. *C. cinereus* CBS 182.61 (CBS Fungal Biodiversity Center, Utrecht, the Netherlands) was cultivated on yeast malt glucose medium (YMG medium) consisting of 4 g yeast extract (Becton Dickinson GmbH, Heidelberg, Germany), 10 g malt extract (Fränkle & Eck, Fellbach, Germany), 10 g glucose and 18 g agar per 1 l tap H$_2$O. The pH was adjusted with 1 N HCl to 5.5 prior to sterilization.

Submerged cultures were grown in a 1 l flask with 500 ml of YMG (27 °C, 120 rpm). Several excised pieces of the fungus grown on a YMG agar plate were used as inoculum. The culture broth was separated from the mycelium by filtration after 4 days, when the glucose was depleted. An intermediate product of the laccase was obtained from 200 ml culture filtrate by ion exchange chromatography using Q-Sepharose Fast Flow (GE Healthcare, Freiburg, Germany) equilibrated and washed after loading with 50 mM Tris-HCl pH 7.5 (buffer A). Elution was maintained with a linear gradient of buffer supplemented with 1 M NaCl. Positive fractions (30 ml) were concentrated to 500 µl with a Centricon Plus-70 centrifugal filter device (Millipore, Darmstadt, Germany). Final purification was achieved using a gel filtration 1 m long XK26/100 column with Superdex 75 prep grade (GE Healthcare, Freiburg, Germany) at a flow rate of 2.5 ml·min^{-1} with buffer A supplemented with 100 mM NaCl as mobile phase.

Further experiments were conducted with a crude extract of a culture supernatant of the fungal strain *Xylaria* sp. IBWF A55-2009. This strain was grown in medium Soybean-medium containing 30 g·l^{-1} soybean meal (Lucas Meyer GmbH, Hamburg), Germany, 15 g·l^{-1} maltose (Applichem GmbH, Darmstadt, Germany) and 5 g·l^{-1} peptone (Carl Roth GmbH, Karlsruhe,

Germany). Submerged cultures were incubated at 27 °C and 120 rpm on an orbital shaker. The cultivation was finished after two weeks. The mycelium was separated from the supernatant by centrifugation at 10,000 rpm for 10 min. For experimental procedures within this study the supernatant stored at -20 °C was used.

The laccase activity was monitored in a liquid assay in 96-well plates. 100 µl culture fluid/protein fraction were supplemented with 100 µl of 2,2'-azino-bis (3-ethylbenzthiazoline-6-sulphonic acid) (ABTS) solution (2 mg·ml^{-1} ABTS in tartaric acid, pH 4.5). The mixture was immediately analysed by photometry over a period of 5 min at room temperature and a wavelength of 420 nm.

5.1.1.1 Synthesis of lignin capsules for hydrophilic substance

The lignin capsules were prepared by a polyaddition reaction performed at the miniemulsion droplet's interface. 100 mg of lignin were mixed with 20 mg of sodium chloride and dissolved in 1.3 g of demineralized water; in case of the investigation the enzymatic cleavage 1 mg of SR101 was added instead of sodium chloride. This solution was added into 7.5 g of cyclohexane containing 80 mg of PGPR at room temperature and stirred at 1000 rpm for 1 h in order to form a pre-emulsion. Then the emulsion was treated with ultrasound (for 180 s at 90% amplitude in a pulse regime (20 s sonication, 10 s pause) under ice cooling). A solution consisting of 5 g of cyclohexane, 30 mg of PGPR and 50, 100 or 150 mg of TDI was then added drop-wise (over a period of 5 min) to the earlier prepared emulsion. The reaction was carried out overnight at room temperature. Then, the nanocapsules were washed twice with cyclohexane.

Redispersion of the capsules in buffer solution

To a stirred nanocapsule dispersion in cyclohexane (1 g with approximately 3% solid content) 5 g of an acetate buffer solution at pH 3 or pH 7 were added drop-wise. The mixture was stirred for 24 h with open cap in order to guarantee evaporation of the solvent, and was then sonicated in an ultrasound bath (25 kHz) for 20 min at 25 °C.

Experimental Part

5.1.1.2 Enzyme-triggered release of lignin capsules

Degradation of lignin nanocapsules by C.Cinereus Laccase Lcc1 and enzyme cocktail from mushroom extraction

To 1 ml of the aqueous nanocapsule dispersion (in buffer solution) 300 µl of a laccase solution (30 µg·ml^{-1}) or an enzyme cocktail (see above) was added. The mixture was kept stirring over a period of time and samples were taken in order to determine the released dye for 24 h at R.T. and 50 °C.

Determination of SR101 dyes after degradation of capsules by enzyme

The lignin nanocapsules were redispersed in water (or buffer) as mentioned above and centrifuged 3000 rpm for 30 min. The supernatant was investigated by fluorescence spectroscopy in order to determine the amount of released SR101. The chemical structure of SR101 is presented in Figure 5.1.
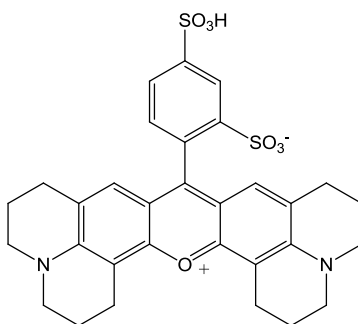
Figure 5.1 Chemical structures of sulforhodamine SR101.

As control, a nanocapsule dispersion that was prepared without fluorescent dye was redispersed in water containing SR101 (the amount is equal to the amount of SR101 that was used in the encapsulation experiments) was used as a reference (blank). The fluorescence signal of the reference sample at difference concentrations of SR101 was used to set up a calibration curve (Note: SR101 has an absorption maximum at 550 nm and the emission was measured at 605 nm). The total release of SR101 from the degraded capsule by enzyme was calculated from the calibration curve.

5.1.2 Lignin carriers for hydrophobic substances, its morphologies and release profiles

Materials and Methods

Lignin was purchased from Sigma Aldrich (kraft lignin, alkali). Prior to the experiment, lignin was extracted with propanol and dried in a vacuum oven for overnight. Kraft lignin data was shown that the amount of hydroxyl groups (aliphatic and phenolic) was 1.24 per 1 phenyl propane unit (PPU or C9 unit, assumed molecular weight of hard wood is 183 g·mol^{-1}).[210] Methacrylic anhydride, triethylamine, isopropyl alcohol, lithium chloride, and dimethylformamide (DMF) were also obtained from Sigma Aldrich. The lithium chloride was dried at 70 °C in a vacuum oven before use. The anionic surfactant sodium dodecylsulfate (SDS) and hexadecane were purchased from Fluka and used as received. Lutensol AT25 nonionic surfactant and Lecithin biodegradation surfactant were obtained from BASF and Carl Roth GmbH & Co. KG, respectively. The structures of three surfactant are shown in Figure 5.2. Diamine molecules (2,2´(ethylenedioxy)bis(ethalamine)) was obtained from Sigma-Aldrich Laccase from Trametes versicolor was obtained from Sigma Aldrich with an activity of ca. ≥ 0.5 U·mg^{-1}.

Sodium dodecyl sulfate (SDS)

R = linear, saturated C$_{16}$C$_{18}$ fatty alcohol

Polyoxyethylene cetylstearyether (Lutensol® AT 25)

Lecithin
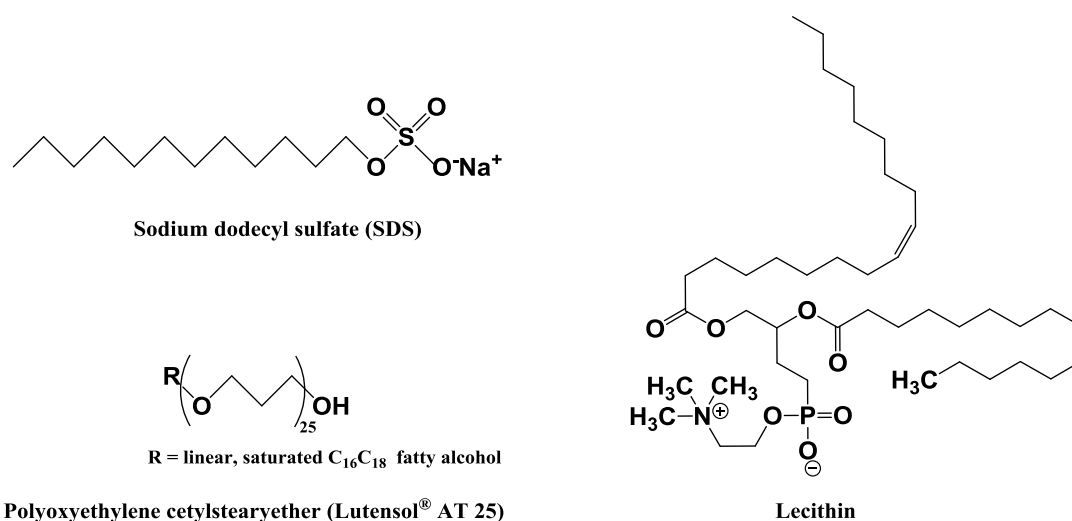
Figure 5.2 Chemical Structures of the surfactants used in this study.

Experimental Part

In order to investigate the structure of lignin and methacrylated-lignin, the FT-IR spectra were obtained by Nicolet iS10. The samples had been dried at room temperature in the vacuum oven. Spectra were recorded between 600 and 4000 cm^{-1} at a resolution of 4 cm^{-1}, and co-adding 32 scans. Proton nuclear magnetic resonance spectroscopy (^{1}H-NMR) was performed by Bruker AVANCE at 500 MHz. Around 2 mg of samples were dissolved in 750 μl of DMSO-d_6 with hexamethycyclo trisiloxane as the internal reference. The degree of functionalization was calculated by dividing the peak area of double bond region (6.5-5.0 ppm) by the peak area of aromatic hydrogen in lignin (7.5-6.5 ppm). The number of moles of methacrylate attached to lignin is given by:

$$mol_{(methacrylate)} = mol_{(int.std)} \times \left(\frac{\text{integral of methyl gr. (2-1.2 ppm)}}{\text{integral of int.std (0.4-(-0.4) ppm)}} \times \frac{18 \text{ (no. proton of int.std)}}{3 \text{ (no.proton of methyl)}}\right)$$

Equation 5.1

The glass transition temperatures (T_g) of lignins were evaluated by using a Mettler Toledo DSC 823 differential scanning calorimeter operating with a heating rate 10 °C·min^{-1} under a nitrogen flow rate of 10 ml·min^{-1}. The T_g values were calculated as the midpoint of the change in heat capacity. The thermal stability of lignin was studied in terms of thermogravimetric analysis (TGA) with a dynamic scan from 30 to 900 °C at 10 °C·min^{-1} was done under nitrogen atmosphere. Before being tested by DSC and TGA, the samples were dried at room temperature under vacuum for overnight.

Interfacial Tensions

The interfacial tension between the core-oils and the various aqueous surfactants (1 wt% of SDS, lutensol and lecithin solutions (liquid-liquid system)) were measured by the spinning drop method using a spinning drop video tensiometer. The temperature of the system was maintained at 22 °C. Automatic measurements were conducted by a horizontally arranged capillary filled with a bulk phase, a surfactant solution (more density), and a drop of lighter phase, hexadecane, is set in rotation. The diameter of the droplet which is elongated by centrifugal force correlates with the interfacial tension.

Solid-liquid interfacial tension of the MA-lignin and the various liquids (oil and aqueous surfactants) were determined by using Young´s equation:

$$\gamma_{sv} = \gamma_{sl} + \gamma_{lv}\cos\Theta \qquad\qquad \text{Equation 5.2}$$

Where γ_{lv}, γ_{sv}, and γ_{sl} are the interfacial tensions of the liquid/vapor, solid/vapor, and solid/liquid, respectively. The contact angles (Θ) of each liquid against a film of MA-lignin were determined by an optical contact angle measurement. Each liquids were measured at least 5 drops on the films (Figure S1). The films were prepared by a 3 wt% solution of MA-lignin in chloroform. This solution was then used in the spin-coating of smooth, thin lignin films onto glass slides which were cleaned thoroughly by ultrasonication three times with firstly surfactant solution, then rinsing with water, and finally with isopropanol and dried in the oven. The contact angle measurements needed to be supplemented with surface tension values for both the liquid and solid. Those for the aqueous surfactants were measured by the du Nuoy ring method and for the solid lignin was calculated from an assumption of Girrfalco and Good [211] as in following equation:

$$\gamma s \approx \gamma l \frac{(1+cos\theta)^2}{4\phi^2} \qquad\qquad \text{Equation 5.3}$$

By means of this assumption, the surface tension of solid surface can be calculated from measurements of the contact angle and the surface tension of liquid. Water was used for this experiment which obtained the solid surface energy of MA-lignin approximately 49.0 mJ·m^{-2}.

5.1.2.1 Synthesis of methacrylated-lignin

Lignin was modified by esterification with methacrylic anhydride (Figure 5-3). 2 g of lignin (10 mmol) were dissolved in 60 ml of 4 wt% lithium chloride (LiCl)/dimethyl formamide (DMF) at 90 °C under argon. After complete dissolution, 1 ml of triethylamine (10 mmol) was added to the lignin solution and stirred for 15 min at 50 °C. 3 ml of methacrylic anhydride

(20 mmol) then were slowly injected into the reaction flask. The reaction was kept at 50 °C overnight. The reaction mixture was precipitated into isopropanol and isolated by centrifugation at 3000 rpm. The product was repeatedly dissolved in chloroform and precipitated in isopropyl alcohol for tree times. The product was dried at room temperature in a vacuum oven. Yields are typically around 50%. ^{1}H NMR spectroscopy proves the successful attachment and purification of the methacrylate moiety to lignin: -CH$_3$, 2.05-1.7 ppm; CH=CH$_2$, 6.2-5.4 ppm.
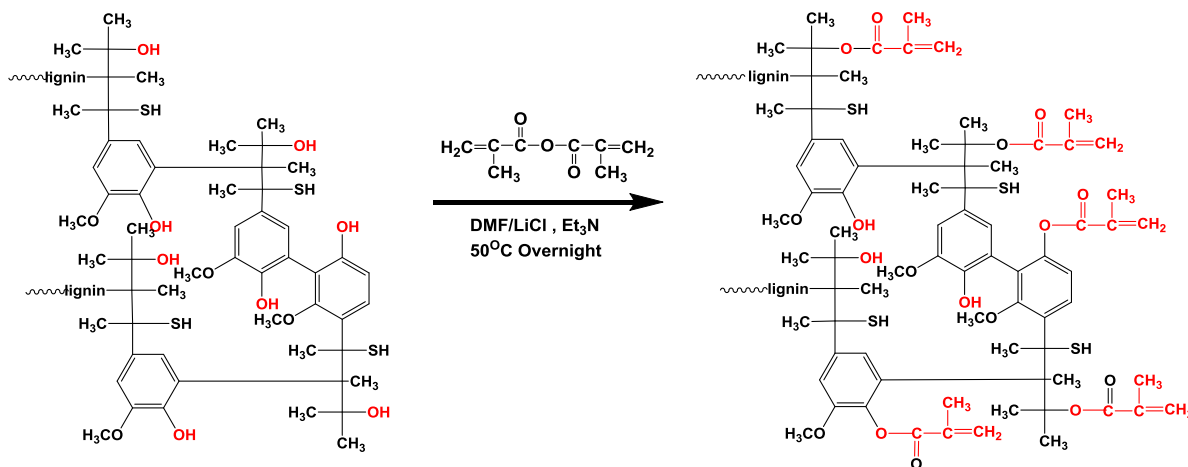
Figure 5.3 Synthesis of methacrylated-lignin.

5.1.2.2 Formation of lignin nanocarrier for hydrophobic molecules

The formation of lignin nanocapsules was carried out by a combined miniemulsion polymerization with subsequent solvent evaporation. The typical procedure is the following: MA-lignin (75 mg, 4.6 µmol), including the hydrophobic oil (25 mg) (hexadecane, olive oil or palm oil) and the initiator (20 mg of azobisisobutyronitrile (AIBN)) were dissolved and mixed in 600 mg of chloroform. This solution was added into an aqueous solution (10 ml) of the surfactant (0.1 or 0.2 wt% of SDS solution) at room temperature and stirred at 1000 rpm for 30 min in order to form a pre-emulsion. Then the emulsion was treated with ultrasound for 3 min (1/2 inch tip, 70% amplitude, 20 s ultrasound followed by 10 s pauses) under ice cooling in order to prevent evaporation of the solvent and the initiation of the polymerization due to heating. After the formation of the stable miniemulsion, the crosslinking polymerization was carried out for 5 h at 60 °C and mild stirring. After the polymerization, the solvent was evaporated from the miniemulsion by stirring it in an open vessel overnight at ambient temperature (ca. 21 °C). The

final volume of dispersions was adjusted to 10 ml with distilled water (typical solid contents of the dispersions were ca. 10 mg·ml^{-1}). For the release studies of the lignin nanocarriers, an UV-active ingredient (2-propylpyridine) was added in oil phase prior to mix in water phase and in some case, natural oils such as olive oil instead of hexadecane were used.

Establishment of the ternary phase diagram

In order to determine the phase separation behavior of MA-lignin, the ternary phase diagram of MA-lignin/hexadecane/chloroform was determined according to the work of Vincent et al.[135] The three components were accurately weighted and mixed with different ratios. The solutions were stirred at room temperature to gradually induce evaporation the volatile chloroform solvent. When the solutions became turbid due to phase separation of lignin, the mixtures were reweighted. The weight loss of the samples correspond to the evaporation of chloroform, the composition at this point were recorded in ternary phase diagram by mass balance.

5.1.2.3 Release profiles of lignin nanocarriers

2-Propylpyridine was used as an UV-active ingredient since it is soluble in the oil phase and also partially soluble in the aqueous phase. The driving force for the release correspond to the oil/water partition coefficient which is 86.3 in the case of 2-propylpyridine. The release study by the dialysis method followed the work of Dowding et al.[212] 3 ml of the emulsion (solid content of 1 wt%) was added to a dialysis tubing and immersed into 197 ml of distilled water. Since 2-propylpyridine has a high coefficient at 260 nm, the release profile of the 2-propylpyridine can be determined by measuring the absorbance of the release medium as a function of time. 5 ml of release medium (distilled water) was taken at different time intervals to determine the concentration of released 2-propylpyridine by UV-Vis spectroscopy. This release profile is defined as the mass of 2-propylpyridine released from the nanocarrier dispersion divided by the mass of 2-propylpyridine initially dissolved in the oil phase.

To investigate the degradation of lignin nanocarriers by laccase, the emulsions were incubated with laccase (30 mg in 3 ml of emulsion) in an acetate buffer (pH 7) at room temperature overnight before using the centrifugation at 12000 rpm for 2 h. The supernatant was

taken and monitored the amount of 2-propylpyridine released from the particle by UV-Vis spectroscopy. In case of control, the lignin emulsion was incubated only in an acetate buffer without laccase.

5.1.3 Potential application of lignin carrier for Esca disease of grapevine

5.1.3.1   Preparation and optimization of lignin nanoparticles for fungicide encapsulation

The crosslinked-lignin particles, loaded and unloaded-drug were prepared by miniemulsion-solvent evaporation. Typically 100 mg (1.1 mmol of PPU) of MA-lignin dissolved in 2.5 g of chloroform ($CHCl_3$). This solution was added into 10 g of water containing 20 mg of surfactant at room temperature and stirred at 1000 rpm for 1 h in order to form a pre-emulsion. Then the emulsion was treated with ultrasound for 3 min (1/2 inch tip, 70% amplitude, 20 s ultrasound followed by 10 s pauses) under ice cooling in order to prevent evaporation of the solvent. A solution of diamine molecules (2,2´(ethylenedioxy)bis(ethalamine)) in water (1:1 mole ratio to MA-lignin was added in the emulsion after sonication process. The reaction was carried out overnight at 50 °C. The solvent was evaporated from the miniemulsion by stirring it for overnight at room temperature. The final volume of dispersions was made up to 10 ml by water. The obtained particles were characterized by DLS and TEM. To study the grafting efficiency of Michael addition between MA-lignin and diamine, the obtained particles were washed with water and chloroform and then dried overnight in vacuum oven. For the encapsulation of pyraclostrobin (fungicide), pyraclostrobin was added to the dispersed phase prior to mix with aqueous phase.

The hydrodynamic diameters of the particles were measured by NICOMP 380 at a fixed angle of 90 degree and a laser diode running at 635 nm, before being measured the sample were diluted. The morphology of particles was observed by TEM with a Joel 1400, an accelerating voltage of 120 kV. Samples were prepared by casting a drop of diluted dispersion on a carbon-coated copper grid (300 square meshes) and dried at room temperature.

Antifungal Drug Loading Content and Encapsulation Efficiency

In order to determine the encapsulation efficiency of fungicide loaded in lignin particles, the amount of pyraclostrobin was measured by high pressure liquid chromatography (HPLC) method. Two possible methods to check the encapsulation efficiency were investigated. By indirect method, sample was centrifuged at 10000 rpm for 60 min. The supernatant which containing free pyraclostrobin were taken, freeze dried and then dissolved in THF. Another way was direct method by using the pellet after centrifugation. The pellet was freeze dried and dissolved in THF to break nanoparticles. The solution from both routes were then passed through a 0.2 μm filter and analyzed by high pressure liquid chromatography (HPLC) method with Agilent Elicpse Plus RP18. The mobile phase was THF:water/ 0.1 wt%. TFA-gradient, injection volume was 10 μl and the column temperature maintained at 20 °C. The analysis was performed at a flow rate of 0.2 ml·min^{-1} with the UV detector at 280 nm. Both methods gave similar results. The encapsulation efficiency (EE) and the loading content (LC) of pyraclostrobin in nanoparticles were determined according to the following equations:

$$LC(\%) = \frac{\text{weight of pyraclostrobin in particles}}{\text{weight of particles}} \times 100$$

$$EE(\%) = \frac{\text{weight of pyraclostrobin in particles}}{\text{initial weight of pyraclostrobin}} \times 100$$

5.1.3.2 *In vitro* and *in planta* antifungal test

Materials and Methods

The microinjection systems were kindly provided by Tree Tech Microinjection Systems Company, 950 S.E. 215th Avenue, Morriston, FL 32668. Furthermore a cordless screwdriver with a 6mm drill head was used (both manufactured by Robert Bosch GmbH, Stuttgart). The holes, which were drilled into the plants were sealed after the injection process by a commercial wound sealant product (Neudorff Lauril® Wundwachs; Neudorff GmbH KG, Emmerthal).

Germination assay: Conidia from 18-day-old agar plate cultures were harvested. After centrifugation at 4000 rpm for 10 minutes the conidia were resuspended in HMG-medium (10 g·l^{-1} malt extract, 10 g·l^{-1} glucose, 4 g·l^{-1} yeast extract, pH 5.5) to a concentration of 1×10^5 per ml. The test was carried out in 96-well microliter plates (Greiner Bio-One GmbH, Frickenhausen) with conidia in 200 µl of YMG-medium and an incubation time of 72 h at 27 °C.[213] The optical density was measured at a wavelength of 600nm (Benchmark Plus Microplate reader, BioRad, Munich). Tests were conducted in triplicates. The concentration of the used fungicide was 5 µg per 200 µl medium in a well.

Evaluation of the field trials: All plants used for the injection tests (as well as the control group) were tested for the presence of Esca-associated fungi. Therefore wood samples of shoots were harvested and analyzed on endophytic fungi afterward using the method of an endophyt isolation protocol: Isolation was from surface-sterilized grapevine plant material (1 min 70% ethanol, 3 min 5% sodium hypochlorite, 30 s 70% ethanol) onto 2% YMG agar augmented with 200 mg·l^{-1} each of penicillin G and streptomycin sulfate (both from, Carl Roth GmbH & Co. KG, Germany). For maintenance and submerged cultivation, YMG medium was used. To solidify media, 2% agar was added. The gross morphological features of the fungus colony were determined on YMG agar. For microscopy, squares of 0.2% malt extract agar were mounted directly in water. For molecular identification, the ITS sequences were obtained and analyzed using the method of Köpcke et al.[214]

The side of the trunk that was selected for the injection was sprayed with 5% sodium hypochlorite to sterilize the wooden surface of the plant. Afterwards an 8 mm deep and 6 mm wide hole was drilled into the grapevine trunk. The chosen plants always had a trunk diameter greater than 20 mm. The drill head was always sterilized in 70% ethanol for 1 min before the next plant was treated. After the drilling the injection system was filled with the lignin particle suspension and inserted to the grapevine trunk hole. The scroll spring pressure system was activated afterwards and the solution was injected into the trunk in less than 24 h. After one day the injection systems were removed and the wound was sealed with grafting wax. The injection application is presented in Figure 5.4.
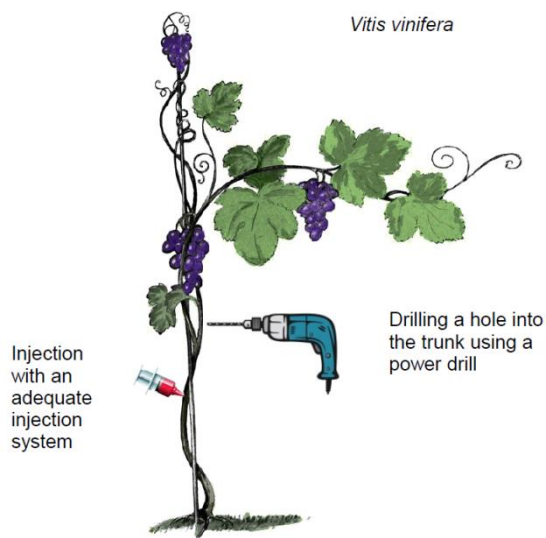
Figure 5.4 Schematic representative of vitis injections assay. (This image was taken from the patent application number: EP16154480.4)

The plants were monitored for five months after the injection. The monitoring ended when the autumn leaf coloration started. The plants were controlled on a six weeks basis for increasing or decreasing foliar Esca symptoms in comparison to their appearance to the previous control and the untreated plants. The discolorations were documented using a digital camera.

5.1.4 Potential application of lignin as bio-resource for carbon nanoparticles

5.1.4.1 Carbon preparation and characterization

Lignin and lignin particles were carbonized in a tubular furnace at 600 °C and 800 °C for 1 h with a heating rate of 5 °C·min^{-1} under N_2 atmosphere at constant flow rate. Surface area and pore size distributions of obtained carbon were determined from the nitrogen adsorption–desorption isotherms at -196 °C using an Autosorb (Quantachrome Clorp.). All samples were outgassed overnight at 110 °C, prior to the adsorption experiments.

XPS was conducted on a Kratos Axis Ultra^{DLD} spectrometer (Kratos, Manchester, England) using an Al Kα excitation source with a photon energy of 1487 eV. The data was acquired in the hybrid mode using a 0$^{°}$ take-off angle, defined as the angle between the surface

normal and the axis of the analyzer lens. A charge neutralizer was always used during spectra collection to compensate charge build-up on the samples. For calculating atomic compositions, spectra were collected with setting analyzer pass energy at 80 eV, and a linear background was subtracted for all peak quantifications. The peak areas were normalized by the manufacturer supplied sensitivity factors and atomic compositions were calculated accordingly with Casa XPS software. C 1s high-resolution spectra were collected with setting analyzer pass energy at 20 eV. The C 1s spectra were self-fitted by individual emissions using Voigt peak profiles and a linear background.

5.1.4.2 Adsorption procedure

The kinetic studies of methylene blue adsorption for obtained carbons were conducted at 25 $^{\circ}$C with initial concentration at 20 m·gl^{-1}. For each time 5 mg carbon and 1 ml solution were mixed and shaken at 200 rpm. Carbons were separated by filtration and the concentration of methylene blue was measured by UV spectroscopy (Lambda 25, PerkinElmer) at γ_{max} 675 nm at time intervals. The experiments were duplicated and the average values were reported. The uptake of methylene blue at time t, q_t (mg·g^{-1}), was calculated by the following equation:

$$q_t = \frac{V\,(C_0 - C_t)}{m}$$
<div align="right">Equation 5.4</div>

where C_0 and C_t are the initial and concentrations of methylene blue in solution at time t (mg·l^{-1}), respectively; V is the volume of the solution (l) and m is the weight of the adsorbent (g).

5.2 Uptake and translocation polymer nanoparticles in plants

Materials and Methods

Lignin was purchased from Aldrich Chemical Co. (kraft lignin, alkali). Prior to the experiment, lignin was extracted with propanol and dried in vacuum oven for overnight. Methacrylic anhydride, triethylamine, isopropyl alcohol, lithium chloride,

2,2´(ethylenedioxy)bis(ethalamine) and dimethyl formamide (DMF) were also obtained from Aldrich Chemical Co. The lithium chloride was dried at 70 °C in a vacuum oven before use. The anionic surfactant sodium dodecylsulfate (SDS) and hexadecane were purchased from Fluka and used as received. Mung bean seeds were purchased from Golden Chef Haricots mungo.

5.2.1 Influence of the nanoparticles on the germination and growth of mung beans

Nanoparticles synthesis

The magnetite nanoparticles coated by polystyrene were produced following the method of Bannwarth et al[181]. Firstly, oleic acid capped iron oxide nanoparticles were synthesized. 24.4 g (90 mmol) ferric chloride and 12.0 g (60 mmol) ferrous chloride were dissolved in 100 ml deionized water. 40 ml of a 28% aqueous ammonium hydroxide solution and 4.0 g (14.2 mmol) of oleic acid were added. The reaction mixture was heated to 70 °C for 1 h followed by a further heating to 100 °C at which temperature the mixture was stirred for additional 2 h under constant refilling of evaporating water. The resulting black precipitate was purified several times by magnetic separation and rinsing with deionized water and finally dried under vacuum overnight. Then finally the oleic acid capped iron oxide nanoparticles were coated with polystyrene. Briefly, 1 g of oleic acid capped iron oxide nanoparticles was redispersed in 2 g of n-octane for 30 min in a sonication bath followed by the addition of 24 g of an aqueous solution containing 25 mg of SDS. The two phase system was sonified with a tip sonifier for 3 min under ice cooling (70% amplitude, 10 s pulse, 5 s pause) and stirred non- magnetic ally (KPG - stirrer) at room temperature. Separately, 1 g of styrene was mixed with 30 mg n-hexadecane and 24 g of a 10 mg SDS containing aqueous solution were added. After sonication at a tip sonifier for 1 min under ice cooling (10% amplitude, 5 s pulse, 5 s pause) the dispersion was added to the magnetite containing dispersion. Nitrogen was bubbled through the combined dispersions for 5 min, KPS and sodium styrene sulfonate were added, and the reaction mixture was heated to 80 °C under stirring for 8 h. Purification of the magnetic polystyrene particles was carried out magnetically and by centrifugation   The hydrodynamic diameter of the particles from dynamic light scattering was found ca. 150 nm.

Experimental Part

The lignin nanoparticles entrapped pyclostrobin fungicide was obtained from miniemulsion process. Firstly, lignin was modified to be methacrylated-lignin as following procedure; 2 g of lignin (10 mmol) was dissolved in 60 ml of LiCl/dimethyl sulfoxide (DMF) at 90 ^{o}C under argon. After complete dissolution, 1 ml of the triethylamine (10 mmol) was added to the lignin solution and stirred for 15 min at 50 ^{o}C. 3 ml of methacrylic anhydride (20 mmol) then was slowly injected into the reaction flask. The reaction was kept at 50°C overnight. The reaction mixture was precipitated in isopropyl alcohol and isolated by centrifugation at 3000 rpm and re-precipitated three times. Then product was dried at room temperature in a vacuum oven. After obtained methacrylated-lignin, the crosslinked-lignin particles loaded and unloaded-fungicide were prepared by miniemulsion-solvent evaporation. Typically 100 mg (1.1 mmol of PPU) of methacrylated-lignin dissolved in 2.5 g of chloroform (CHCl$_3$). This solution was added into 10 g of water containing 20 mg of surfactant at room temperature and stirred at 1000 rpm for 1 h in order to form a pre-emulsion. Then the emulsion was treated with ultrasound for 3 min (1/2 inch tip, 70 % amplitude, 20 s ultrasound followed by 10 s pauses) under ice cooling in order to prevent evaporation of the solvent. A solution of diamine molecules (2,2´(ethylenedioxy)bis(ethalamine)) in water (1:1 mole ratio to methacrylated-lignin was added in the emulsion after sonication process. The reaction was carried out overnight at 50 ^{o}C. The solvent was evaporated from the miniemulsion by stirring it for overnight at room temperature. The final volume of dispersions was made up to 10 ml by water. The obtained particles were characterized by DLS and TEM. To study the grafting efficiency of Michael addition between methacrylated-lignin and diamine, the obtained particles were washed with water and chloroform and then dried overnight in vacuum oven. For the encapsulation of pyraclostrobin (fungicide), 5 mg of pyraclostrobin was added to the dispersed phase prior to mix with aqueous phase. The magnetite nanoparticles coated by polystyrene were produced following the method of Bannwarth et al.[215]. The hydrodynamic diameter of the particles from dynamic light scattering was found ca. 150 nm. The lignin nanoparticles entrapped pyclostrobin fungicide was obtained from the 5.1.3.1. section which were ca. 250 nm of diameter.

Seed germination

Mung seeds were surface-sterilized by 10% H$_2$O$_2$ solution for 10 min and then rinsed with deionized (DI) water 3 times. The 20 sterilized seeds were immersed in 2 ml of DI-water,

magnetite coated polystyrene nanoparticles (PS-FeNPs) (14, 28 µg·ml^{-1}) and lignin nanoparticles (1, 5 mg·ml^{-1}) dispersion for 2 days. Young seedlings were then transferred to separate container; there were 10 seeds per container, filled with 2 ml of medium containing magnetite nanoparticle and lignin nanoparticles at the same concentration in germination step as mentioned above and were incubated in a dark warm place at 30±1 °C. The treatment experiment included: (1) control (DI water only), (2) 1.4 mg·ml^{-1}of PS-FeNPs, (3) 2.8 mg·ml^{-1} of PS-FeNPs, (4) 1 mg·ml^{-1}of lignin NPs and (5) 5 mg·ml^{-1}of lignin NPs. The bean sprouts of all treatments were drenched every day with DI-water. They were exposed to the nanoparticles dispersion for 5 days before measured the length of the stem and later scarified for the extraction process to quantify the accumulation of the nanoparticles in the specific part of the pant by ICP or HPLC.

Fe determination - Acid digestion method

After harvesting of the young mung bean plant, roots stem and shoots were cut separately and washed three times with DI-water, then cut and grind each part of the young plant into small pieces. After preparation of the plant tissue, 5 ml of 69.0–70.0% trace-metal grade HNO_3 was added to each digestion flask at room temperature and then 25% H_2O_2 was slowly added. The digestion was heated to 90 °C and allowed to sit around 1 h. The sample solution appeared translucent slightly dark yellow. Prior to filtration and dilution, the samples were cooled down. All digest experiments were washed with 1:1 ratio of conc. HCl:H_2O in filtration step and made up to 25.0 ml by DI-water for inductively coupled plasma spectroscopy (ICP; ACTIVA Simultaneous CCD-ICP-OES Spectrometer, Horiba). Detection limits for Fe tested were approximately 5 µg·ml^{-1}.

Fungicide determination - Extraction method

The fungicide (pyclostrobin) was extracted from the plant by solvent extraction. After harvesting of the young mung bean plant, roots stem and shoots were cut separately and washed three times with DI-water, then cut each part of the young plant into small pieces. The samples were dried overnight by freeze dryer before grinding. The grinded samples were immerged in to gas chromatography analysis grade tetrahydrofuran (THF), shaken and then filtrated. Finally, the extraction fractions were collected three times for each sample and the quantification of pyclostrobin was done by high-pressure liquid chromatography (HPLC). The solution sample

were then passed through a 0.2 μm filter and analyzed by high pressure liquid chromatography (HPLC) method with Agilent Elicpse Plus RP18. The mobile phase was THF:water 0.1 wt% TFA-gradient, injection volume was 10 μl and the column temperature maintained at 20ºC. The analysis was performed at a flow rate of 0.2 ml·min^{-1} with the UV detector at 280 nm.

5.2.2 Uptake and distribute of the nanoparticles in plant

Sample preparation for TEM of plant tissues

After a 14 d treatment, plants were washed with deionized water thoroughly and hand cut to separate root, stem and leaf tissues and then firstly fixed in 2.5 wt% glutaraldehyde in 0.1 M phosphate buffer solution, pH 7.4 for overnight at 4 °C. After three times washing with phosphate buffer solution, then second fixed in 1vol% osmium tetroxide in 0.1M phosphate buffer, pH 7.4 for 1 h. Then after three times washing with phosphate buffer solution, they were dehydrated in a graded acetone series of acetone: the solutions used contained 10%, 30%, 50%, 70%, 90% acetone in pure water and finally with 100% acetone. Each solution was left on the tissues for 15 minutes. Acetone was then replaced by a 30:70 of EPON 812:acetone mixture, followed by a 50:50 mixture and a 70:30 mixture each mixture for overnight. Finally 100% EPON 812 was left on the tissues overnight, replaced by new EPON on the next day and left to polymerize at 60 °C for 3 days. Ultrathin sections (60 nm) were obtained using a Leica Ultracut UCT equipped with a 35° Diatome diamond knife. The sections were collected on copper grids followed by staining with 1% ruthenium tetraoxide solution and observed on a Tecnai F20 (FEI, USA) transmission electron microscope operating at 120 kV. TEM/EDX spectra were collected on a TEM equipped with energy dispersive X-ray spectrometer (EDAX, USA) with a beam diameter of 25 nm.

5.3 Glutathione responsive material

Materials and Method

For the kinetic study, bucillamine was obtained from Biozol diagnostic Vertrieb GmbH. 1,4-bis(3-(2-pyridyldithio)propionamido) butane (BPB), 1,1′-(Methylenedi-4,1-phenylene) bismaleimide, triethylene amine (TEA), THF-*d8*, D$_2$O, and chloroform-*d* were obtained from Sigma-Aldrich. The oil-soluble surfactant polyglycerol polyricinoleate (PGPR) was used for the preparation of the inverse miniemulsion systems. Hexamethylcyclo trisiloxane was used as internal standard. All chemicals were used without further purification.

5.3.1 Competing and simultaneous click reactions at the interface and in solution

5.3.1.1 Solution reaction of thiol-maleimide and thiol-disulfide interchange reaction

Appoximately 2.2 mg (10 µmol) of bucillamine and ca. 2.2 mg (10 µmol of hexamethylcyclo trisiloxane was dissolved in 500 ml of THF-*d8*. 50 µl (10 µmol) of 0.3 M TEA solution in THF-*d8* was also dropped in this solution. And, separately, a second solution of 3.6 mg (1 µmol of bismaleimide in 250 ml of THF-d8 was also prepared. These two solution was mixed in NMR tube and immediately introduced in the NMR spectrometer (Bruker Avance III 700 MHz) with the temperature of the experiment previously equilibrated (298 K or 283 K). In case of thiol-disulfide interchange reaction, a solution of 4.8 mg (10 µmol) of BPB in 150 ml of THF-d8 was prepared instead of bismaleimide solution. For dual reaction, 1.8 mg (0.5 µmol) of bismeimide and 2.4 mg (0.5 µmol) of BPB in 150 ml of THF-d8 was prepared and mixed with bucillamie solution.

5.3.1.2 Interfacial reaction of thiol-maleimide and thiol-disulfide interchange reaction in inverse-miniemulsion

For kinetics study of thiol-maleimide reaction, ca. 2.2 mg (10 µmol) of bucillamine and 0.5 mg of sodium chloride were dissolved in 100 mg of D_2O. 500 µl of a stock solution of chloroform-d/PGPR (0.8 wt%) was added and the mixture was stirred at 1000 rpm for 1 h. Meanwhile, a second solution composed of 3.6 mg (10 µmol) of bismaleimide and ca. 2.2 mg (10 µmol) of hexamethylcyclo trisiloxane was dissolved in 150 µl of chloroform-d. After 1 h, the pre-emulsificated mixture was submitted to a pulsed ultrasonication process in an ice bath for 60 s (2.5 s sonication, 5 s paused) at 60% amplitude using a 1/8" tip Branson 450W sonifier. The obtained miniemulsion was immediately transferred into a conventional NMR tube. A NMR spectrometer (Bruker Avance III 700 MHz) was previously equilibrated at the temperature of the experiment (283 K). The second solution containing the bismaleimide and hexamethylcyclo trisiloxane used as reference for the spectrum, were added to the NMR tube, homogenized and the tube was immediately introduced in the spectrometer. In case of thiol-disulfide interchange reaction, a solution of 4.8 mg (10 µmol) of BPB in 150 ml of chloroform-d was prepared instead of bismaleimide solution. For dual reaction, 1.8 mg (0.5 µmol) of bismaleimide and 2.4 mg (0.5 µmol) of BPB in 150 ml of chloroform-d was prepared. For each experiment, 100 ^{1}H NMR spectra were collected consecutively, using 32 transients with an 11 ms long 90° pulse. A 12600 Hz spectral width together with a recycling delay time of 3 s, resulting in a total time of 5 min for the collection of each spectrum and a total time of 600 min, was used for each experiment.

5.3.1.3 Determination of fluorescent dye sulforhodamine (SR101) after degradation of capsules by glutathione

The capsules were prepare by following the procedure in 5.1.3.2 for two "click" reactions thiol-maleimide addition and thiol-disulfide exchange. 10 µl of SR101 dye (5.5 mg·ml^{-1}) were added into water phase.

The capsules were re-dispersed in phosphate buffer solution at pH7 after the formation of the capsules in inverse miniemulsion. The capsules dispersion in cyclohexane was added into 4 ml of the buffer solution. The mixture was stirred for 24 h with open cap in order to guarantee evaporation of the solvent.

To 1 ml of the aqueous capsule dispersion (in buffer solution), 500 µl of glutathione in phosphate buffer solution (10 mg·ml^{-1}) was added. The mixture was kept stirring over 7 hours and then centrifuge at 10000 rpm for 30 min. The supernatant was investigated by fluorescence spectroscopy in order to determine the amount of released SR101. As control, a capsule dispersion that fluorescent dye was encapsulated was incubated with phosphate buffer at pH 7, room temperature for 7 h. The fluorescence signal of SR101 at difference concentrations was used to set up a calibration curve (Note: SR101 has an absorption maximum at 550 nm and the emission was measured at 605 nm). The total release of SR101 from the degraded capsule by enzyme was calculated from the calibration curve.

Kinetics

The curves of the kinetics measurements were fitted using the software Origin 9.0.

^{1}H NMR and 2D ^{1}H,^{1}H TOCSY

The ^{1}H NMR experiments were recorded with a 5 mm BBI 1 H/Xz- gradient on a 700 MHz spectrometer with a Bruker Avance III system. For the 1H NMR spectrum 64 transients were used with an 11µ s long 90° pulse and a 12600 Hz spectral width together with a recycling delay of 5 s. The assignment was accomplished by ^{1}H,^{1}H TOCSY (total correlated spectroscopy). The spectroscopic widths of the homo-nuclear 2D TOCSY, experiments were typically 13600 Hz in both dimension (f1 and f2) and the relaxation delay 2s. The mixing time used in the 2D TOSCY was kept at 100 ms.

2D ^{1}H, ^{13}C-HSQC

The experiments were done with a 5 mm triple resonance TXI ^{1}H/^{13}C/^{15}N probe with z-gradient on the 850 MHz spectrometer on a Bruker Avance III system. The data were analysed with Topspin 3.1 software from the Bruker Company.

For a ^{1}H NMR spectrum 128 transients were used with an 9.4 µs long 90° pulse and a 17600 Hz spectral width together with a recycling delay of 5s.

Experimental Part

The proton (850 MHz), carbon (213 MHz) were measured in a mixture of DMSO-d$_6$ at 298,3K and the spectra were referenced with the residual DMSO-d$_5$H at $\delta(^1H)$ = 2.49 ppm, DMSO-d$_6$ $\delta(^{13}C$ heptett) = 40,3 ppm.

The 2D ^{1}H,^{13}C-HSQC (heteronuclear single quantum correlations via double inept transfer and phase sensitive using Echo/Antiecho-TPPI gradient selection with decoupling during acquisition) and HSQC-edited (with multiplicity editing during selection step) experiments were run with 2048 points in f2 and 512 points in f1 dimension. The following parameters were used to obtain optimal results: ^{1}J$_{CH}$=145Hz for optimizing observable intensities of cross peaks from one bond ^{1}H-^{13}C correlation.

The spectral widths for ^{1}H and ^{13}C were 12000 Hz (14 ppm) for ^{13}C and 43000 Hz (199 ppm). Before Fourier transformation, the data were zero filled to 1024 points in f1 and multiplied by a window function (q-sine bell or sine bell) in both dimension. The carbon signals of the product from miniemulsion was extracted from the cross peaks ^{1}H,^{13}C-HSQC due to the poor signal intensities in a 1D ^{13}C NMR measurement.

5.4 Instrumentation

Ultra-sonication

The emulsion was treated with ultrasound by using a Branson Sonifier W-450-Digital. The tip size used depends on the sonified volume. For volume exceeding 10 ml, the tip size was 10 mm and for smaller volumes, a tip size of 6.5 mm was chosen. Ultrasonication was generally performed at 0 °C with ice cooling in order to prevent polymerization.

Infrared (IR) spectroscopy

The chemical composition of lignin and crosslinked-lignin was studied by FT-IR spectroscopy. The sample powder was obtained by freeze-drying of the capsule dispersion for overnight at -70 °C under reduced pressure. The dry samples were recorded a spectrum between 4000 and 400 cm^{-1} was recorded using a Nicolet iS10.

Transmission electron microscopy

Transmission electron Microscope (TEM) images were obtained on JEOL 1400. TEM samples were prepared by placing sample dilution on the 300 mesh carbon coated copper grid and dried under ambient conditions.

Scanning electron microscopy

Scanning electron microscopy (SEM) images were taken by a 1530 Gemini LEO from Zeiss with accelerating voltages between 100 V to 30 kV. For the SEM studies, the Samples were diluted in cyclohexane or water, placed onto a 5x5 mm silicon wafer and dried under ambient conditions.

Dynamic light scattering (DLS)

The average capsule size and the size distribution were measured using a PSS NicompParticle Sizer 380 (Nicomp Particle Sizing Systems, USA) equipped with a detector at 90° scattering mode at 20 °C. The samples were dilute in cyclohexane or water, then sonicated for 5 min in sonication bath.

Fluorescence spectroscopy

The degradation and permeability of the capsule's shell was studied on SR101-containing capsules redispersed in water using a fluorescence spectrometer (NanoDrop ND-3300, PEQLab).

Differential Scanning Calorimeter (DSC)

DSC measurements were made with samples of about 10 mg on a Mettler Toledo DSC 823 differential scanning calorimeter operating with a cooling and heating rate 10 °C·min^{-1} under a nitrogen flow rate of 10 ml·min^{-1}.

Experimental Part

Nuclear Magnetic Resonance (NMR)

Proton nuclear magnetic resonance (1H-NMR) spectra, Diffusion-ordered NMR spectroscopy (DOSY NMR) were recorded on a Bruker Avance spectrometer 700 MHz.

Diffusion ordered spectroscopy NMR (DOSY-NMR) experiments were conducted on a Bruker Avance-III 700 MHz NMR Spectrometer employing a 5 mm BBI 1H/X z-gradient probe with a gradient strength of 5.35 [$G \cdot mm^{-1}$]. The gradient strength was properly calibrated by analysis of a sample of $2H_2O/1H_2O$ at a defined temperature and comparison with the theoretical diffusion coefficient of $2H_2O/1H_2O$. The temperature was kept constant at 298.3 K using the Bruker Topspin 3.1 software monitoring a standard 1H methanol NMR sample. The gradient strength was varied in 32 or 64 steps from 2% to 100%. The diffusion time was 350 ms, while the gradient pulse length was 1.1 ms. For the diffusion measurements a 2D sequence (Bruker program: dstebpgp3s) was employed using double stimulated echo for convection compensation.

Gel permeation chromatography (GPC) analysis

The apparent molecular weight was determined by gel permeation chromatography (Agilent Technologies 1260 Infinity). After 10 h of reaction from NMR spectrometer, the samples were directly analyzed by GPC. Solutions of the final materials with concentrations of 1 $mg \cdot ml^{-1}$ were prepared in DMF, injected at a flow of 1 $ml \cdot min^{-1}$ with DMF as eluent phase. The signal was detected with a UV-Vis detector S-3702 (Soma) and the molecular weight was obtained with the software PSS-WinGPC UniChrom (PSS) against PS standards.

Thermogravimetry

Gravimetric measurements were performed with a Mettler-Toledo TGA851 with a heating rate 10 °C·min^{-1} under a nitrogen flow rate of 10 $ml \cdot min^{-1}$.

Tensiometry

Surface tension measurements of the latexes were carried out at 22 °C using a DCAT11 tensiometer from Dataphysics, employing the Du Nouy ring method. The ring radius of the Pt-Ir ring is 9.4425 mm and the wire radius is 0.185 mm. Each measurement was repeated 10 times

and the average value was taken as result. The liquid-liquid system were measured by the spinning drop method using a Spinning drop video tensiometer SVT 20N (Dataphysic).

Contact angle

The contact angles of polymer film and liquid were measured by a video-based optical contact angle measuring system OCA20 from Dataphysic.

Ultraviolet-Visible Spectroscopy (UV-Vis)

UV analyses were carried out with a Perkin Elmer UV-Vis spectrometer Lambda25. The measurements were done between 250 and 800 nm.

X-ray Photoelectron Spectroscopy (XPS)

X-ray photoelectron spectroscopy (XPS) analysis was performed using an a Kratos Axis Ultra^{DLD} spectrometer (Kratos, Manchester, England) using an Al Kα excitation source with a photon energy of 1487 eV. The data was acquired in the hybrid mode using a $0°$ take-off angle, defined as the angle between the surface normal and the axis of the analyzer lens

6.   References

1.   Calvo-Flores, F. G.; Dobado, J. A.; Isac-García, J.; Martín-Martínez, F. J., *Lignin and Lignans as Renewable Raw Materials: Chemistry, Technology and Applications*. John Wiley & Sons, Ltd.: 2015; p 512.

2.   De Franceschi, S.; Kouwenhoven, L., Nanotechnology: Electronics and the single atom. *Nature* **2002,** 417, (6890), 701-702.

3.   Wang, Z. L.; Wu, W., Nanotechnology-enabled energy harvesting for self-powered micro-/nanosystems. *Angew. Chem., Int. Ed.* **2012,** 51, (47), 11700-11721.

4.   Moghimi, S. M.; Hunter, A. C.; Murray, J. C., Nanomedicine: current status and future prospects. *FASEB J.* **2005,** 19, (3), 311-330.

5.   Zhang, J.; Li, M.; Fan, T.; Xu, Q.; Wu, Y.; Chen, C.; Huang, Q., Construction of novel amphiphilic chitosan copolymer nanoparticles for chlorpyrifos delivery. *J. Polym. Res.* **2013,** 20, (3), 1-11.

6.   Perez-de-Luque, A.; Rubiales, D., Nanotechnology for parasitic plant control. *Pest Manage. Sci.* **2009,** 65, (5), 540-545.

7.   Montané, D.; Torné-Fernández, V.; Fierro, V., Activated carbons from lignin: kinetic modeling of the pyrolysis of Kraft lignin activated with phosphoric acid. *Chem. Eng.J.* **2005,** 106, (1), 1-12.

8.   Chatterjee, S.; Clingenpeel, A.; McKenna, A.; Rios, O.; Johs, A., Synthesis and characterization of lignin-based carbon materials with tunable microstructure. *RSC Adv.* **2014,** 4, (9), 4743-4753.

9.   Hatakeyama, H.; Hatakeyama, T., Lignin structure, properties, and applications. *Adv. Polym. Sci.* **2010,** 232, (Biopolymers), 1-63.

10.   Boerjan, W. Bio-Energy. (Accessed on January 20, 2016), Retrieved from http://www.psb.ugent.be/bio-energy/313-lignin

11.   Cells - What is a Cell Wall? (Accessed on January 20, 2016), Retrieved from http://www.kidsbiology.com/biology_basics/cells_tissues_organs/cell_wall6.php

12.   Calvo-Flores, F. G.; Dobado, J. A., Lignin as renewable raw material. *ChemSusChem* **2010,** 3, (11), 1227-1235.

13.   Joseph, L. M.; Aminul, I., Lignin chemistry, technology, and utilization: A brief history. In *Lignin: Historical, Biological, and Materials Perspectives*, American chemical society: 1999; Vol. 742, pp 2-99.

14.   Adler, E., Lignin chemistry - past, present and future. *Wood Sci. Technol.* **1977,** 11, (3), 169-218.

15.   Gupta, P. R.; Goring, D. A. I., Physicochemical studies of alkali lignins: I. Preparatioan and properties of fractions. *Can. J. Chem.* **1960,** 38, (2), 248-258.

References

16. Gupta, P. R.; Goring, D. A. I., Physicochemical studies of alkali lignins: III. Size and shape of the machoolecule. *Can. J. Chem.* **1960,** 38, (2), 270-279.

17. Gupta, P. R.; Robertson, R. F.; Goring, D. A. I., Physicochemical studies of alkali lignins: II. Ultracentrifugal sedimentation analysis. *Can. J. Chem.* **1960,** 38, (2), 259-269.

18. Rezanowich, A.; Goring, D. A. I., Polyelectrolyte expansion of a lignin sulfonate microgel. *J. Colloid Sci.* **1960,** 15, (5), 452-471.

19. Dong, D.; Fricke, A. L., Intrinsic viscosity and the molecular weight of kraft lignin. *Polymer* **1995,** 36, (10), 2075-2078.

20. Pla, F., Light Scattering. In *Methods in Lignin Chemistry*, Lin, S. Y.; Dence, C. W., Eds. Springer Berlin Heidelberg: Berlin, Heidelberg, 1992; pp 498-508.

21. Glasser, W. G.; Davé, V.; Frazier, C. E., Molecular weight distribution of (semi-) commercial lignin derivatives. *J. Wood Chem. Technol.* **1993,** 13, (4), 545-559.

22. Lora, J. H.; Glasser, W. G., Recent industrial applications of lignin: a sustainable alternative to nonrenewable materials. *J. Polym. Environ.* **2002,** 10, (1/2), 39-48.

23. Zakzeski, J.; Bruijnincx, P. C. A.; Jongerius, A. L.; Weckhuysen, B. M., The catalytic valorization of lignin for the production of renewable chemicals. *Chem. Rev.* **2010,** 110, (6), 3552-3599.

24. Hofrichter, M.; Steinbuechtel, A., *Biopolymers, Volume 1: Lignin, Humic Substances and Coal*. Wiley-VCH Verlag GmbH: 2001; p 513 pp.

25. Bollag, J. M.; Shuttleworth, K. L.; Anderson, D. H., Laccase-mediated detoxification of phenolic compounds. *Appl. Environ. Microbiol.* **1988,** 54, (12), 3086-91.

26. Palmore, G. T. R.; Kim, H.-H., Electro-enzymic reduction of dioxygen to water in the cathode compartment of a biofuel cell. *J. Electroanal. Chem.* **1999,** 464, (1), 110-117.

27. Barriere, F.; Kavanagh, P.; Leech, D., A laccase-glucose oxidase biofuel cell prototype operating in a physiological buffer. *Electrochim. Acta* **2006,** 51, (24), 5187-5192.

28. Vianello, F.; Cambria, A.; Ragusa, S.; Cambria, M. T.; Zennaro, L.; Rigo, A., A high sensitivity amperometric biosensor using a monomolecular layer of laccase as biorecognition element. *Biosens. Bioelectron.* **2004,** 20, (2), 315-321.

29. Tan, Y.; Deng, W.; Li, Y.; Huang, Z.; Meng, Y.; Xie, Q.; Ma, M.; Yao, S., Polymeric bionanocomposite cast thin films with in situ laccase-catalyzed polymerization of dopamine for biosensing and biofuel cell applications. *J. Phys. Chem.* **2010,** 114, (15), 5016-5024.

30. Christopher, L. P.; Yao, B.; Ji, Y., Lignin biodegradation with laccase-mediator systems. *Frontiers in Energy Research* **2014,** 2.

31. Gosselink, R. J. A.; de Jong, E.; Guran, B.; Abacherli, A., Co-ordination network for lignin-standardisation, production and applications adapted to market requirements (EUROLIGNIN). *Ind. Crops Prod.* **2004,** 20, (2), 121-129.

32. Tecnaro website. (Accessed on January 22, 2016) Retrieved from http://www.tecnaro.de/english/willkommen.htm?section=we.

33. Thielemans, W.; Wool, R. P., Lignin esters for use in unsaturated thermosets: Lignin modification and solubility modeling. *Biomacromolecules* **2005,** 6, (4), 1895-1905.

34. Akato, K.; Tran, C. D.; Chen, J.; Naskar, A. K., Poly(ethylene oxide)-assisted macromolecular self-Assembly of lignin in ABS matrix for sustainable composite applications. *ACS Sustainable Chem. Eng.* **2015,** 3, (12), 3070-3076.

35. Sivasankarapillai, G.; Li, H.; McDonald, A. G., Lignin-based triple shape memory polymers. *Biomacromolecules* **2015,** 16, (9), 2735-2742.

36. Kai, D.; Tan, M. J.; Chee, P. L.; Chua, Y. K.; Yap, Y. L.; Loh, X. J., Towards lignin-based functional materials in a sustainable world. *Green Chem.* **2016,** 18, (5), 1175-1200.

37. Duval, A.; Lawoko, M., A review on lignin-based polymeric, micro- and nano-structured materials. *React. Funct. Polym.* **2014,** 85, 78-96.

38. Gupta, C.; Washburn, N. R., Polymer-Grafted Lignin Surfactants Prepared via Reversible Addition-Fragmentation Chain-Transfer Polymerization. *Langmuir* **2014,** 30, (31), 9303-9312.

39. Yu, J.; Wang, J.; Wang, C.; Liu, Y.; Xu, Y.; Tang, C.; Chu, F., UV-Absorbent Lignin-Based Multi-Arm Star Thermoplastic Elastomers. *Macromol. Rapid Commun.* **2015,** 36, (4), 398-404.

40. Ganesh, V. A.; Baji, A.; Ramakrishna, S., Smart functional polymers - a new route towards creating a sustainable environment. *RSC Adv.* **2014,** 4, (95), 53352-53364.

41. Lu, Y.; Sun, W.; Gu, Z., Stimuli-responsive nanomaterials for therapeutic protein delivery. *J. Controlled Release* **2014,** 194, 1-19.

42. Confortini, O.; Du Prez, F. E., Functionalized thermo-responsive poly(vinyl ether) by living cationic random copolymerization of methyl vinyl ether and 2-chloroethyl vinyl ether. *Macromol. Chem. Phys.* **2007,** 208, (17), 1871-1882.

43. Hoogenboom, R., Poly(2-oxazoline)s: A Polymer class with numerous potential applications. *Angew. Chem. Int. Ed.* **2009,** 48, (43), 7978-7994.

44. Schattling, P.; Jochum, F. D.; Theato, P., Multi-stimuli responsive polymers - the all-in-one talents. *Polym. Chem.* **2014,** 5, (1), 25-36.

45. Lutz, J.-F., Polymerization of oligo(ethylene glycol) (meth)acrylates: Toward new generations of smart biocompatible materials. *J. Polym. Sci. Part B Polym. Chem.* **2008,** 46, (11), 3459-3470.

References

46. Saeed, A. O.; Magnusson, J. P.; Moradi, E.; Soliman, M.; Wang, W.; Stolnik, S.; Thurecht, K. J.; Howdle, S. M.; Alexander, C., Modular construction of multifunctional bioresponsive cell-targeted nanoparticles for gene delivery. *Bioconjugate Chem.* **2011,** 22, (2), 156-168.

47. Shiraishi, Y.; Miyamoto, R.; Hirai, T., Spiropyran-conjugated thermoresponsive copolymer as a colorimetric thermometer with linear and reversible color change. *Org Lett.* **2009,** 11, (7), 1571-1574.

48. Albini, A.; Fasani, E.; Faiardi, D., Charge-transfer and exciplex pathway in the photocycloaddition of 9-anthracenecarbonitrile with anthracene and naphthalenes. *J. Org. Chem.* **1987,** 52, (1), 155-157.

49. Jochum, F. D.; Theato, P., Temperature and light sensitive copolymers containing azobenzene moieties prepared via a polymer analogous reaction. *Polymer* **2009,** 50, (14), 3079-3085.

50. Hirakura, T.; Nomura, Y.; Aoyama, Y.; Akiyoshi, K., Photoresponsive nanogels formed by the self-assembly of spiropyrane-bearing pullulan that act as artificial molecular chaperones. *Biomacromolecules* **2004,** 5, (5), 1804-1809.

51. Zhao, Y., Photocontrollable block copolymer micelles: what can we control? *J. Mater. Chem.* **2009,** 19, (28), 4887-4895.

52. Irvin, D. J.; Goods, S. H.; Whinnery, L. L., Direct measurement of extension and force in conductive polymer gel actuators. *Chem. Mater*. **2001,** 13, (4), 1143-1145.

53. Kumar, A.; Srivastava, A.; Galaev, I. Y.; Mattiasson, B., Smart polymers: Physical forms and bioengineering applications. *Prog. Polym. Sci.* **2007,** 32, (10), 1205-1237.

54. Xiongjun, Y.; Shaobing, Z.; Xiaotong, Z.; Tao, G.; Yu, X.; Botao, S., A biodegradable shape-memory nanocomposite with excellent magnetism sensitivity. *Nanotechnology* **2009,** 20, (23), 235702.

55. Cuevas, J. M.; Alonso, J.; German, L.; Iturrondobeitia, M.; Laza, J. M.; Vilas, J. L.; León, L. M., Magneto-active shape memory composites by incorporating ferromagnetic microparticles in a thermo-responsive polyalkenamer. *Smart Mater. Struct.* **2009,** 18, (7), 075003.

56. Varga, Z.; Filipcsei, G.; Zrínyi, M., Magnetic field sensitive functional elastomers with tuneable elastic modulus. *Polymer* **2006,** 47, (1), 227-233.

57. Nunes, S. P.; Behzad, A. R.; Hooghan, B.; Sougrat, R.; Karunakaran, M.; Pradeep, N.; Vainio, U.; Peinemann, K.-V., Switchable pH-responsive polymeric membranes prepared via block copolymer micelle assembly. *ACS Nano* **2011,** 5, (5), 3516-3522.

58. Jia, H.; Wildes, A.; Titmuss, S., Structure of pH-responsive polymer brushes grown at the gold–water interface: Dependence on grafting density and temperature. *Macromolecules* **2012,** 45, (1), 305-312.

59.   Liu, R.; Liao, P.; Liu, J.; Feng, P., Responsive polymer-coated mesoporous silica as a pH-sensitive nanocarrier for controlled release. *Langmuir* **2011,** 27, (6), 3095-3099.

60.   Dai, S.; Ravi, P.; Tam, K. C., pH-Responsive polymers: synthesis, properties and applications. *Soft Matter* **2008,** 4, (3), 435-449.

61.   Zhang, H.; Mardyani, S.; Chan, W. C. W.; Kumacheva, E., Design of biocompatible chitosan microgels for targeted pH-mediated intracellular release of cancer therapeutics. *Biomacromolecules* **2006,** 7, (5), 1568-1572.

62.   Lin, Y.-H.; Sonaje, K.; Lin, K. M.; Juang, J.-H.; Mi, F.-L.; Yang, H.-W.; Sung, H.-W., Multi-ion-crosslinked nanoparticles with pH-responsive characteristics for oral delivery of protein drugs. *J. Controlled Release* **2008,** 132, (2), 141-149.

63.   Wu, W.; Shen, J.; Banerjee, P.; Zhou, S., Chitosan-based responsive hybrid nanogels for integration of optical pH-sensing, tumor cell imaging and controlled drug delivery. *Biomaterials* **2010,** 31, (32), 8371-8381.

64.   Tong, W.; Gao, C.; Moehwald, H., pH-responsive protein microcapsules fabricated via glutaraldehyde mediated covalent layer-by-layer assembly. *Colloid Polym. Sci.* **2008,** 286, (10), 1103-1109.

65.   Wu, Y.; Chakrabortty, S.; Gropeanu, R. A.; Wilhelmi, J.; Xu, Y.; Er, K. S.; Kuan, S. L.; Koynov, K.; Chan, Y.; Weil, T., pH-Responsive Quantum Dots via an Albumin Polymer Surface Coating. *J. Am. Chem. Soc.* **2010,** 132, (14), 5012-5014.

66.   Narayani, R.; Rao, K. P., pH-responsive gelatin microspheres for oral delivery of anticancer drug methotrexate. *J. Appl. Polym. Sci.* **1995,** 58, (10), 1761-9.

67.   Zhang, Y.; Wang, Z.; Wang, Y.; Zhao, J.; Wu, C., Facile preparation of pH-responsive gelatin-based core-shell polymeric nanoparticles at high concentrations via template polymerization. *Polymer* **2007,** 48, (19), 5639-5645.

68.   Mahdavinia, G. R.; Pourjavadi, A.; Hosseinzadeh, H.; Zohuriaan, M. J., Modified chitosan. 4. Superabsorbent hydrogels from poly(acrylic acid-co-acrylamide) grafted chitosan with salt- and pH-responsiveness properties. *Eur. Polym. J.* **2004,** 40, (7), 1399-1407.

69.   Yuan, L.; Tang, Q.; Yang, D.; Zhang, J. Z.; Zhang, F.; Hu, J., Preparation of pH-responsive mesoporous silica nanoparticles and their application in controlled drug delivery. *J. Phys. Chem. C* **2011,** 115, (20), 9926-9932.

70.   Xu, S.; Luo, Y.; Haag, R., Water-soluble pH-responsive dendritic core-shell nanocarriers for polar dyes based on poly(ethylene imine). *Macromol. Biosci.* **2007,** 7, (8), 968-974.

71.   Burke, S. E.; Barrett, C. J., pH-Responsive properties of multilayered poly(L-lysine)/hyaluronic acid surfaces. *Biomacromolecules* **2003,** 4, (6), 1773-1783.

References

72. Motoyama, K.; Koike, T.; Akita, M., Remarkable switching behavior of bimodally stimuli-responsive photochromic dithienylethenes with redox-active organometallic attachments. *Chem. Commun.* **2008**, (44), 5812-5814.

73. Akhoury, A.; Bromberg, L.; Hatton, T. A., Redox-responsive gels with tunable hydrophobicity for controlled solubilization and release of organics.*ACS Appl. Mater. Interfaces.* **2011,** 3, (4), 1167-1174.

74. Song, J.; Janczewski, D.; Ma, Y.; Hempenius, M.; Xu, J.; Vancso, G. J., Redox-controlled release of molecular payloads from multilayered organometallic polyelectrolyte films. *J. Mater. Chem. B* **2013,** 1, (6), 828-834.

75. Liu, R.; Zhao, X.; Wu, T.; Feng, P., Tunable redox-responsive hybrid Nanogated Ensembles. *J. Am. Chem. Soc.* **2008,** 130, (44), 14418-14419.

76. Ishii, S.; Kaneko, J.; Nagasaki, Y., Dual stimuli-responsive redox-active injectable gel by polyion complex based flower micelles for biomedical applications. *Macromolecules.* **2015,** 48, (9), 3088-3094.

77. Oyaizu, K.; Nishide, H., Radical polymers for organic electronic devices: A radical departure from conjugated polymers? *Adv. Mater.* **2009,** 21, (22), 2339-2344.

78. Ito, Y.; Casolaro, M.; Kono, K.; Imanishi, Y., An insulin-releasing system that is responsive to glucose. *J. Controlled Release* **1989,** 10, (2), 195-203.

79. Chu, L.-Y.; Li, Y.; Zhu, J.-H.; Wang, H.-D.; Liang, Y.-J., Control of pore size and permeability of a glucose-responsive gating membrane for insulin delivery. *J. Controlled Release* **2004,** 97, (1), 43-53.

80. Hassan, C. M.; Doyle, F. J., III; Peppas, N. A., Dynamic behavior of glucose-responsive poly(methacrylic acid-g-ethylene glycol) hydrogels. *Macromolecules* **1997,** 30, (20), 6166-6173.

81. Podual, K.; Doyle, F. J., III; Peppas, N. A., Preparation and dynamic response of cationic copolymer hydrogels containing glucose oxidase. *Polymer* **2000,** 41, (11), 3975-3983.

82. Kashyap, N.; Viswanad, B.; Sharma, G.; Bhardwaj, V.; Ramarao, P.; Kumar, M. N. V. R., Design and evaluation of biodegradable, biosensive in situ gelling system for pulsatile delivery of insulin. *Biomaterials* **2007,** 28, (11), 2051-2060.

83. Kataoka, K.; Miyazaki, H.; Bunya, M.; Okano, T.; Sakurai, Y., Totally synthetic polymer gels responding to external glucose concentration: Their preparation and application to on-off regulation of insulin release. *J. Am. Chem. Soc.* **1998,** 120, (48), 12694-12695.

84. Andrieu, J.; Kotman, N.; Maier, M.; Mailänder, V.; Strauss, W. S. L.; Weiss, C. K.; Landfester, K., Live monitoring of cargo release from peptide-based hybrid nanocapsules induced by enzyme cleavage. *Macromol. Rapid Commun.* **2012,** 33, (3), 248-253.

85.   Fuchs, A. V.; Kotman, N.; Andrieu, J.; Mailander, V.; Weiss, C. K.; Landfester, K., Enzyme cleavable nanoparticles from peptide based triblock copolymers. *Nanoscale* **2013,** 5, (11), 4829-4839.

86.   Baier, G.; Cavallaro, A.; Vasilev, K.; Mailänder, V.; Musyanovych, A.; Landfester, K., Enzyme responsive hyaluronic acid nanocapsules containing polyhexanide and their exposure to bacteria to prevent infection. *Biomacromolecule.* **2013,** 14, (4), 1103-1112.

87.   Vincent, B., *Colloid Science : Principles, methods and application*. John Wiley & Son Ltd.: 2010.

88.   Cosgrove, T., Polymers and Polymer Solutions. In *Colloid Science*, Blackwell Publishing Ltd.: 2009; pp 98-112.

89.   Antonietti, M.; Landfester, K., Polyreactions in miniemulsions. *Prog. Polym. Sci.* **2002,** 27, (4), 689-757.

90.   Verschueren, K., *Handbook of Environmental Data of Organic Chemicals*. 2 ed.; Van Nostrand Reinhold Co.: New York, NY, 1983.

91.   Weiss, C. K.; Landfester, K., Miniemulsion polymerization as a means to encapsulate organic and inorganic materials. *Adv. Polym. Sci.* **2010,** 233, (Hybrid Latex Particles), 185-236.

92.   Landfester, K.; Bechthold, N.; Tiarks, F.; Antonietti, M., Formulation and stability mechanisms of polymerizable miniemulsions. *Macromolecules* **1999,** 32, (16), 5222-5228.

93.   Fickert, J.; Rupper, P.; Graf, R.; Landfester, K.; Crespy, D., Design and characterization of functionalized silica nanocontainers for self-healing materials. *J. Mater. Chem.* **2012,** 22, (5), 2286-2291.

94.   Malzahn, K.; Marsico, F.; Koynov, K.; Landfester, K.; Weiss, C. K.; Wurm, F. R., Selective interfacial olefin cross metathesis for the preparation of hollow nanocapsules. *ACS Macro. Lett.* **2014,** 3, (1), 40-43.

95.   Crespy, D.; Stark, M.; Hoffmann-Richter, C.; Ziener, U.; Landfester, K., Polymeric nanoreactors for hydrophilic reagents synthesized by interfacial polycondensation on miniemulsion droplets. *Macromolecules* **2007,** 40, (9), 3122-3135.

96.   Landfester, K.; Tiarks, F.; Hentze, H.-P.; Antonietti, M., Polyaddition in miniemulsions: A new route to polymer dispersions. *Macro. Chem. Phys.* **2000,** 201, (1), 1-5.

97.   Tiarks, F.; Landfester, K.; Antonietti, M., One-step preparation of polyurethane dispersions by miniemulsion polyaddition. *J. Polym. Sci., Part A: Polym. Chem.* **2001,** 39, (14), 2520-2524.

98.   Barrere, M.; Landfester, K., High Molecular Weight Polyurethane and Polymer Hybrid Particles in Aqueous Miniemulsion. *Macromolecules* **2003,** 36, (14), 5119-5125.

References

99.   Crespy, D.; Landfester, K., Anionic polymerization of ε-caprolactam in miniemulsion: Synthesis and characterization of polyamide-6 nanoparticles. *Macromolecules* **2005,** 38, (16), 6882-6887.

100.   Weiss, C. K.; Ziener, U.; Landfester, K., A route to nonfunctionalized and functionalized poly(n-butylcyanoacrylate) nanoparticles: preparation in miniemulsion. *Macromolecules* **2007,** 40, (4), 928-938.

101.   Landfester, K.; Weiss, C. K., Encapsulation by miniemulsion polymerization. *Adv. Polym. Sci.* **2010,** 229, (Modern Techniques for Nano- and Microreactors/-Reactions), 1-49.

102.   Reis, C. P.; Neufeld, R. J.; Ribeiro, A. J.; Veiga, F., Nanoencapsulation. II. Biomedical applications and current status of peptide and protein nanoparticulate delivery systems. *Nanomedicine* **2006,** 2, (2), 53-65.

103.   Park, S.-J.; Arshady, R., Microcapsules for fragrances and cosmetics. *Microspheres, Microcapsules Liposomes* **2003,** 6, 157-198.

104.   Brannon-Peppas, L., Controlled release in the food and cosmetics industries. *ACS Symp. Ser.* **1993,** 520, (Polymeric Delivery Systems), 42-52.

105.   Suntivich, R.; Shchepelina, O.; Choi, I.; Tsukruk, V. V., Ink-jet-assisted layer-by-layer printing of encapsulated arrays. *ACS Appl. Mater. Interfaces* **2012,** 4, (6), 3102-3110.

106.   Ziegler, A.; Landfester, K.; Musyanovych, A., Synthesis of phosphonate-functionalized polystyrene and poly(methyl methacrylate) particles and their kinetic behavior in miniemulsion polymerization. *Colloid Polym. Sci.* **2009,** 287, (11), 1261-1271.

107.   Lorenz, M. R.; Kohnle, M.-V.; Dass, M.; Walther, P.; Hoecherl, A.; Ziener, U.; Landfester, K.; Mailaender, V., Synthesis of fluorescent polyisoprene nanoparticles and their uptake into various cells. *Macromol. Biosci.* **2008,** 8, (8), 711-727.

108.   Zhao, X.; Zhou, S.; Chen, M.; Wu, L.; Gu, G., Encapsulation of hydrophilic dyes with polystyrene using double miniemulsion technique. *J. Appl. Polym. Sci.* **2011,** 119, (6), 3615-3622.

109.   Baier, G.; Friedemann, K.; Leuschner, E.-M.; Musyanovych, A.; Landfester, K., pH Stability of poly(urethane/urea) capsules synthesized from different hydrophilic monomers via interfacial polyaddition in the inverse miniemulsion process. *Macromol. Symp.* **2013,** 331-332, (1), 71-80.

110.   Schreiber, E.; Ziener, U.; Manzke, A.; Plettl, A.; Ziemann, P.; Landfester, K., Preparation of narrowly size distributed metal-containing polymer latexes by miniemulsion and other emulsion techniques: Applications for nanolithography. *Chem. Mater.* **2009,** 21, (8), 1750-1760.

111.   Theisinger, S.; Schoeller, K.; Osborn, B.; Sarkar, M.; Landfester, K., Encapsulation of a fragrance via miniemulsion polymerization for temperature-controlled release. *Macromol. Chem. Phys.* **2009,** 210, (6), 411-420.

112. Tiarks, F.; Landfester, K.; Antonietti, M., Encapsulation of carbon black by miniemulsion polymerization. *Macromol. Chem. Phys.* **2001,** 202, (1), 51-60.

113. Steiert, N.; Landfester, K., Encapsulation of organic pigment particles via miniemulsion polymerization. *Macromol. Mater. Eng.* **2007,** 292, (10-11), 1111-1125.

114. Xu, Z. Z.; Wang, C. C.; Yang, W. L.; Deng, Y. H.; Fu, S. K., Encapsulation of nanosized magnetic iron oxide by polyacrylamide via inverse miniemulsion polymerization. *J. Magn. Magn. Mater.* **2004,** 277, (1–2), 136-143.

115. Wormuth, K., Superparamagnetic latex via inverse emulsion polymerization. *J. Colloid Interface Sci.* **2001,** 241, (2), 366-377.

116. Ramirez, L. P.; Landfester, K., Magnetic polystyrene nanoparticles with a high magnetite content obtained by miniemulsion processes. *Macromol. Chem. Phys.* **2003,** 204, (1), 22-31.

117. Landfester, K.; Ramirez, L. P., Encapsulated magnetite particles for biomedical application. *J. Phys.: Condens. Matter* **2003,** 15, (15), S1345-S1361.

118. Tong, W.; Song, X.; Gao, C., Layer-by-layer assembly of microcapsules and their biomedical applications. *Chem. Soc. Rev.* **2012,** 41, (18), 6103-6124.

119. Wang, Y.; Angelatos, A. S.; Caruso, F., Template synthesis of nanostructured materials via layer-by-layer assembly. *Chem. Mater.* **2008,** 20, (3), 848-858.

120. Landfester, K., The generation of nanoparticles in miniemulsions. *Adv. Mater.* **2001,** 13, (10), 765-768.

121. Cao, Z.; Ziener, U., A versatile technique to fabricate capsules: miniemulsion. *Curr. Org. Chem.* **2013,** 17, (1), 30-38.

122. Torza, S.; Mason, S. G., Three-phase interactions in shear and electrical fields. *J. Colloid Interface Sci.* **1970,** 33, (1), 67-83.

123. van Zyl, A. J. P.; Sanderson, R. D.; de Wet-Roos, D.; Klumperman, B., Core/shell particles containing liquid cores: Morphology prediction, synthesis, and characterization. *Macromolecules* **2003,** 36, (23), 8621-8629.

124. Fernandez-Perez, M.; Villafranca-Sanchez, M.; Flores-Cespedes, F.; Daza-Fernandez, I., Ethylcellulose and lignin as bearer polymers in controlled release formulations of chloridazon. *Carbohdr. Polym* **2011,** 83, (4), 1672-1679.

125. Flores-Céspedes, F.; Figueredo-Flores, C. I.; Daza-Fernández, I.; Vidal-Peña, F.; Villafranca-Sánchez, M.; Fernández-Pérez, M., Preparation and characterization of imidacloprid lignin–polyethylene glycol matrices coated with ethylcellulose. *J. Agric. Food Chem.* **2011,** 60, (4), 1042-1051.

References

126. Ciolacu, D.; Oprea, A. M.; Anghel, N.; Cazacu, G.; Cazacu, M., New cellulose-lignin hydrogels and their application in controlled release of polyphenols. *Mater. Sci. Eng. C Mater. Biol. Appl.* **2012,** 32, (3), 452-463.

127. Yiamsawas, D.; Baier, G.; Thines, E.; Landfester, K.; Wurm, F. R., Biodegradable lignin nanocontainers. *RSC Adv.* **2014,** 4, (23), 11661-11663.

128. Faria, F. A. C.; Evtuguin, D. V.; Rudnitskaya, A.; Gomes, M. T. S. R.; Oliveira, J. A. B. P.; Graca, M. P. F.; Costa, L. C., Lignin-based polyurethane doped with carbon nanotubes for sensor applications. *Polym. Inter.* **2012,** 61, (5), 788-794.

129. Gao, G.; Dallmeyer, J. I.; Kadla, J. F., Synthesis of Lignin nanofibers with ionic-responsive shells: Water-expandable lignin-based nanofibrous mats.. *Biomacromolecules* **2012,** 13, (11), 3602-3610.

130. Tiarks, F.; Landfester, K.; Antonietti, M., Preparation of polymeric nanocapsules by miniemulsion polymerization. *Langmuir* **2001,** 17, (3), 908-918.

131. Landfester, K.; Weiss, C. K., Encapsulation by miniemulsion polymerization. In *Modern Techniques for Nano- and Microreactors/-Reactions*, Caruso, F., Ed. 2010; Vol. 229, pp 1-49.

132. Rosenbauer, E.-M.; Wagner, M.; Musyanovych, A.; Landfester, K., Controlled release from polyurethane nanocapsules via pH-, UV-light- or temperature-induced stimuli. *Macromolecules* **2010,** 43, (11), 5083-5093.

133. Baier, G.; Musyanovych, A.; Dass, M.; Theisinger, S.; Landfester, K., Cross-linked starch capsules containing dsDNA prepared in inverse miniemulsion as "nanoreactors" for polymerase chain reaction. *Biomacromolecules* **2010,** 11, (4), 960-968.

134. Nghi, D. H.; Bittner, B.; Kellner, H.; Jehmlich, N.; Ullrich, R.; Pecyna, M. J.; Nousiainen, P.; Sipilä, J.; Huong, L. M.; Hofrichter, M.; Liers, C., The Wood rot ascomycete Xylaria polymorpha produces a novel GH78 glycoside hydrolase that exhibits α-l-Rhamnosidase and feruloyl esterase activities and releases hydroxycinnamic acids from lignocelluloses. *Appl. Environ. Microbiol.* **2012,** 78, (14), 4893-4901.

135. Loxley, A.; Vincent, B., Preparation of poly(methyl methacrylate) microcapsules with liquid cores. *J. Colloid Interface Sci.* **1998,** 208, (1), 49-62.

136. Berg, J.; Sundberg, D.; Kronberg, B., Microencapsulation of emulsified oil droplets by in-situ vinyl polymerization. *J. Microencapsulation* **1989,** 6, (3), 327-37.

137. McDonald, C. J.; Bouck, K. J.; Chaput, A. B.; Stevens, C. J., Emulsion polymerization of voided particles by encapsulation of a nonsolvent. *Macromolecules* **2000,** 33, (5), 1593-1605.

138. Dowding, P. J.; Atkin, R.; Vincent, B.; Bouillot, P., Oil core-polymer shell microcapsules prepared by internal phase separation from emulsion droplets. I. Characterization and release rates for microcapsules with polystyrene shells. *Langmuir* **2004,** 20, (26), 11374-11379.

139. Lavergne, F.-M.; Cot, D.; Ganachaud, F., Polymer microcapsules with "foamed" membranes. *Langmuir* **2007,** 23, (12), 6744-6753.

140. Rojas, O. J.; Bullon, J.; Ysambertt, F.; Forgiarini, A.; Salager, J.-L.; Argyropoulos, D. S., Lignins as emulsion stabilizers. *ACS Symp. Ser.* **2007,** 954, (Materials, Chemicals, and Energy from Forest Biomass), 182-199.

141. Selyanina, S. B.; Trufanova, M. V.; Afanas'ev, N. I.; Selivanova, N. V., Surfactant properties of kraft lignins. *Russ. J. Appl. Chem.* **2007,** 80, (11), 1832-1835.

142. Hofmeister, I.; Landfester, K.; Taden, A., Controlled formation of polymer nanocapsules with high diffusion-barrier properties and prediction of encapsulation efficiency. *Angew. Chem. Int. Ed.* **2015,** 54, (1), 327-330.

143. Chiarappa, L., Wood decay of the Grapevine and its relationship with black measles disease. *Phytopathology* **1959,** 49, (8), 510-519 pp.

144. Mugnai, L.; Graniti, A.; Surico, G., Esca (black measles) and brown wood-streaking: two old and elusive diseases of grapevines. *Plant Dis.* **1999,** 83, (5), 404-418.

145. Khan, A.; Eskalen, A.; Gubler, W. D., Rootstock susceptibility to *Phaeomoniella chlamydospora* and *Phaeoacremonium. Phytopathol. Mediterr.* **2001,** 40, 433-438.

146. Herche, R., C Control strategies for trunk diseases of grapevine (Vitis vinifera L.). *UC Davis - Department of Plant Pathology* **2009**.

147. Martin, M. T.; Cobos, R., Identification of fungi associated with grapevine decline in castilla y León (Spain). *Phytopathol. Mediterr.* **2007,** 46, (1), 18-25.

148. Bertsch, C.; Ramírez-Suero, M.; Magnin-Robert, M.; Larignon, P.; Chong, J.; Abou-Mansour, E.; Spagnolo, A.; Clément, C.; Fontaine, F., Grapevine trunk diseases: complex and still poorly understood. *Plant Pathology* **2013,** 62, (2), 243-265.

149. Moreno-Sanz, P.; Lucchetta, G.; Zanzotto, A.; Loureiro, M. D.; Suarez, B.; Angelini, E., Fungi associated to grapevine trunk diseases in young plants in Asturias (Northern Spain). *Hortic. Sci.* **2013,** 40, (3), 138-144.

150. Murolo, S.; Romanazzi, G., Effects of grapevine cultivar, rootstock and clone on esca disease. *Australasian Plant Pathol.* **2014,** 43, (2), 215-221.

151. Lecomte, P.; Darrieutort, G.; Pieri, P.; Rey, P.; Fermaud, M., Esca in France: increase, possible causes and symptoms. *10e Conférence Internationale sur les Maladies des Plantes, Tours, France, 3, 4 & 5 Décembre,* **2012**, 391-402.

152. Larignon, P.; Darne, G.; Menard, E.; Desache, F.; Dubos, B., Comment agissait l'arsénite de sodium sur l'esca de la vigne? *Le Progrès agricole et viticole* **2008,** 125, (23), 642-651.

153. Evidente, A.; Sparapano, L. O. R. E. N. Z. O.; Andolfi, A.; Bruno, G. I. O. V. A. N. N. I., Two naphthalenone pentaketides from liquid cultures of Phaeoacremonium aleophilum -

a fungus associated with esca of grapevine. *Phytopathol. Mediterr.* **2000,** 39, (1), 162-168.

154. Andolfi, A.; Mugnai, L.; Luque, J.; Surico, G.; Cimmino, A.; Evidente, A., Phytotoxins produced by fungi associated with grapevine trunk diseases. *Toxins* **2011,** 3, (12), 1569.

155. Bruno, G.; Sparapano, L.; Graniti, A., Effects of three esca-associated fungi on Vitis vinifera L.: IV. Diffusion through the xylem of metabolites produced by two tracheiphilous fungi in the woody tissue of grapevine leads to esca-like symptoms on leaves and berries. *Physiol. Mol. Plant Pathol.* **2007,** 71, (1–3), 106-124.

156. Di Marco, S.; Osti, F.; Cesari, A., Experiments on the control of Esca by Thricoderma. *Phytopathol. Mediterr.***2004,** 43, (1), 108-115.

157. Fourie, P. H.; Halleen, F., Proactive control of petri disease of grapevine through treatment of propagation material. *Plant Dis* **2004,** 88, (11), 1241-1245.

158. Di Marco, S.; Osti, F., Applications of Trichoderma to prevent Phaeomoniella chlamydospora infections in organic nurseries. *Phytopathol. Mediterr.* **2007,** 46, (1), 73-83.

159. Rolshausen, P. E.; Úrbez-Torres, J. R.; Rooney-Latham, S.; Eskalen, A.; Smith, R. J.; Gubler, D., Evaluation of pruning wound susceptibility and protection against fungi associated with grapevine trunk diseases. *Am. J. Enol. Vitic.* **2010,** 61, (1), 113-119.

160. Mazzullo, A.; Cesari, A.; Calzarano, F.; Di Marco, S., The Contro of Esca : Status and perspectives. *Phytopathol. Mediterr.* **2000,** 39, (1), 232-240.

161. Darrieutort, G.; Lecomte, P., Evaluation of a trunk injection technique to control grapevine wood diseases. *Phytopathol. Mediterr.* **2007,** 46, (1), 50-57.

162. Loskill, B.; Rosswog, K.; Kappes, E.; Berkelmann-Loehnertz, B., Investigations on the control of Esca disease by means of stem injection. *IOBC/wprs Bulletin* **2006,** 29, (11), 119-122.

163. Bechthold, N.; Tiarks, F.; Willert, M.; Landfester, K.; Antonietti, M., Miniemulsion polymerization: applications and new materials. *Macromol. Symp.* **2000,** 151, (Polymers in Dispersed Media), 549-555.

164. Pastor, A. C.; Rodriguez-Reinoso, F.; Marsh, H.; Martinez, M. A., Preparation of activated carbon cloths from viscous rayon. Part I. Carbonization procedures. *Carbon* **1999,** 37, (8), 1275-1283.

165. Servin, A.; Elmer, W.; Mukherjee, A.; De la Torre-Roche, R.; Hamdi, H.; White, J. C.; Bindraban, P.; Dimkpa, C., A review of the use of engineered nanomaterials to suppress plant disease and enhance crop yield. *J. Nanopart. Res.* **2015,** 17, (2), 1-21.

166. Mukhopadhyay, S. S., Nanotechnology in agriculture: prospects and constraints. *Nanotechnol., Sci. Appl.* **2014,** 7, 63-71.

167. Eapen, S.; D'Souza, S. F., Prospects of genetic engineering of plants for phytoremediation of toxic metals. *Biotechnol. Adv.* **2005,** 23, (2), 97-114.

168. Kumar, S.; Chauhan, N.; Gopal, M.; Kumar, R.; Dilbaghi, N., Development and evaluation of alginate-chitosan nanocapsules for controlled release of acetamiprid. *Int. J. Biol. Macromol.* **2015,** 81, 631-637.

169. Maysinger, D., Nanoparticles and cells: good companions and doomed partnerships. *Org. Biomol. Chem.* **2007,** 5, (15), 2335-2342.

170. Nair, R.; Varghese, S. H.; Nair, B. G.; Maekawa, T.; Yoshida, Y.; Kumar, D. S., Nanoparticulate material delivery to plants. *Plant Sci. (Shannon, Irel.)* **2010,** 179, (3), 154-163.

171. Kang, B.; Okwieka, P.; Schoettler, S.; Winzen, S.; Langhanki, J.; Mohr, K.; Opatz, T.; Mailaender, V.; Landfester, K.; Wurm, F. R., Carbohydrate-based nanocarriers exhibiting specific cell targeting with minimum influence from the protein corona. *Angew. Chem., Int. Ed.* **2015,** 54, (25), 7436-7440.

172. Soppimath, K. S.; Aminabhavi, T. M.; Kulkarni, A. R.; Rudzinski, W. E., Biodegradable polymeric nanoparticles as drug delivery devices. *J. Controlled Release* **2001,** 70, (1-2), 1-20.

173. Horcajada, P.; Chalati, T.; Serre, C.; Gillet, B.; Sebrie, C.; Baati, T.; Eubank, J. F.; Heurtaux, D.; Clayette, P.; Kreuz, C.; Chang, J.-S.; Hwang, Y. K.; Marsaud, V.; Bories, P.-N.; Cynober, L.; Gil, S.; Ferey, G.; Couvreur, P.; Gref, R., Porous metal-organic-framework nanoscale carriers as a potential platform for drug delivery and imaging. *Nat. Mater.* **2010,** 9, (2), 172-178.

174. Lunov, O.; Syrovets, T.; Loos, C.; Beil, J.; Delacher, M.; Tron, K.; Nienhaus, G. U.; Musyanovych, A.; Mailander, V.; Landfester, K.; Simmet, T., Differential uptake of functionalized polystyrene nanoparticles by human macrophages and a monocytic cell line. *ACS Nano* **2011,** 5, (3), 1657-1669.

175. Mailander, V.; Landfester, K., Interaction of nanoparticles with cells. *Biomacromolecules* **2009,** 10, (9), 2379-400.

176. De Jong, W. H.; Borm, P. J. A., Drug delivery and nanoparticles: applications and hazards. *Int. J. Nanomed.* **2008,** 3, (2), 133-149.

177. Chung, Y.-C.; Chen, I. H.; Chen, C.-J., The surface modification of silver nanoparticles by phosphoryl disulfides for improved biocompatibility and intracellular uptake. *Biomaterials* **2008,** 29, (12), 1807-1816.

178. Panyala, N. R.; Pena-Mendez, E. M.; Havel, J., Gold and nano-gold in medicine: overview, toxicology and perspectives. *J. Appl. Biomed.* **2009,** 7, (2), 75-91.

179. Zhu, H.; Han, J.; Xiao, J. Q.; Jin, Y., Uptake, translocation, and accumulation of manufactured iron oxide nanoparticles by pumpkin plants. *J. Environ. Monit.* **2008,** 10, (6), 713-717.

References

180.   Dan, Y.; Zhang, W.; Xue, R.; Ma, X.; Stephan, C.; Shi, H., Characterization of gold nanoparticle uptake by tomato plants using enzymatic extraction followed by single-particle inductively coupled plasma-mass spectrometry analysis. *Environ. Sci. Technol.* **2015,** 49, (5), 3007-3014.

181.   Bannwarth, M. B.; Kazer, S. W.; Ulrich, S.; Glasser, G.; Crespy, D.; Landfester, K., Well-defined nanofibers with tunable morphology from spherical colloidal building blocks. *Angew. Chem. Int. Ed.* **2013,** 52, (38), 10107-10111.

182.   Carrion, N.; Fernandez, A.; Eljuri, E. J.; Murillo, M.; Franceschetto, M., Trace metal determination in plant tissue by inductively coupled plasma-atomic emission spectrometry with slurry sample introduction. *At. Spectrosc.* **1991,** 12, (5), 162-8.

183.   Kanicky, V.; Toman, J.; Povolny, A.; Kopicova, Z., Determination of trace metals in soil extracts and plant tissues by ICP-OES [inductively coupled plasma-optical emission spectrometry]. *Chem. Listy* **1989,** 83, (2), 194-204.

184.   Gonzalez-Melendi, P.; Fernandez-Pacheco, R.; Coronado, M. J.; Corredor, E.; Testillano, P. S.; Risueno, M. C.; Marquina, C.; Ibarra, M. R.; Rubiales, D.; Perez-de-Luque, A., Nanoparticles as smart treatment-delivery systems in plants: assessment of different techniques of microscopy for their visualization in plant tissues. *Ann Bot* **2008,** 101, (1), 187-95.

185.   Peng, J.; Sun, Y.; Liu, Q.; Yang, Y.; Zhou, J.; Feng, W.; Zhang, X.; Li, F., Upconversion nanoparticles dramatically promote plant growth without toxicity. *Nano Res.* **2012,** 5, (11), 770-782.

186.   Rico, C. M.; Majumdar, S.; Duarte-Gardea, M.; Peralta-Videa, J. R.; Gardea-Torresdey, J. L., Interaction of nanoparticles with edible plants and their possible implications in the food chain. *J. Agric. Food Chem.* **2011,** 59, (8), 3485-3498.

187.   Fleischer, A.; O'Neill, M. A.; Ehwald, R., The pore size of non-graminaceous plant cell walls is rapidly decreased by borate ester cross-linking of the pectic polysaccharide rhamnogalacturonan II. *Plant Physiol.* **1999,** 121, (3), 829-838.

188.   Navarro, E.; Baun, A.; Behra, R.; Hartmann, N. B.; Filser, J.; Miao, A.-J.; Quigg, A.; Santschi, P. H.; Sigg, L., Environmental behavior and ecotoxicity of engineered nanoparticles to algae, plants, and fungi. *Ecotoxicology* **2008,** 17, (5), 372-386.

189.   Wang, Z.; Li, J.; Zhao, J.; Xing, B., T Toxicity and internalization of CuO nanoparticles to prokaryotic alga microcystis aeruginosa as affected by dissolved organic matter. *Environ. Sci. Technol.* **2011,** 45, (14), 6032-6040.

190.   Wang, Z.; Xie, X.; Zhao, J.; Liu, X.; Feng, W.; White, J. C.; Xing, B., Xylem- and phloem-based transport of CuO nanoparticles in maize (Zea mays L.). *Environ. Sci. Technol.* **2012,** 46, (8), 4434-4441.

191.   Paiphansiri, U.; Baier, G.; Kreyes, A.; Yiamsawas, D.; Koynov, K.; Musyanovych, A.; Landfester, K., Glutathione-responsive DNA-based nanocontainers through an

"interfacial click" reaction in inverse miniemulsion. *Macromol. Chem. Phys.* **2014,** 215, (24), 2457-2462.

192. Chan, J. W.; Hoyle, C. E.; Lowe, A. B., Sequential phosphine-catalyzed, nucleophilic thiol-ene/radical-mediated thiol-yne reactions and the facile orthogonal synthesis of polyfunctional materials. *J. Am. Chem. Soc.* **2009,** 131, (16), 5751-5753.

193. Hoyle, C. E.; Lee, T. Y.; Roper, T., Thiol–enes: Chemistry of the past with promise for the future. *Journal of Polymer Science Part A: Polymer Chemistry* **2004,** 42, (21), 5301-5338.

194. Killops, K. L.; Campos, L. M.; Hawker, C. J., Robust, efficient, and orthogonal synthesis of dendrimers via thiol-ene "click" chemistry.*J. Am. Chem. Soc.* **2008,** 130, (15), 5062-5064.

195. Connal, L. A.; Kinnane, C. R.; Zelikin, A. N.; Caruso, F., Stabilization and functionalization of polymer multilayers and capsules via thiol-ene click chemistry. *Chem. Mater.* **2009,** 21, (4), 576-578.

196. Gress, A.; Völkel, A.; Schlaad, H., Thio-click modification of poly[2-(3-butenyl)-2-oxazoline]. *Macromolecules* **2007,** 40, (22), 7928-7933.

197. Chan, J. W.; Yu, B.; Hoyle, C. E.; Lowe, A. B., Convergent synthesis of 3-arm star polymers from RAFT-prepared poly(N,N-diethylacrylamide) via a thiol-ene click reaction. *Chem. Commun.* **2008**, (40), 4959-4961.

198. Chan, J. W.; Hoyle, C. E.; Lowe, A. B.; Bowman, M., Nucleophile-initiated thiol-michael reactions: Effect of organocatalyst, thiol, and ene. *Macromolecules* **2010,** 43, (15), 6381-6388.

199. Koo, S. P. S.; Stamenovic, M. M.; Prasath, R. A.; Inglis, A. J.; Du Prez, F. E.; Barner-Kowollik, C.; Van Camp, W.; Junkers, T., Limitations of radical thiol-ene reactions for polymer-polymer conjugation. *J. Polym. Sci., Part A: Polym. Chem.* **2010,** 48, (8), 1699-1713.

200. Sun, J.; Schlaad, H., Thiol-ene clickable polypeptides. *Macromolecules.* **2010,** 43, (10), 4445-4448.

201. Krishnaveni, N. S.; Surendra, K.; Rao, K. R., Study of the Michael addition of [small beta]-cyclodextrin-thiol complexes to conjugated alkenes in water. *Chem. Commun.* **2005**, (5), 669-671.

202. Lowe, A. B., Thiol-ene "click" reactions and recent applications in polymer and materials synthesis: a first update. *Polym. Chem.* **2014,** 5, (17), 4820-4870.

203. Lai, K. K.; Renneberg, R.; Mak, W. C., Bioinspired protein microparticles fabrication by peptide mediated disulfide interchange. *RSC Advances* **2014,** 4, (23), 11802-11810.

204. Bauhuber, S.; Hozsa, C.; Breunig, M.; Göpferich, A., Delivery of nucleic acids via disulfide-based carrier systems. *Adv. Mater.* **2009,** 21, (32-33), 3286-3306.

References

205. Paiphansiri, U.; Baier, G.; Kreyes, A.; Yiamsawas, D.; Koynov, K.; Musyanovych, A.; Landfester, K., G Glutathione-responsive DNA-based nanocontainers through an "interfacial click" reaction in inverse miniemulsion. *Macro. Chem. Phys.* **2014,** 215, (24), 2457-2462.

206. Northrop, B. H.; Frayne, S. H.; Choudhary, U., Thiol-maleimide "click" chemistry: evaluating the influence of solvent, initiator, and thiol on the reaction mechanism, kinetics, and selectivity. *Polym.Chem.* **2015,** 6, (18), 3415-3430.

207. Lowe, A. B., Thiol-ene "click" reactions and recent applications in polymer and materials synthesis. *Polym. Chem.* **2010,** 1, (1), 17-36.

208. Alexandrino, E. M.; Buchold, P.; Wagner, M.; Fuchs, A.; Kreyes, A.; Weiss, C. K.; Landfester, K.; Wurm, F. R., A molecular "screw-clamp": accelerating click reactions in miniemulsions. *Chem. Commun.* **2014,** 50, (72), 10495-10498.

209. Alkan, A.; Natalello, A.; Wagner, M.; Frey, H.; Wurm, F. R., Ferrocene-containing multifunctional polyethers: monomer sequence monitoring via quantitative ^{13}C NMR spectroscopy in bulk. *Macromolecules* **2014,** 47, (7), 2242-2249.

210. Rudnitskaya, A.; Evtuguin, D. V.; Costa, L. C.; Graca, M. P. F.; Fernandes, A. J. S.; Correia, M. R. P.; Gomes, M. T. S. R.; Oliveira, J. A. B. P., Potentiometric chemical sensors from lignin-poly(propylene oxide) copolymers doped by carbon nanotubes. *Analyst* **2013,** 138, (2), 501-508.

211. Girifalco, L. A.; Good, R. J., A theory for the estimation of surface and interfacial energies. I. Derivation and application to interfacial tension. *J. Phys. Chem.* **1957,** 61, 904-9.

212. Dowding, P. J.; Atkin, R.; Vincent, B.; Bouillot, P., Oil core-polymer shell microcapsules prepared by internal phase separation from emulsion droplets. I. Characterization and release rates for microcapsules with polystyrene shells. *Langmuir* **2004,** 20, (26), 11374-9.

213. Kettering, M.; Valdivia, C.; Sterner, O.; Anke, H.; Thines, E., Heptemerones A-G, seven novel diterpenoids from Coprinus heptemerus: producing organism, fermentation, isolation and biological activities. *J Antibiot (Tokyo)* **2005,** 58, (6), 390-6.

214. Kopcke, B.; Weber, R. W. S.; Anke, H., Galiellalactone and its biogenetic precursors as chemotaxonomic markers of the Sarcosomataceae (Ascomycota). *Phytochemistry* **2002,** 60, (7), 709-714.

215. Bannwarth, M. B.; Weidner, T.; Eidmann, E.; Landfester, K.; Crespy, D., Reversible redox-responsive assembly/disassembly of nanoparticles mediated by metal complex rormation. *Chem. Mater.* **2014,** 26, (3), 1300-1302.

7. Curriculum Vitae

Doungporn Yiamsawas

Born the August 26th 1980 in Samut Sakhon, Thailand

Thai nationality

Professional Experiences

Period		Activities
May 2006 – Present	:	National Nanotechnology Center (NANOTEC) Thailand. Position : Research Assistant
Apr 2001- May 2001	:	Department of Industrial Work, Ministry of Industry, Thailand Position : Trainee

Educational Background

Period		Degrees
Oct 2012 – Apr 2016		PhD. Max Planck Institute for Polymer Research (Mainz - Germany)
May 2002 - May 2005	:	M.Sc. (Petrochemistry and Polymer Science) Chulalongkhorn University, Thailand
May 1998 - Mar 2002	:	B.Sc. (Chemistry) Silpakhon University, Thailand

8. Publications

(Related to PhD thesis)

(1)   Yiamsawas D, Baier G, Thines E, Landfester K, Wurm FR. Biodegradable lignin nanocontainers. RSC Adv. 2014;4:11661-3.

(2)   Paiphansiri U, Baier G, Kreyes A, Yiamsawas D, Koynov K, Musyanovych A, Landfester K. Glutathione-Responsive DNA-Based Nanocontainers Through an "Interfacial Click" Reaction in Inverse Miniemulsion. Macromolecular Chemistry and Physics. 2014;215:2457-62.

(3)   Lignin Biomaterial as Agricultural Drug Carrier. (the patent application number: EP16154480.4)

(4)   Yiamsawas D, Landfester K, Wurm FR. Nanoparticles as a delivery vehicle for plants. (ready to submit)

(5)   Yiamsawas D, Lu H, Landfester K,Wurm FR. Lignin Nanoparticles for drug delivery and as precursors for carbon-materials. (ready to submit)

(6)   Yiamsawas D, Wagner M, Landfester K, Wurm FR. Competing and simultaneous click reactions at the interface and in solution. (ready to submit)

(7)   Yiamsawas D, Fischer J, Landfester K, Thines E, Wurm, FR. Targeted drug delivery with lignin nanoparticles cure Esca-infected wine plants. *In preparation*